Republic of Iraq
Ministry of Higher Education
And Scientific Research
University of Baghdad
College of Education for Pure Sciences / Ibn Al-Haitham
Department of Physics

Study the Effect of Doping and Annealing On the Structure and Optical Properties for ZnO Thin Films Using Image Processing

A thesis

Submitted to the Council of Education for Pure Sciences / Ibn Al-Haitham - University of Baghdad in Partial Fulfillment of The Requirements for the Degree of Master of Science in Physics

By

Shahd Ali Hussain

BSc. in Physics / 2011

Supervised by

Assist.Prof. Dr. Auday Hattem Shaban

2018 A.D *1439 A.H*

بِسْمِ اللهِ الرَّحْمنِ الرَّحِيمِ

" وَيَسْأَلُونَكَ عَنِ الرُّوحِ ۖ قُلِ الرُّوحُ مِنْ أَمْرِ رَبِّي
وَمَا أُوتِيتُمْ مِنَ الْعِلْمِ إِلَّا قَلِيلًا "

صدق الله العظيم

سورة الاسراء الاية (٨٥)

Supervisors certification

I certify that this thesis entitled " **Study the Effect of Doping and Annealing On the Structure and Optical Properties for ZnO Thin Films Using Image Processing** " was prepared by **Shahd Ali Hussain** under my supervision at Physics Department, College of Education for Pure Sciences Ibn -Al-Haitham University of Baghdad as partial requirement for the degree of Master of Science in Physics.

Signature: A.H. Shaban

Name: **Assist. Prof. Dr. Auday Hattem shaban**

Address: Collage of Education for Pure Sciences

Ibn-Al-Haitham / University of Baghdad

Date: 19/ 10/ 2017

Certification of the head of physics Department

In view of the available recommendation, I forward this thesis for debate by the examination committee.

Signature:

Name: **Prof. Dr. Kareem Ali Jasim**

Address: Collage of Education for Pure Sciences

Ibn-Al-Haitham / University of Baghdad

Date: 19/ 10/ 2017

Committee Certification

We certify that we have read this thesis titled " **Study the Effect of Doping and Annealing On the Structure and Optical Properties for ZnO Thin Films Using Image Processing** " submitted by (**Shahd Ali Hussain**) and as examining committee examined the student in its content and that in our opinion it is adequate with standard as thesis for the Degree of Master of Science in Physics.

Signature: S. A. Maki
Name: *Prof. Dr. Samir A. Maki*
Address: University of Baghdad
(Chairmen)
Date: 14/ 3/ 2018

Signature:
Name: *Prof. Dr. Ziad M. Abood*
Address: University of Mustansyria
(Member)
Date: 14/ 3/ 2018

Signature:
Name: *Dr. Ali H. Abd Alrazak*
Address: University of Baghdad
(Member)
Date: 14/ 3 / 2018

Signature: A. H. Shaban
Name: *Assist Prof. Dr. Auday H. shaban*
Address: University of Baghdad
(Member-Supervisor)
Date: 14/ 3 / 2018

Approved by the Council of the College of Education for Pure Sciences Ibn-Al-Haitham / University of Baghdad

Signature: K. F. Ali
Name: *Prof. Dr. Khalid Fahad Ali*
Address: **Dean of college**
Date: 14/ 3/ 2018

Dedication

To

The soul of my grandmother

My dears mother, father &

My brother mohammed

and my friends Rand, Maitham & Rasheed

for their love, endless support and

encouragement

Shahd

Acknowledgments

First, I would like to express my deep thanks to the Almighty, ALLAH JALA JALALAH, for what I have been.

Great thanks and deepest gratitude to my supervisor Dr.Auday H. Shaban, for his valuable scientific guidance.

Additionally, I'd faithfully like to express my deepest and profound respect to (Prof. Dr. Samir Atta Maki) and (Prof. Dr. Alia A. Shehab) for their serious help all over the period of preparing this research,

Many thanks and gratefulness to all my family members who always support me and alleviate difficulties I have faced during my works.

Finally, My thanks are extended to postgraduate colleagues and all my friends in the Physics Department in the College of Education of Ibn-Alhaitham for their support.

Abstract

In this research, the Zinc Oxide (ZnO) thin film has been prepared and studied the optical and structural properties which prepared by thermal evaporation under vacuum. The pure Zinc metal (Zn) was deposited on a glass substrate at room temperature (300)K. The thin films prepared at thickness about (200) nm, also, Oxidation process applied to Zinc Films at a temperature (673K) at one hour with exhaust air flow (2.5) lit/s, then we studied the effect of doping by Tin metal (Sn) at different ratios on the structural and optical properties (3 to 9 step 2)wt%. Furthermore, we study the influence of annealing process, at a temperature (473K), on the structural and optical properties. X-Ray diffraction pattern revealed that all the prepared films (undoped and Sn-doped) are polycrystalline and have a hexagonal structure. The crystallite size increases from (29.9 nm) for pure ZnO to (30.4 nm) for doped films at (5%) then it will decrease at percentages (7 & 9)wt%. annealing process at (473K) affects, the average grain size for the thin film continuously decreasing with increasing the doping percentages. This research involved also the study of optical properties for all films Prepared (pure and Sn-doped). UV-Vis spectroscopy shows that the (300-1100) nm were used to calculate the value of optical energy gap (direct transition, transmittance, and absorbance).

Image processing techniques were applied to (AFM) images. The images have been enhanced, transformed, and applied edge detection to the images. These techniques used to observe the nature of the thin films surface. Many images processing methods had been used to achieve a reference and determine the quality of the prepared thin films. The other procedure that been used is the effects of doping and annealing on the surface image parameters. Histogram techniques show good results in classifying the quality of thin films.

Table of Content

List of Figures

List of tables

List of some Symbols

Symbol	Description	Unit
a	Lattice Constant	nm
c	Speed of light	m/s
d	Lattice plane	nm
Eg	Energy Gap	eV
T	Transmission	%
A	Absorption	%
t	Film Thickness	nm
λ	Wavelength	cm
ν	Frequency	Hz
D	Crystallite Size	nm
h	Planck Constant	J.s
δ	Dislocation Density	$Line/cm^2$
2θ	Diffraction Angle	Degree
α	Absorption Coefficient	cm^{-1}
E^{op}	Direct energy gap	eV
θ	Bragg's angle	Degree
d_{hkL}	The Inter-Planar Distance	nm
k_B	Boltzmann constant	J/K
m	mass	g
ρ	density	g/cm^3
h	height	cm

List of Abbreviations

JCPDS	Joint Committee On Powder Diffraction Standerds
I_A	Intensity Of Absorbed Radiation
I_o	Intensity Of Incident Radiation
I	Intensity Of Transmitted Radiation
AFM	Atomic Force Microscopy
SPM	Scanning Probe Microscopy
RMS	Root Mean Square
FWHM	Full Width At Half Maximum
Eu	Urbach Energy
hν	Photon Energy
L.R.O	Long Range Order
S.R.O	Short Rang Order
XRD	X-Ray Diffraction
UV	Ultraviolet
IR	Infrared
VIS	Visible
λ cutoff	Cutoff Wavelength
RGB	Red, Green, Blue
DCT	Discrete Cosine Transform
N	Row
M	Column

Chapter One

Introduction & Literature Review

1.1 Introduction

The material science and engineering have the ability to comprehend the novel material with a combination of chemical, physical and mechanical properties have changed the society. There is an increasing technological progress. Modern technology requires thin films for multiple applications [1].

One of the modern physical terms in which how is the lack of material thickness and its effects on material properties described. Thin film technique is used for making a material with one or several layers, therefore the thin films thickness range can be from several nanometers to less than one microns[2].

Thin film technology is the basis of development in solid-state electronics. The usefulness of the optical properties of metal films, and scientific about the behavior of two-dimensional solids has been responsible for great interest in the study science and technology of the thin films. Thin film studies have directly or indirectly advanced many new areas of research in solid state physics and chemistry which are based on phenomena uniquely characteristic of the thickness, geometry, and structure of the film [3].

Thin film's physical properties will be different from the original bulk material because the thickness is very small. Thin film's work mainly depends on the surface formation and how the crystal nucleation [4,5].

Thin films the first appearance were on the practical side in (1838), where they manufactured by using electrolysis technique, thus working on thin-film manufacturing has become more modern and more different techniques, so they have been developing since that time till now, and due to their importance, good efficiency, low cost, and small size, they are used in filters industry, coatings, detectors, sensors and solar cells….etc [6].

One of the beauties of thin film physics is that it is a very multidisciplinary subject. Through thin films, we can explore areas in solid state physics, surface science, chemistry, vacuum science, crystal growth, and still more [7]**.** The process of preparation of thin film back to the late of the eighteenth century. So techniques evaporation developed over the years, in order to get the best specifications thin films in terms of thickness homogeneous and area. So thin films become emerged in the research of applied physics sold state[8]. There are several techniques available for thin films deposited on a substrate such as thermal evaporation, chemical decomposition and evaporation of source material by the irradiation of energetic species or photons [9].

Image processing and digital image acquisition became over the last decades, the most valuable tools in the characterization of materials. The strong development of Micro and Nanosciences and technologies in recent years brought special demands to the non-invasive inspection and characterization of thin films and nanostructures. Digital image processing can be successfully applied to different types of microscopy images [10].

1.2 Thin films deposition methods

The deposition of the thin films has been studied for almost a century. Some of the techniques developed during the past five decades and widely used in the industries. The film deposition involves heterogeneous processes such as heterogeneous chemical reactions, evaporation, adsorption, and desorption on growth surfaces. The growth of films of Nano scale thickness involves nucleation and growth on the surface of the substrate. The nucleation step is very important because it governs the crystallinty and microstructure of the film [11,12]. The deposition processing and fabrication techniques classify in following methods:

1-physical deposition process [13,14].

a- Sputtering

- Glow discharge DC sputtering.
- Radio Frequency sputtering.
- Magnetron and Ion beam sputtering.
- A.C sputtering.

b- Evaporation

- Vacuum evaporation.
- Laser evaporation.

- Electron beam evaporation.
- Resistive heating evaporation.

2-chemical deposition process[15].

a- Gas Phase

- Chemical vapor deposition.
- Laser chemical vapor deposition.
- Plasma enhanced vapour deposition
- Photo-chemical vapour deposition.

b- Liquid Phase.

- Electro-deposition.
- Chemical bath deposition.
- Electroless deposition.
- Molecular beam epitaxy.
- Sol-gel / Spin Coating / Spray –pyrolysis technique.

1.3 Semiconductor doping methods

The properties of the semiconductor are strongly affected by the addition of some impurities or cause some defects in it, these impurities are increase the conductivity of the semiconductor and become one type of charge carriers are the majority and the others type are a minority. These mechanisms are desirable in most practical applications. There are several methods of doping semiconductor by (thermal diffusion, ion implantation, laser and dissolution by the solution). [16]

1.4 Diffusion in solid

Many reaction processes that are important in the treatment of material rely on the transfer of mass either within solid, liquid, gas, or another solid phase will necessarily accomplish by diffusion. The phenomena of material transport by atomic motion or stepwise migration of atoms from lattice site to another. There must be a vacancy and the atom must have sufficient energy to break bonds with its neighbor atoms and then cause some lattice distortion during the displacement, this energy is vibration in nature [17].

1.4.1 Interchange diffusion

This process also called "ring diffusion", the exchange of two atomic sites or more inside the structure of the crystal [18]. This process illustrated in figure (1-1).

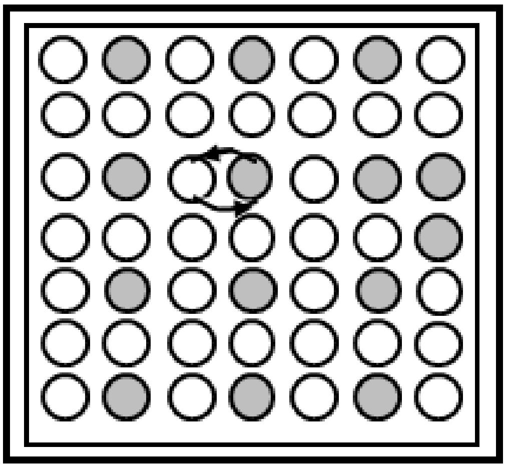

Figure (1-1) : interchange (ring) diffusion[19].

1.4.2 Vacancies diffusion

Vacancies play an important role in the diffusion of atoms in solids. the interchange of an atom from normal lattice sites to an adjacent vacant lattice site or vacancy as shown in figure (1-2). This could be occurred at a temperature higher than absolute zero, due to atoms vibrations. [18].

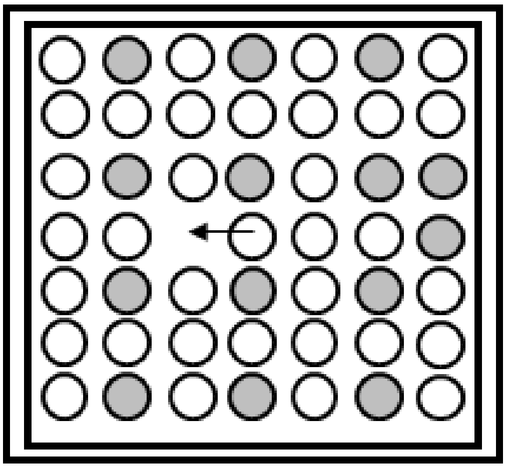

Figure (1-2) : vacancies diffusion[19].

1.4.3 Interstitials vacancies diffusion

The third type of diffusion involves interstitial atoms moves from one place to another without occupying a lattice site, as shown in figure (1-3). the mechanism is interstitial diffusion. The diffusion flux along direction x is proportional to the concentration gradient according to the Fick's first law [19]:

$$F = -D(\frac{dC}{dX}) \quad ....(1\text{-}1)$$

Where :

F: a flex as the number of dopants (atoms /cm^2 s).

D: diffusion constant (cm^2 s^{-1}).

$\frac{dc}{dX}$: concentration gradient.

The concentration of atoms was also determined by distance (x) and is a function of time according to the Fick's second law [20]:

$$\frac{dc}{dt} = D(\frac{d2c}{dx2}) ......(1\text{-}2)$$

Where:

$\frac{dc}{dt}$ = rate of concentration.

$\frac{d2c}{dx2}$ = second derivative of the concentration's gradiant for host's atoms [19].

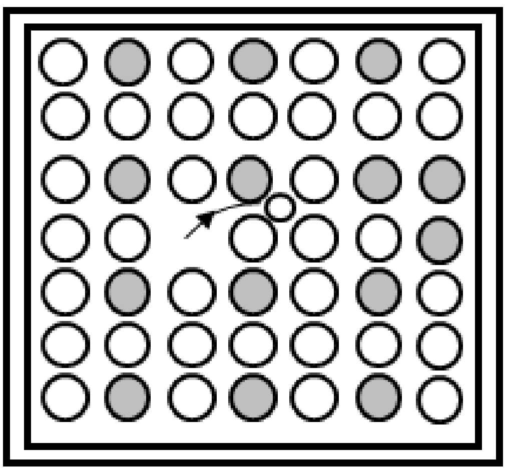

Figure (1-3) :Interstitials diffusion[19].

The diffusion of impurities affected by several variables [20,21]:

1- Diffusion's temperature, the diffusion rate will increase with rising of temperature.

2- The gradient of impurities concentration refers to the diffusion force.

3- The degree of distortion through crystal growth.

4- The difference between the radius of impurities and the original atoms.

1.5 Chemical and physical properties of Zinc Oxide (ZnO):

1- Zinc Oxide is an II-VI compound semiconductor [22], Pure Zinc Oxide is a white solid compound, change in color to yellows when heated due to the lattice distortions, it is Non-toxic material, not soluble in a water and alcohol, it dissolved in acetic acid, mineral acids, ammonia.

2- The preparation of Zinc Oxide chemically by burn Zinc element in the air or by thermal.

3- Zinc Oxide is one of the transparent conducting Oxides semiconductors (TCOs) it exhibit a high transmission in the visible range and reflection in the infrared wavelength range, in addition, it has a good electrical conductivity of (n-type).[23,24]

4- Zinc Oxide has a wide band gap of (3.37 eV), so it has huge technological importance and application in an optoelectric device such as solar cell, a light emitting diode (LED), heating mirrors, gas sensing devices [22].

5- Zinc Oxide has a binding energy gap (60 meV) due to a wide direct band gap energy, large exciton binding, excellent optical properties.[25]

6- Zinc Oxide is composed of large Oxygen atoms and small Zinc atoms, it crystallizes in three forms i.e hexagonal wurtzite, cubic Zinc blende, and cubic rock salt. The wurtzite structure is most stable at ambient conditions [26] and thus most common are shown in figure (1-4), and Table (1-1) illustrated some properties of Zinc Oxide [27].

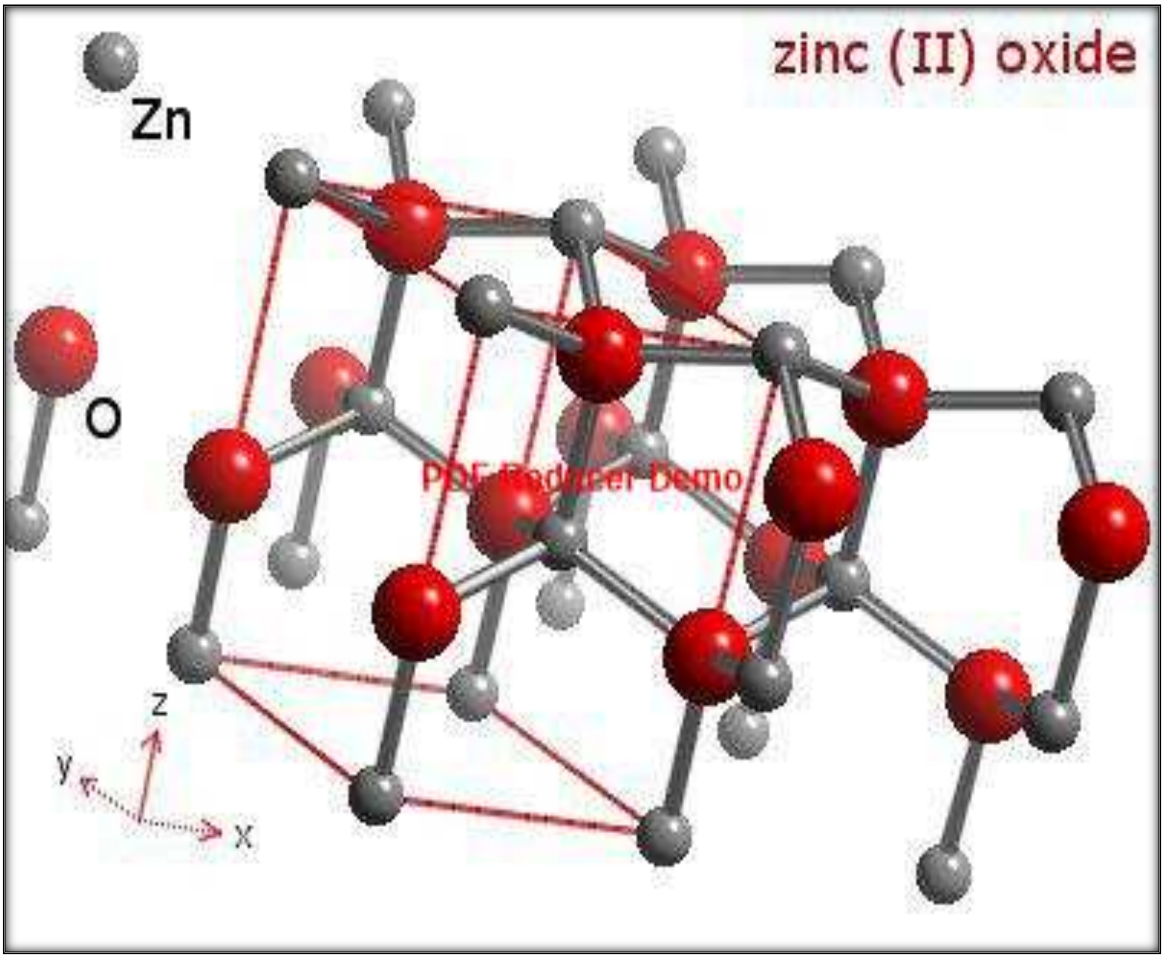

Figure (1-4): Hexagonal structure of ZnO.[26]

Table (1-1) some of the physical properties of Zinc Oxide.[27]

Zinc Oxide symbol	ZnO
phase	solids
color	White
Crystal structure	Hexagonal
Melting point	2243 (K)
Atomic radius Zn , O	Zn= 0.153 nm, O= 6.5 nm
Energy gap	3.37 (eV) (direct)
Molar mass	81.38 (g/mol)
Density	5.6706 (g/cm^3)

1.6 Tin (Sn)

Tin is a chemical element with symbol Sn and atomic number 50. It has a crystalline tetragonal in the group (4) of the periodic table. It is obtained chiefly from the mineral cassiterite, which contains tin dioxide SnO_2 [28]. Tin metal has good properties that it can be used in the manufacture of a wide range of products because of its ability to be in the form required [29].

Due to its nature of its electronic distribution especially in the secondary shells of the external orbits of its atoms, enable it to be present in two main oxidation states, +2 and the slightly more stable +4. It tends to be present slightly more stable +4. This term of energy levels for external orbital electrons, therefore tin classified as donor impurities which donate its electrons that are lies in the external orbits and make the semiconductor (n-type) [30]. Table (1-2) show some of the physical properties of Tin Users often include in coating systems as an external coating material to produce the coated material from corrosion oxidation or chemical reaction. as in the canned food as well as other uses [31] Also, it used to produce the metal alloys and to manufacture of solder alloys. it has a low melting point used in soldering metal surface or electrodes in electrical circuits [32].

Table (1-2) physical properties of Tin.[29, 31]

Tin symbol	Sn
phase	solid
Color	Silver-white (beta,β) or gray (α,β)
Crystal structure	White (β) ,tetragonal
Melting point	504.93 (K)
Atomic radius	0.172 nm
Molar mass	118.71(g/mol)
Density	7.265 (g/cm^3)

1.7 Literature Survey:

1) Reem .S et.al (2008) [33] a number of digital image processing techniques have been applied to digital images of (CdO: Sb, CdO) thin film which could obtain using optical microscopy and a digital camera connected to the computer. It has been found that there is a clear chromatic differentiation between thin films before and after doping and annealing and the average of grain size equal (48.86,50.53) pixel before and after annealing respectively.

2) S. Aksoy, et al (2010) [34], Tin doped ZnO thin films with a different doping were deposited by a spray pyrolysis method and thickness is (600) nm. The transmission was about 76% in the visible range. The value of optical energy gap decrease with increasing of Sn content from (3.37) eV for pure ZnO thin films and for doped with Sn (3.26 -3.25 and 3.18) eV.

3) N. Chahmat, et al (2012) [35], Tin doped Zinc Oxide thin films with percentage (2, 4, 6, 8 and 10) wt% prepared by chemical reactive liquid phase (spray). The results of XRD are polycrystalline with hexagonal wurtzite structure and preferential grains orientation along the direction (002). The peak intensity increases with increasing Sn, and the value of crystalline size increase from (31 to 41.37) nm for Sn and 29 nm for ZnO. The transmission decrease slightly when percentage up to 8%. The energy gap increases with Sn content from 3.2 eV for ZnO to 3.3 eV for ZnO doped by Sn. The energy gap decrease above of 8%.

4) S. Palimar et al (2013) [36], Zinc Oxide thin films doped with indium and indium Oxide by thermal evaporation, ZnO thin film has excellent transmission up to 90% in the visible range and does not affect by doping. The optical energy gap of the ZnO thin film that doped (In & In_2O_3) is widened from 3.26 to 3.3 eV when doped with indium oxide and with metallic indium it decreases to 3.2 eV. thickness of thin film is 200 nm, all pure and doped films were annealing at 300K for 2 hours, thin films are amorphous in nature as well as after annealing.

5) S. J. Mohammed (2013) [37], prepared pure ZnO thin film doped with Ni by chemical deposition with percentage doping (1 to 7 step 2) wt%. The transmission of pure ZnO is around between (82 to 90)%. Then decrease with doping from (0.8 to 0.79)% while the absorption increase with doping from (0.08 to 0.10) %. absorption coefficient increases rapidly with increasing photon energy through the range (3.2 to 3.3)eV. The energy gap is direct transition increase with doping (3.24, 3.16, 3.14, 3.18 and 3.10) eV.

6) N. S. Kamar et al (2013) [38], ZnO nanofiber thin films have been deposited by spray pyrolysis technique. The result of XRD shows that films have a polycrystalline with the hexagonal structure, the preferred orientation is (002) after annealing changes the preferred orientation (100) direction. The dislocation density with annealing at one hour increase then decrease with (4 to 6) hours and found the energy gap 3.29 eV which increases to 3.2 eV as the annealing time increases. It was found from AFM images that RMS and Roughness increase with annealing time.

7) K. chongsri et al (2013) [39] , Sn-doped ZnO thin films prepared by a sol-gel spin coating method, Sn-doped with ZnO with various content (2,4,6,8 and 10) wt%, then annealing at 773 K. the structure properties show a polycrystalline structure, all films have a high transmission in visible region (80-95)% as doping increased. Sn-doped increases the crystalline decreases accompanying grain size. The energy gap increase with various doped from (3.22-3.25) eV.

8) M. Fakhar-E-Alam et al (2014) [40], ZnO thin films with thickness (180) nm that have been deposition by thermal evaporation Then annealing from 350-450 C. the result of XRD show the preferred orientation is (101) and the crystalline size increase with doping. The transmission increase with annealing from 87% to 90%. The result of SEM that the grain size is increased with doping

9) N. chahmat et al (2014) [41], Zinc Oxide doped with Tin by spray pyrolysis, all thin films is a crystalline hexagonal wurtzite. Crystalline size increase from (20)nm to (200)nm. At doping of (10)%, the crystalline properties are slightly degraded. The optical energy increase with increasing Sn up to (6)% from (3.22 to 3.28) eV then decrease at higher Sn concentration from (8 to10)% thin films have the highest transmission above 85% for ZnO and 4% doped thin films

10) S. I. Saleh (2014) [42], ZnO thin films and Mg-doped ZnO prepared by chemical spray pyrolysis. Thickness was around 0.3μm. The preferred orientation is (002) when doped with the percentage (2 & 4)% the preferred orientation become (101). The FWHM decreases as Mg increases. The average grain size increases with Mg content. The transmission of pure and doped ZnO increase with doping up to 90% the energy gap increases by Mg doping from (3.23 to 3.54) eV.

11) F.Z. Bedia et al (2015) [43], ZnO Oxide thin film doped with Sn prepared spray pyrolysis. The result of XRD shows that all films have polycrystalline with (002) plane. The percentage doping of Sn is (1, 2)% the maximum intensity at 1% Sn concentration. At 2% the peaks position has slightly shifted, the FWHM decreases with increasing Sn content means that the average crystallite size increasing reaches a maximum value of 1% then decreases.the high transmission of ZnO: Sn increase with Sn content from (84 to 86)%. The energy gap of thin films doping increase from (3.27 to 3.29) eV to reach 1% then decrease at 2% (3.28) eV.

12) Mugwanga Fk, et al (2015) [44], Al doped Zinc Oxide thin films with percentage (2, 3, 4, 5 and 6) wt% prepared by thermal evaporation. ZnO thin films have a transmission higher than 70% and have a direct band gap 3.3eV. The transmission decrease as an Aluminum concentration increases. The energy gap decrease between (3.34-3.18) eV from (0 to 3)% the energy gap widening between (4-6)%.

13) Sheeba.N.H et al (2015) [45], ZnO and ZnO: Sn thin films deposited by multisource vacuum evaporation. The result of XRD show a polycrystalline ZnO and ZnO: Sn films with preferred orientation are (002), the crystalline size increased 16-20 nm. The optical properties show enhancement of transmission (80-90)% in visible range. Thin films show a wide of band gap films (3.21-3.24) eV.

14) A. Zaier et al (2015) [46], ZnO thin films deposited by thermal evaporation technique using ZnO powder, then annealing at a different temperature. The results of XRD that thin films have a good crystalline hexagonal wurtzite. The optical properties show high transmission about 90% within the visible range. the optical energy gap increased from 3.13-3.25 eV.

15) Musaab Khudhr M et al (2016) [47], Al doped ZnO thin films with doping percentage (0, 0.002, 0.004 and 0.006) wt%. were deposited by thermal evaporation method and thickness is (125) nm. The transmission was increased with increasing doping content for all wavelength, The absorption decreased with increasing doping content and the value bandgap increase with doping. Optical constants decrease with increasing doping content.

16) Al-Jamal (2016) [48], ZnO and SnO2 thin film have been prepared with different molar using (Matlab R2010a), initial treatment was done for the samples that have been obtained from the AFM and SEM with different concentrations (0.05, 0.1, 0.15) M, the grain size and surface roughness were calculated.

1.8 Aim of thesis

1- Preparation and characterization of Zinc Oxide (ZnO) thin films by thermal evaporation.

2- study the effect of adding Tin (Sn) as impurities by Study the structural and optical properties of different preparation conditions and annealing temperature.

3- Applying digital image processing techniques to the images of thin films surface that been produced from (AFM) techniques. These procedures maintain the characteristic of thin films with respect to the structure observed visually.

Chapter Two

Theoretical Part

Part one

Structural and Optical properties

2.1 Introduction

This chapter includes the theoretical principles for structural and optical properties for thin films studies.

2.2 Semiconductor

Solid state material can be divided into three types (insulator, semiconductor, and conductor). The material in nature is classified in term of electrical conductivity and resistivity value. Conductor material conductivity is usually between (10^6 - 10^4) (Ω cm)$^{-1}$, While the insulator has conductivity (10^{-10}) (Ω.cm)$^{-1}$ and some materials have conductivity between (10^4-10^{-10}) Ω.cm^{-1} are called as semiconductor [49]. The major characteristic of the semiconductor is the duel types of charge carrier which consisting of electrons and holes. According to the theory of energy bands, the semiconductor at low temperature has a valence band occupied by electrons while the conduction band is usually empty of electrons because there is not enough energy to across the electrons to the conduction band. The temperature has a clear effect on semiconductor characteristics as the degree of electrical conductivity of the semiconductor increases as the temperature increases [50].

The semiconductors are characterized by being insulation at absolute zero and have an electrical conductivity at high temperature. The other characteristic of this materials is the ability to add impurities or defects in their crystalline structure. Semiconductors are affected by heat, light and the magnetic field makes it a very important material in electrical applications, detector, solar cells and resistors [51].

2.3 The crystal of semiconductor

The solids classified into three types according to the nature of crystalline structure:

2.3.1 single crystal

Characterized by the atoms or molecular have a periodicity or regular geometric arrangement. the single crystal structure has a high degree of ordering and thus have (long range order) (L.R.O) in three dimensions as shown in figure (2-1a)[52].

2.3.2 polycrystalline

The structure of polycrystalline characterized by a high degree of order over many small regions called (grains) each grain is collected from thousands of unit cells and separated from one another by grain boundaries as shown in figure (2-1b)[52].

2.3.3 amorphous

The structure of amorphous characterize by (short-range order) (S.R.O) .the arrangement atoms or molecular will be random and the periodicity is absent in three dimensions and the order within a few atomic or molecular dimension as shown in figure (2-1c) [53].

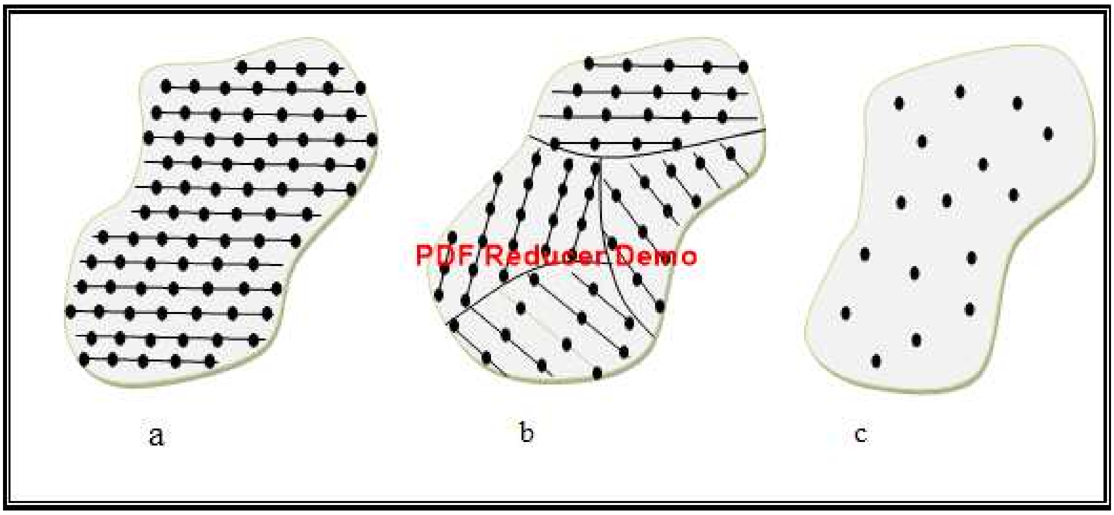

Figure (2-1) The types of materials structure a: single crystal b: polycrystalline c: amorphous[54].

2.4 Doping of semiconductor

The most suitable methods for controlling the conductivity of the semiconductor are adding a small and limited percentage of impurities to the semiconductor crystal, which is called doping. The process of doping is more desirable than heat to control the conduction of semiconductor.

2.5 Extrinsic semiconductor

when some suitable impurities or doping has been added in small amounts to a pure semiconductor are called "extrinsic or doped semiconductors". It increases the conductivity of these materials depending on the type of impurities used for doping and can be divided into two types (N-type semiconductor and p-type semiconductor)[55]. The impurities are merged into the material in these two ways (Substitution impurities or Interstitial impurities).

2.6 Structure properties

Structural characterization is carried out using X-ray diffraction analysis (XRD), atomic force microscope (AFM) and thickness measurement.

2.6.1 X-ray diffraction

X-rays are defined as electromagnetic radiation between ultraviolet waves and gamma waves and have relatively high energy and specific wavelengths within range (0.1-100) Å. This range of wavelength lies within the lattice spacing [56]. The most effective methods are X-ray diffraction is a basic tool used to study the crystal structure and give information about lattice parameters, crystalline phase, defect, and crystallite size. X-ray diffraction consists of constructive interference of reflected monochromatic rays from any position of lattice space at certain angles as shown in figure (2-2). The spacing between diffraction planes and incident angles is determined by Bragg's law given by following equation [57]:

$n\lambda = 2d \sin \theta$……(2-1)

Where ; (n): reflection order 1.2.3,…

λ_{ave}: wavelength of incident X-ray diffraction (0.1541838 nm).

d: lattice plane.

θ: Bragg angle.

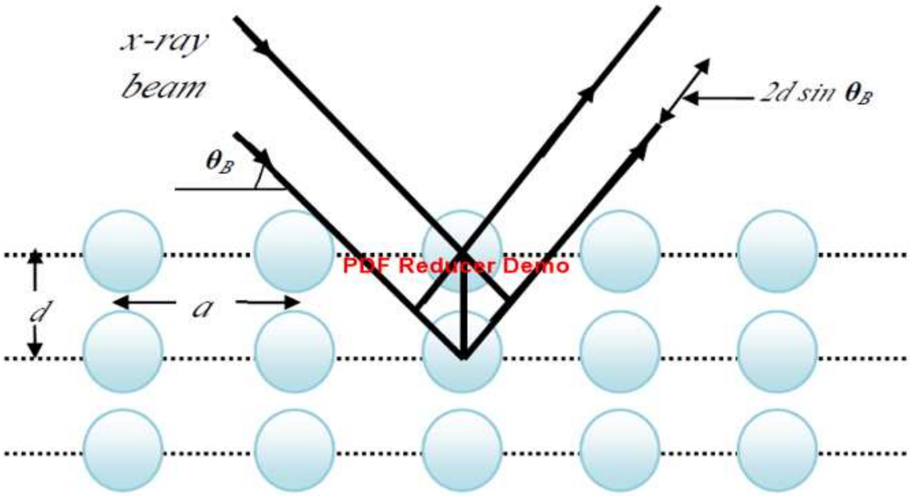

Figure (2-2) X-ray diffraction [58].

X-ray diffraction is used to determine many parameters such as :

- **Lattice constant**

The domain pattern for ZnO thin films is hexagonal (hcp) structure. (a, b, c) is a lattice dimension as shown in figure (2-3) if (a=b) can determine this parameter by measuring different values for (d) and through using equation [59]:

$$\frac{1}{d^2} = \frac{4}{3}\frac{h^2+k^2+l^2}{a^2} + \frac{l^2}{c^2} \text{......(2-2)}$$

Where (hkl) represents miller indices.

- **Full width at half maximum (**FWHM**)**

The FWHM is equal to the width of the curve at the half of maximum intensity (unit degree) [60] and converted into (Radian Units) when applying crystalline size law.

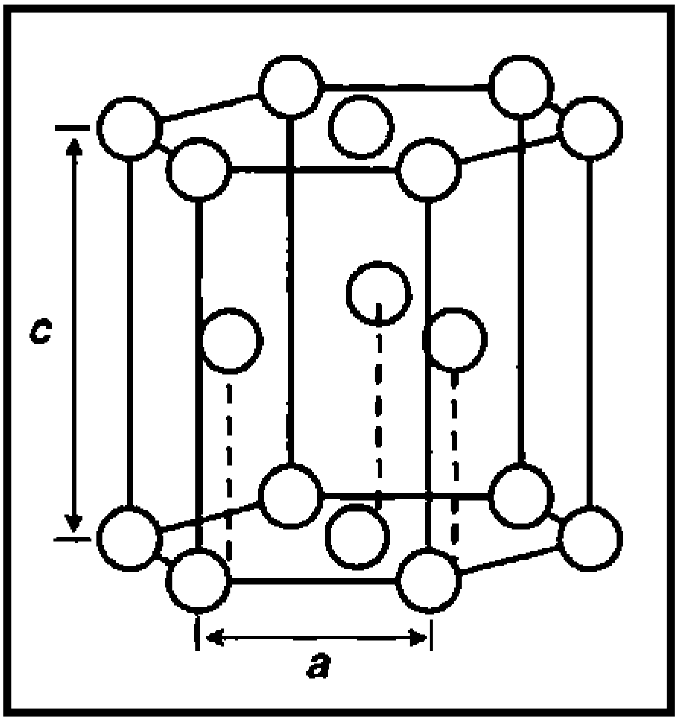

Figure (2-3) Hexagonal structure [59].

- **Crystallite size (C.S)**

The average crystallite size (C.S) can be calculated by using Scherrer's equation [46]:

$C.S = \frac{0.9\,\lambda}{\beta\cos\theta}$ ……………..(2-3)

- **Dislocation density (δ)**

The dislocation density that lies in a unit area in the crystal. It can be a calculated by following equation (Williamson and Smallmans)[61] :

$\delta = \frac{1}{(C.S)^2}$ ………………(2-4)

2.6.2 Atomic Force Microscopy (AFM)

Atomic force microscopy (AFM) is one of the scanning probe microscopy (SPM) developer depending on the technique of the scanning tunnel provide a very high-resolution of (0.1-1.0 nm) type with fractions of a nanometer and the magnification is $(5\times10^{2}-10^{8})$ µm. (AFM) is suitable to use with the surface of insulators, conductor, and semiconductor. (AFM) provide extremely accurate information of surface roughness and average grain size. (AFM) analysis the surface features of the sample and the instrument produces two and three-dimensional images of the surface [63]. Figure (2-4) shows the diagram of atomic force microscope.

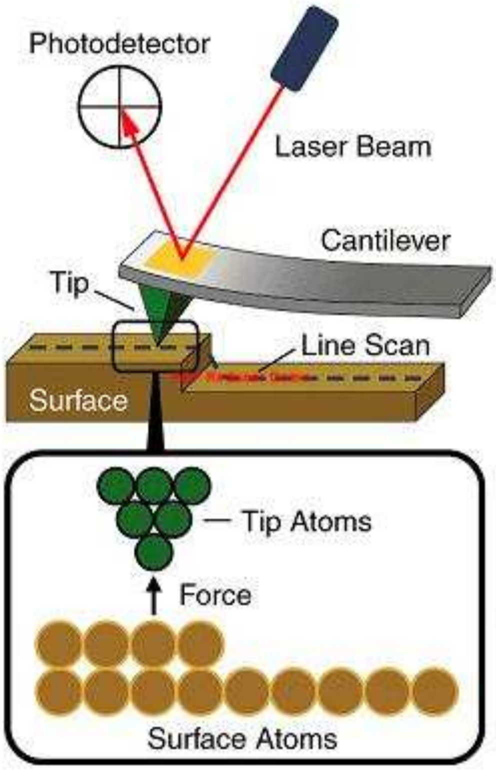

Figure(2-4) cross section of atomic force microscope [63].

2.7 Optical properties of semiconductor

The study of the optical properties of semiconductor provides information on the quality of electronic transitions occurring in the material and the structure of energy band as well as the properties that determine the interaction of light with the material [64]. The optical properties of semiconductor thin film generally depend on the method and conditions such as temperature, annealing temperature, pressure, deposition rate if any change in one of the factors leads to the deviation of the absorption edge to higher or lower energies [65].

2.8 Fundamental absorption edge

Is the rapid increase in absorption when the photon energy of incident radiation (hυ) equal to the forbidden energy gap (E_g represents the smallest difference in energy between the highest point in the valence band and the lowest point in the conduction band), it gets a quick and sudden absorption of the incident light .this characteristically is common to all semiconductor materials. This absorption is rapid and sharp in single crystal material while being less sharp in polycrystalline material. The cutoff wavelength (λ_{cutoff}) at the edge is calculated by following equation :

$$(h\nu)_{photon} = E_g = \frac{hc}{\lambda_{cutoff}} \quad \ldots\ldots\ldots\ldots\ldots\ldots(2\text{-}5)$$

$$\therefore \lambda_{cut\,off}(nm) = \frac{1240}{E_g(eV)} \quad \ldots\ldots\ldots\ldots\ldots\ldots(2\text{-}6)$$

Where; h: is plank's constant = 6.626×10^{-34} J.s.

c is the speed of light = 3×10^{8} m/s.

(λ_{cutoff}) is the wavelength that relates to energy gap for the semiconductor where at that point, the optical absorption will start to illustrate the fundamental absorption edge [66].

2.9 Absorption Regions

2.9.1 High Absorption Region (A)

The high absorption region has a high absorption coefficient has value ($\alpha \geq 10^4$) cm^{-1}, the relation with photon energy in this region is calculated as the value of the Tauc's equation [68]:

$$\alpha h\upsilon = B_\circ (h\upsilon - E_g^{opt})^r \quad \ldots\ldots\ldots\ldots\ldots\ldots(2\text{-}7)$$

where :

$B_\circ$: transition constant.

hυ : photon energy (e.V).

E_g^{opt} : optical energy gap (e.V).

r: exponential constant (2,3,1/2,3/2) depending on the type of material and the type of transition.

From figure (2-5A), this region is due to the transition between the extended states of the valence and condition bands.

2.9.2 Exponential Absorption Region(B)

This region has an absorption coefficient ranges from ($1< \alpha< 10^4$) cm^{-1} and the absorption coefficient is described by the Urbach equation:

$\alpha= \alpha_o \exp (h\upsilon /E_u)$ ………(2-8)

where :

Eu is Urbach energy.

From figure (2-5B), this region is due to the transition between the tail states of the valence band and extended states of the condition band or extended state of the valence band to tail states of the conduction band.

2.9.3 Weak Absorption Region (c)

From figure (2-5C), in this region, the absorption coefficient has the value (α < 1) cm^{-1} below the exponential part of the absorption edge, i.e. a tail absorption .this region depends on the nature of the material in terms of (purity), the conditions, and method of preparation. The transition for A, B, C part is illustrated in figure (2-5).

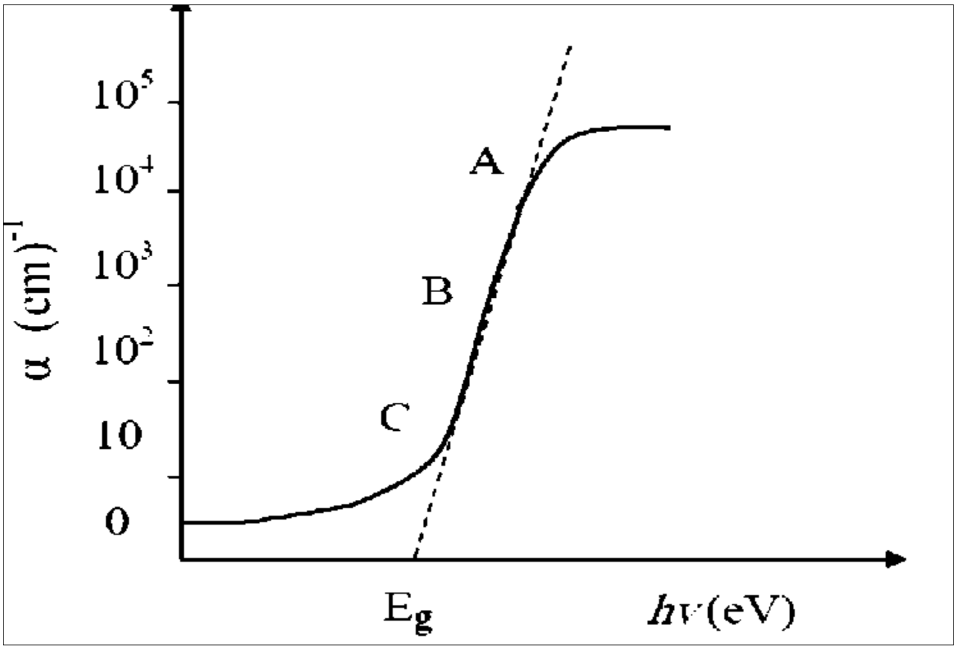

Figure (2-5) absorption regions (A) High Absorption Region. (B) Exponential Absorption Region. (C) Weak Absorption Region[69].

2.10 Optical constants

2.10.1 Absorption (A):

The definition of (absorption) is the ratio between the intensity of absorbed radiation by a thin film (I_A) to the intensity of incident radiation (I_o), and its given by following equation :

$A = \frac{I_A}{I_o}$………(2-9)

This relation represents the decrease in the energy of the electromagnetic radiation when passing through a medium. [70].

2.10.2 Transmittance (T):

The definition of transmittance is the ratio between the intensity of transmitted radiation through thin films (I) to the intensity of incident radiation (Io) and the transmittance is a quantity free of units, given by following equation :

$T = \frac{I}{I_o}$……..(2-10)

The transmission and absorption are related to the following equation [71] :

$A = \text{Log}_{10}\left(\frac{1}{T}\right) = \text{Log}_{10}\left(\frac{I_o}{I}\right)$ ....(2-11)

$\therefore T = e^{-2.303\,A} = 10^{-A}$.......(2-12)

2.10.3 Absorption coefficient (α):

The change in energy as the wave passes through a layer is a constant of the material for a given wavelength. Absorption coefficient depends on the incident of photon energy (hυ) and semiconductor properties. It is given Lambert's equation for absorption after it's derivation [72] :

$I = I_o\, e^{-\alpha t}$.......(2-13)

$\alpha = 2.303\,\frac{A}{t}$ ....(2-14)

Where:

I_o : the intensity of incident radiance.

I: the intensity of transmittance radiance.

α : absorption coefficient.

t : thickness of thin film.

2.10.4 Optical Energy Gap (Eg):

The optical energy gap is the least energy needed for electrons to move from the top of the valence band to the bottom of the conduction band. The value of the energy gap changes due to the change in temperature, impurity and the preparation method. This effect is either increased, or decreased depending on the type of semiconductor material. The (Eg^{opt}) for pure semiconductor is not completely free because it has structure defects [73]. The energy gap of the prepared thin films can be calculated in a standard manner using Taus equation (2-7).

To drawing the value of $(\alpha h\nu)^2$ plotted against photon energy $(h\nu)$. Stretch the straight line of the curve until the energy axis is cut at (α=0) which represented the optical energy gap.

Part two

Image Processing Technique

2.11 Introduction

This part is interested in studying the theoretical side aspect of the science of image processing. Its included some basic concepts of important image processing terms and display the image processing techniques used in the current study.

At present using different methods in order to enhance image information for interpreting and analysis due to wide spread for these images in multi-field of daily life, for example, in the field of medicine using technique to enhance X-ray image, and within military field to improve the thermal image and in space image. This techniques used also to inhance finger print images, and images that use in the operations of mineral exploration by using the seismic waves .

2.12 Digital image

Digital images are electronic snapshots taken of a scene or scanned from documents, such as photographs, manuscripts, printed texts, and artwork. The digital image is sampled and mapped as a grid of dots or picture elements pixels. Each pixel is assigned a tonal value (black, white, shades of gray or color), which is represented in binary code zeros and ones. The binary digits (bits) for each pixel are stored in a sequence by a computer and often reduced to a mathematical representation compressed. The bits are then interpreted and read by the computer to produce an analog version for display or printing [74].

2.12.1 Binary image

Binary images are the simplest type of images and can take on two values, typically black and white or 0 and 1. a binary image is referred to as (1 bit/pixel) image, because it takes only 1 binary digit to represent each pixel. this type of images is the most commonly used in applications that require only information form in general form or outline for example application of computer vision [75]. Pixel Values: As shown in this bitonal image, Figure (2-7) each pixel is assigned a tonal value, in this example 0 for black and 1 for white.

1	1	1	1	1	1	1	1	1	1
1	0	0	0	1	1	0	0	0	1
1	1	0	1	1	1	1	0	1	1
1	1	0	1	1	1	1	0	1	1
1	1	0	1	1	1	1	0	1	1
1	1	0	0	0	0	0	0	1	1
1	1	0	1	1	1	1	0	1	1
1	1	0	1	1	1	1	0	1	1
1	1	0	1	1	1	1	0	1	1
1	0	0	0	1	1	0	0	0	1
1	1	1	1	1	1	1	1	1	1

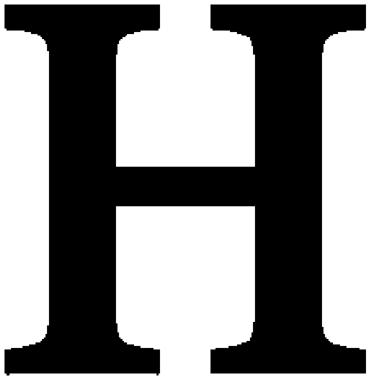

Figure (2-7) binary image [76].

2.12.2 Gray level image

a grayscale image is an image in which the value of each pixel is a single value, that carries only intensity information, and also known as black-and-white, are composed exclusively of shades of gray, varying from black at the weakest intensity to white at the strongest.

Grayscale images are often the result of measuring the intensity of light at each pixel in a single band of the electromagnetic spectrum e.g. infrared, visible light, ultraviolet, etc.

They number of different brightness level (bits) used for each pixel determines the number of different gray levels available. The typical gray-scale images contain 8 bit/pixel data [75], which allows us to have (0-255) or (256) different brightness gray levels, as shown in figure (2-8) [77].

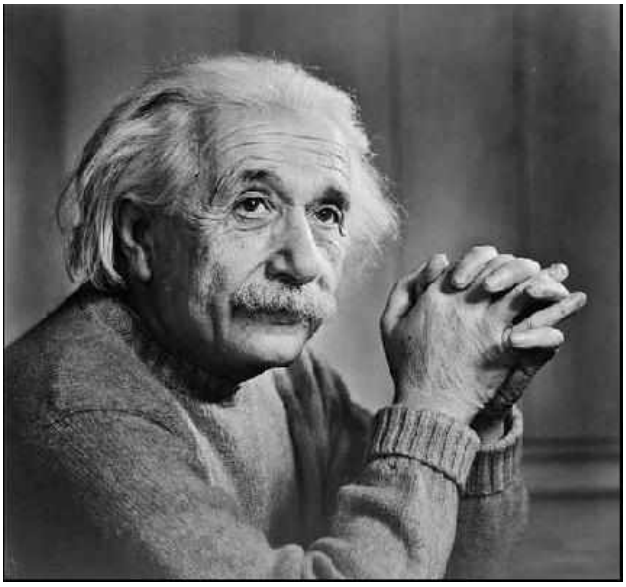

Figure (2-8) Gray level image [78].

2.12.3 Color image

A digital color image is a digital image that includes color information for each pixel. For visually acceptable results, it is necessary and almost sufficient to provide three samples color channels for each pixel, which are interpreted as coordinates in some color space. The (RGB) color space is commonly used in computer displays. Using the (8-bit) monochrome standard as a model, the corresponding color image would have (24 bit/pixel -8 bit) for each color bands red, green and blue as shown in figure (2-9).[79].

Figure (2-9) Colored image [80] .

2.12.4 Multispectral image

A multispectral image is one that captures image data within specific wavelength ranges across the electromagnetic spectrum. The wavelengths may be separated by filters or by the use of instruments that are sensitive to particular wavelengths, including light from frequencies beyond the visible light range, i.e. infrared and ultra-violet, X-ray, acoustic or radar data. source of these types of the image includes satellite systems, underwater sensor systems, and medical diagnostics imaging systems [81]. Spectral imaging can allow extraction of additional information the human eye fails to capture with its receptors for red, green and blue. Multispectral image shown in figure (2-10).

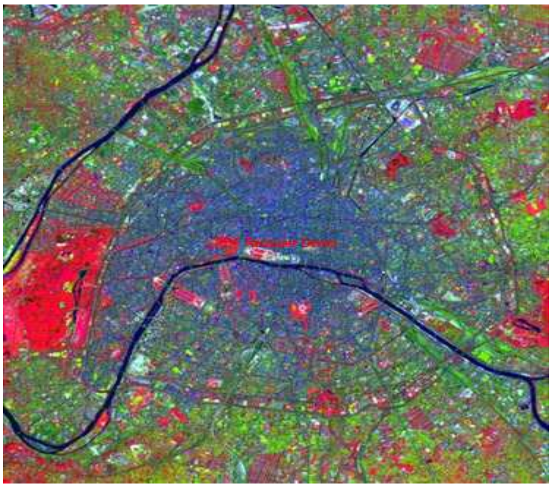

Figure (2-10) Finding Vegetation in a Multispectral image [82].

https://www.mathworks.com/help/images/examples/finding-vegetation-in-a-multispectral-image.html

2.13 Image Histogram

An image histogram is a graphical representation of the number of pixels in an image as a function of their intensity. Histograms are a way of visualizing the predominant intensities of an image. As a definition, image histograms are a count of the number of pixels that are at certain intensity. When represented as a plot, the x-axis is the intensity value, and the y-axis is the number of pixels with that intensity value. Histograms have many uses in image processing. We can predict about an image by just looking at its histogram.

The second use of histogram is for brightness purposes. The histograms have wide application in image brightness like adjusting the contrast of an image. Another important use of histogram is to equalize an image and thresholding. This is mostly used in computer vision [83].

2.14 Histogram Specification

Histogram Specification is a generalized version of histogram equalization, a standard image processing operation. An equalized image has an equal number of pixels at all brightness levels, resulting in a straight horizontal line on the histogram graph. When you specify a histogram, you actually define the desired shape of the histogram, and a nonlinear stretch operation is applied to force the image histogram to have that shape. Histogram specification is useful for compressing the dynamic range of an image in order to remove pixel values that contain very little information. This makes an image easier to view on a video monitor. It also allows you to emphasize information that appears at certain brightness levels. You can specify the curve by drawing it manually or select from the pre-defined list of curves. Predefined curves include Uniform, Exponential, Lognormal, Gaussian, Rayleigh, and Straight-Line [83].

2.15 Contrast

Contrast generally refers to the difference in luminance or gray level values in an image and is an important characteristic. It can be defined as the ratio of the maximum intensity to the minimum intensity over an image. Contrast ratio has a strong bearing on the resolving power and detectability of an image. The histogram of this image is shown in figure (2-11). Contrast enhancement techniques expand the range of brightness values in an image so that the image can be efficiently displayed in a manner desired by the analyst. The density values in a scene are literally pulled farther apart, that is, expanded over a greater range. The effect is to increase the visual contrast between two areas of different uniform densities. This enables the analyst to discriminate easily between areas initially having a small difference in density [84][85].

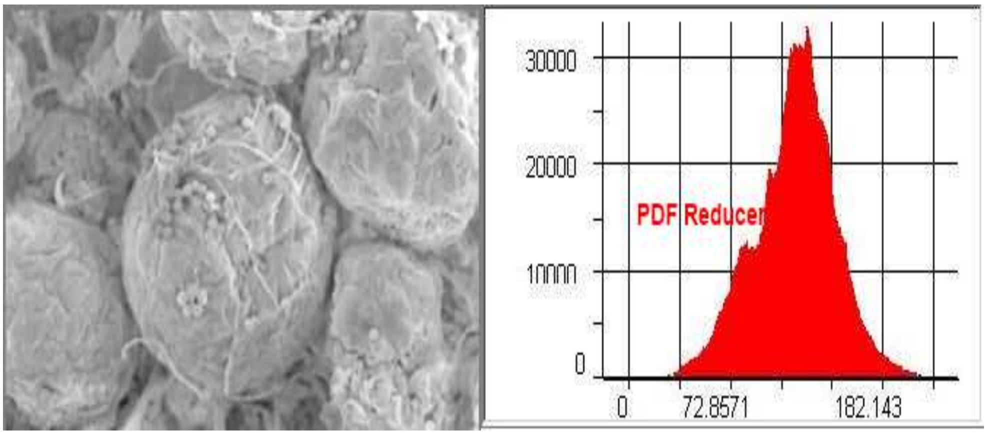

Figure (2-11) Histogram of an image.

https://www.google.iq/search?q=histogram+stretch+images&source=lnms&tbm=isch&sa=X&ved=0ahUKEwikuObsvtPZAhVHKuwKHegKCo4Q_AUICigB&biw=1366&bih=662#imgrc=f00ADMiS8i1E_M

The formula for stretching the histogram of the image to increase the contrast is

$$g\,(x,y) = \frac{f\,(x,y) - f_{min}}{f_{max} - f_{min}} \times 2^{bpp} \ldots\ldots\ldots\ldots(2\text{-}16)$$

The formula requires finding the minimum and maximum pixel intensity multiply by levels of gray. In our case, the image is 8bpp, so levels of gray are 256.

The minimum value is 0 and the maximum value is 225. So the formula in our case is

$$g\,(x,y) = \frac{f\,(x,y) - 0}{225 - 0} x255 \quad \ldots\ldots\ldots..(2\text{-}17)$$

where f(x,y) denotes the value of each pixel intensity. For each f(x,y) in an image, we will calculate this formula. After doing this, we will be able to enhance our contrast. The following image appears after applying histogram stretching.

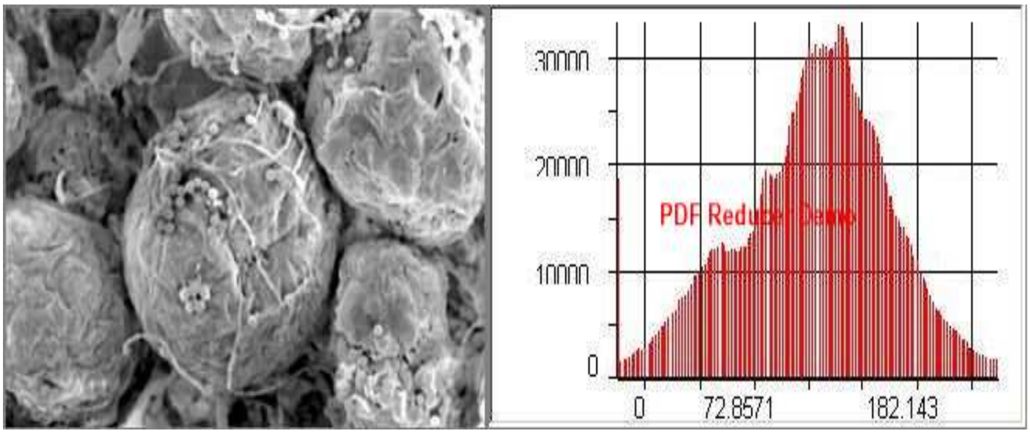

Figure (2-12) image after histogram stretch.

https://www.google.iq/search?q=histogram+stretch+images&source=lnms&tbm=isch&sa=X&ved=0ahUKEwikuObsvtPZAhVHKuwKHegKCo4Q_AUICigB&biw=1366&bih=662#imgrc=f00ADMiS8i1E_M

The stretched histogram of this image has been shown in figure (2-12).

Note the shape and symmetry of histogram. The histogram is now stretched or in other means expand. Have a look at it. In this case, the contrast of the image can be calculated as Contrast = 240. Hence we can say that the contrast of the image is increased.

2.15.1 Linear Contrast Stretch

This is the simplest contrast stretch algorithm. The gray values in the original image and the modified image follow a linear relation in this algorithm. A density number in the low range of the original histogram is assigned to extremely black and a value at the high end is assigned to extremely white. The remaining pixel values are distributed linearly between these extremes, as shown in figure (2-13). To provide optimal contrast and color variation in color composites the small range of gray values in each band is stretched to the full brightness range of the output or display unit [86].

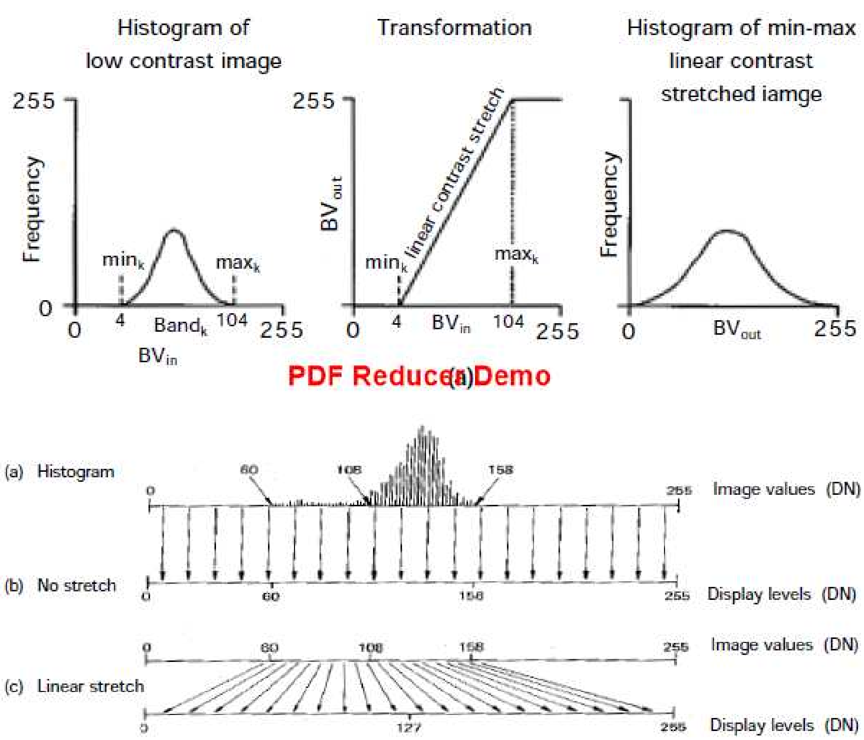

Figure (2-13) Linear Contrast Stretch [86].

2.15.2Non-Linear Contrast Enhancement

The general form of the nonlinear contrast enhancement is defined by y=f(x), where (x) is the input data value and (y) is the output data value. The nonlinear contrast enhancement techniques have been found to be useful for enhancing the color contrast between the near classes and subclasses of the main class.

A type of non linear contrast stretch involves scaling the input data logarithmically. This enhancement has the greatest impact on the brightness values found in the darker part of the histogram. It could be reversed to enhance values in brighter part of the histogram by scaling the input data using an inverse log function.

Histogram equalization is another nonlinear contrast enhancement technique. In this technique, ahistogram of the original image is redistributed to produce a uniform population density. This is obtained by grouping certain adjacent gray values. Thus the number of gray levels in the enhanced image is less than the number of gray levels in the original image [87].

2.16 Image Enhancement

Image enhancement aims to process an image, so that the output image is more suitable than the original. It is used to solve some computer imaging problems, or to improve image quality visually and brings out detail that is obscured, or simply highlights certain features of interest in an image. Enhancement methods tend to be problem specific [77]. For example, a method that is to enhance satellite images may not suitable for enhancing medical images. Image enhancement techniques include smoothing, sharpening, highlighting features, or normalizing illumination for display or analysis.

Image enhancement approaches are classified into categories :

- *Spatial domain methods***:** are based on direct manipulation of pixels in an image.
- *Frequency domain methods***:** are based on modifying the Fourier transform of an image [88].

2.16.1 Image enhancement in the spatial domain

The term spatial domain refers to the image plane itself and approaches in this categories are based on direct manipulation of a pixel in an image i.e the total number of pixels composing an image. To enhance an image in the spatial domain we transform an image by changing pixel value or moving them around[89] . A spatial process is denoted by the expression:

$$g(x,y) = T[\, f\,(x,y)] \qquad \text{......................(2-18)}$$

where f (x,y) is input image, T is operater on f, defined over the neighborhood of f (x,y), g (x,y) is aproccssed image .

2.16.2 Image enhancement in the frequency domain

- **The Discrete Cosine Transform (DCT) [90,91]**

The discrete cosine transform (DCT) helps separate the image into parts (or spectral sub-bands) of differing importance (with respect to the image's visual quality). The (DCT) is similar to the discrete Fourier transform: it transforms a signal or image from the spatial domain to the frequency domain as shown Figure (2-14).

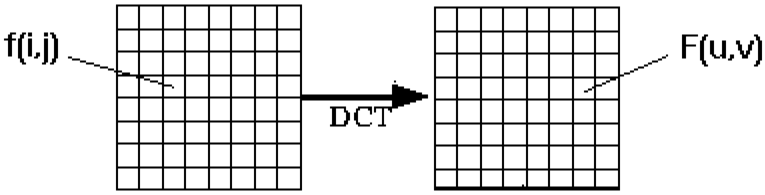

Figure (2-14) transform image from spatial domain to the frequency domain.

- **DCT Encoding**

The general equation for a 1D (N data items) DCT is defined by the following equation:

$$F(u) = \left(\frac{2}{N}\right)^{\frac{1}{2}} \sum_{i=0}^{N-1} \Lambda(i).cos\left[\frac{\pi.u}{2.N}(2i+1)\right] f(i)$$ …………….(2-19)

and the corresponding ***inverse*** 1D DCT transform is simple $F^{-1}(u)$, i.e.:

where

$$\Lambda(i) = \begin{cases} \frac{1}{\sqrt{2}} & \text{for} \xi = 0 \\ 1 & \text{otherwise} \end{cases}$$ …………………..(2-20)

The general equation for a 2D (N by M image) DCT is defined by the following equation:

$$F(u,v) = \left(\frac{2}{N}\right)^{\frac{1}{2}} \left(\frac{2}{M}\right)^{\frac{1}{2}} \sum_{i=0}^{N-1} \sum_{j=0}^{M-1} \Lambda(i).\Lambda(j).cos\left[\frac{\pi.u}{2.N}(2i+1)\right] cos\left[\frac{\pi.v}{2.M}(2j+1)\right] .f(i,j)$$

………………..(2-21)

and the corresponding ***inverse*** 2D DCT transform is simple $F^{-1}(u,v)$, i.e.:

where

$$\Lambda(\xi) = \begin{cases} \frac{1}{\sqrt{2}} & \text{for} \xi = 0 \\ 1 & \text{otherwise} \end{cases}$$ ……………………(2-22)

The basic operation of the DCT is as follows:

- The input image is N by M;
- f(i,j) is the intensity of the pixel in row i and column j;
- F(u,v) is the DCT coefficient in row k1 and column k2 of the DCT matrix.
- For most images, much of the signal energy lies at low frequencies; these appear in the upper left corner of the DCT.
- Compression is achieved since the lower right values represent higher frequencies, and are often small - small enough to be neglected with little visible distortion.
- The DCT input is an 8 by 8 array of integers. This array contains each pixel's grayscale level;
- 8-bit pixels have levels from 0 to 255.
- Therefore an 8 point DCT would be:

where

$$\Lambda(\xi) = \begin{cases} \frac{1}{\sqrt{2}} & \text{for} \xi = 0 \\ 1 & \text{otherwise} \end{cases}$$ …………………..(2-23)

- **Wavelet transform**

Wavelets can be used to extract information from many different kinds of data, including audio signals and images. A wavelet is a wave-like oscillation with an amplitude that begins at zero, increases, and then decreases back to zero. Wavelets allow complex information such as music, speech, images, and patterns to be decomposed into elementary forms at different positions and subsequently reconstructed with high precision. The wavelet method is the one which least distorts the spectral characteristics of the data. The distortions are minima the wavelet-based method is the most efficient in preserving the spectral information contained in the original multispectral images. Wavelets have the great advantage of being able to separate the fine details in a signal. Very small wavelets can be used to isolate very fine details in a signal, while very large wavelets can identify coarse details. A wavelet transform can be used to decompose a signal into component wavelets [92].

2.17 Image segmentation

image segmentation is the process of partitioning a digital image into multiple segments (sets of pixels, also known as superpixels). The goal of segmentation is to simplify and/or change the representation of an image into something that is more meaningful and easier to analyze[93]. Image segmentation is typically used to locate objects and boundaries (lines, curves, etc.) in images. More precisely, image segmentation is the process of assigning a label to every pixel in an image such that pixels with the same label share certain characteristics.

The result of image segmentation is a set of segments that collectively cover the entire image or a set of contours extracted from the image (see edge detection). Each of the pixels in a region is similar with respect to some characteristic or computed property, such as color, intensity, or texture. Adjacent regions are significantly different with respect to the same characteristics[94]. When applied to a stack of images, typical in medical imaging, the resulting contours after image segmentation can be used to create 3D reconstructions with the help of interpolation algorithms like Marching cubes.

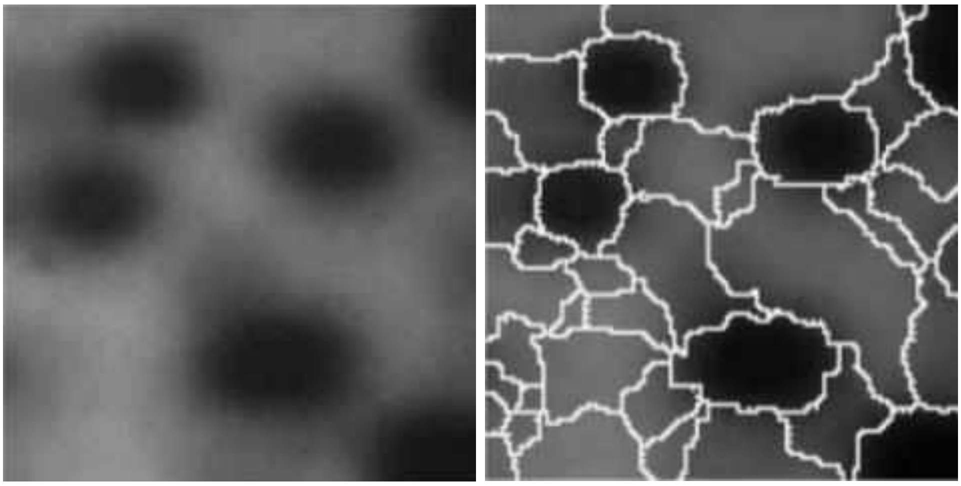

Figure (2-15) Model of a segmentation by morphology watersheds.

https://www.imageprocessingbook.com

2.18 Edge Detection Techniques

Edge detection is one of the most commonly used operations in image analysis, and there are probably more algorithms in the literature for enhancing and detecting edges than any other single subject. The reason for this is that edges form the outline of an object. An edge is the boundary between an object and the background and indicates the boundary between overlapping objects [95].

2.18.1 Sobel Operator

The operator consists of a pair of 3×3 convolution kernels as shown in Figure (2-16). One kernel is simply the other rotated by 90°.

Gx

-1	0	+1
-2	0	+2
-1	0	+1

Gy

+1	+2	+1
0	0	0
-1	-2	-1

Figure (2-16) Sobel 3×3 convolution kernels

These kernels are designed to respond maximally to edges running vertically and horizontally relative to the pixel grid, one kernel for each of the two perpendicular orientations. The kernels can be applied separately to the input image, to produce separate measurements of the gradient component in each orientation (call these *Gx* and *Gy*) [96]. The gradient magnitude is given by:

$|G| = \sqrt{Gx^2 + Gy^2}$………………..(2-24)

Typically, an approximate magnitude is computed using [97]:

$|G| = |Gx| + |Gy|$

which is much faster to compute. The angle of orientation of the edge (relative to the pixel grid) giving rise to the spatial gradient is given by:

$\theta = \arctan\frac{Gy}{Gx}$…………………(2-25)

2.18.2 Robert's cross operator:

The Roberts Cross operator performs a simple, quick to compute, 2-D spatial gradient measurement on an image. The operator consists of a pair of 2×2 convolution kernels as shown in Figure (2-17). One kernel is simply the other rotated by 90°. This is very similar to the Sobel operator.

Gx

+1	0
0	-1

Gy

0	+1
-1	0

Figure (2-17) Robert's 2×2 convolution kernels

These kernels are designed to respond maximally to edges running at 45° to the pixel grid, one kernel for each of the two perpendicular orientations. The kernels can be applied separately to the input image, to produce separate measurements of the gradient component in each orientation (call these *Gx* and *Gy*). The gradient magnitude is given by:

$|G| = \sqrt{Gx^2 + Gy^2}$………………..(2-26)

although typically, an approximate magnitude is computed using:

$|G| = |Gx| + |Gy|$……………..(2-27)

which is much faster to compute.

The angle of orientation of the edge giving rise to the spatial gradient (relative to the pixel grid orientation) is given by[98]:

$\theta = \arctan\frac{Gy}{Gx} - \frac{3\pi}{4}$..........................(2-28)

2.18.3 Prewitt's operator:

Prewitt operator is similar to the Sobel operator and is used for detecting vertical and horizontal edges in images [99].

$h_1 = \begin{bmatrix} 1 & 1 & 1 \\ 0 & 0 & 0 \\ -1 & -1 & -1 \end{bmatrix} h_1 = \begin{bmatrix} -1 & 0 & 1 \\ -1 & 0 & 1 \\ -1 & 0 & 1 \end{bmatrix}$....................(2-29)

2.18.4 Laplacian of Gaussian:

The Laplacian is a 2-D isotropic measure of the (2nd) spatial derivative of an image. The Laplacian is often applied to an image that has been first smoothed with something approximating a Gaussian Smoothing filter in order to reduce its sensitivity to noise. The operator normally takes a single gray level image as input and produces another gray level image as output.

The laplacian(x,y) of an image with pixel intensity values I(x,y) is given by:

$L(x,y) = \frac{\partial^2 I}{\partial x^2} + \frac{\partial^2 I}{\partial y^2}$............................(2-30)

Three commonly used small kernels are shown a figure (2-18).

0	1	0
1	-4	1
0	1	0

1	1	1
1	-8	1
1	1	1

-1	2	-1
2	-4	2
-1	2	-1

Figure (2-18) Laplacian small kernels.

2.18.5 Canny's Edge Detection Algorithm

Canny edge detector is the optimal and most widely used algorithm for edge detection. Compared to other edge detection methods like Sobel, etc canny edge detector provides robust edge detection, localization and linking.

Comparison of Edge detection Algorithm

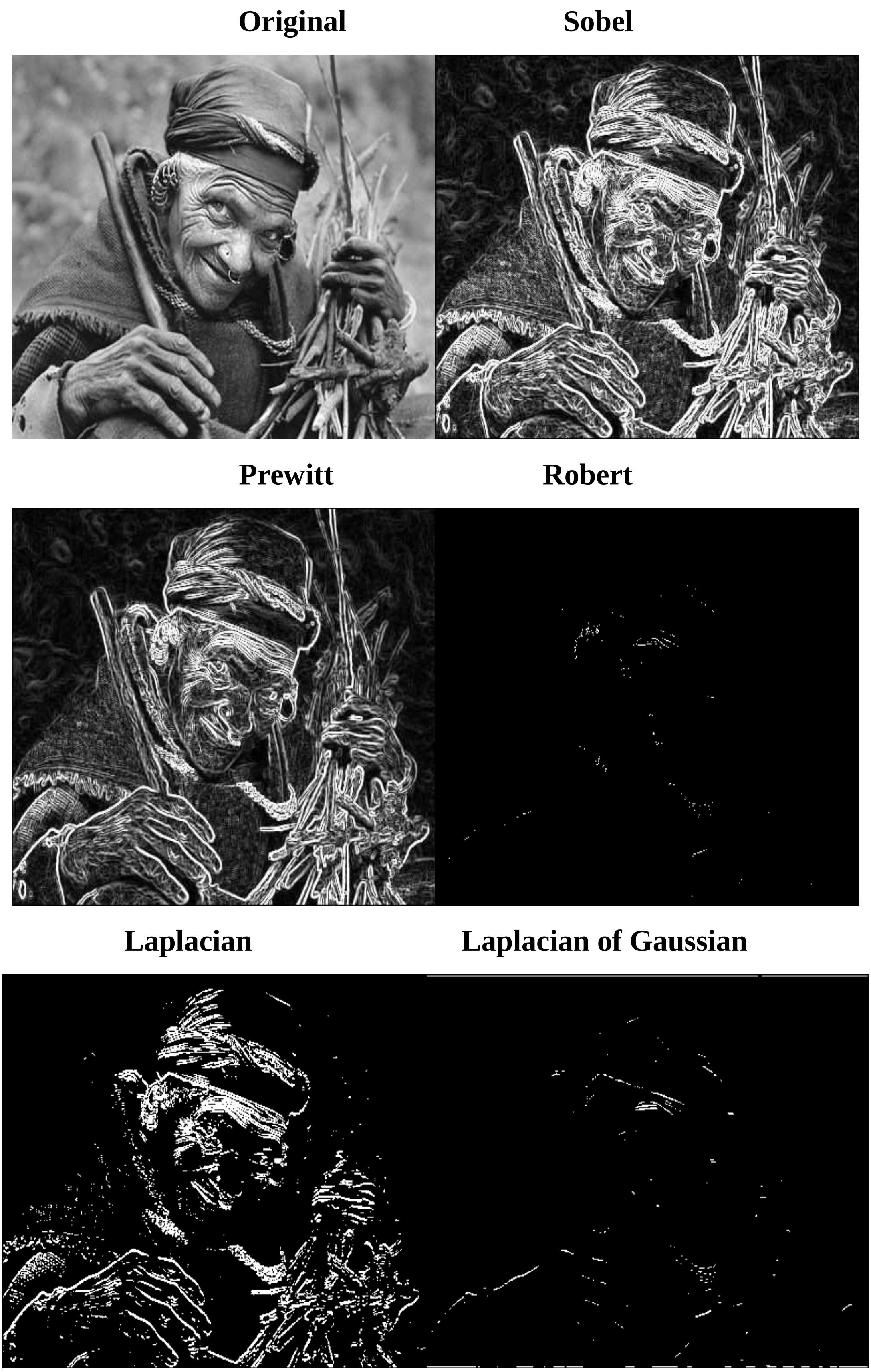

Figure (4-19) Performance of Edge Detection Algorithms.

Chapter Three

Experimental Work

Part one

Experimental work

3.1 Introduction

This chapter included an explanation of how to prepare Zinc Oxide (ZnO) thin film and doping by Tin (Sn). The evaporation mechanism is used to deposit the thin films. The process for examining ZnO thin films will be explained for structural, optical properties and image processing with a clear of function steps. Figure (3-1) illustrated the diagram of the first part including thin films preparations and measurements.

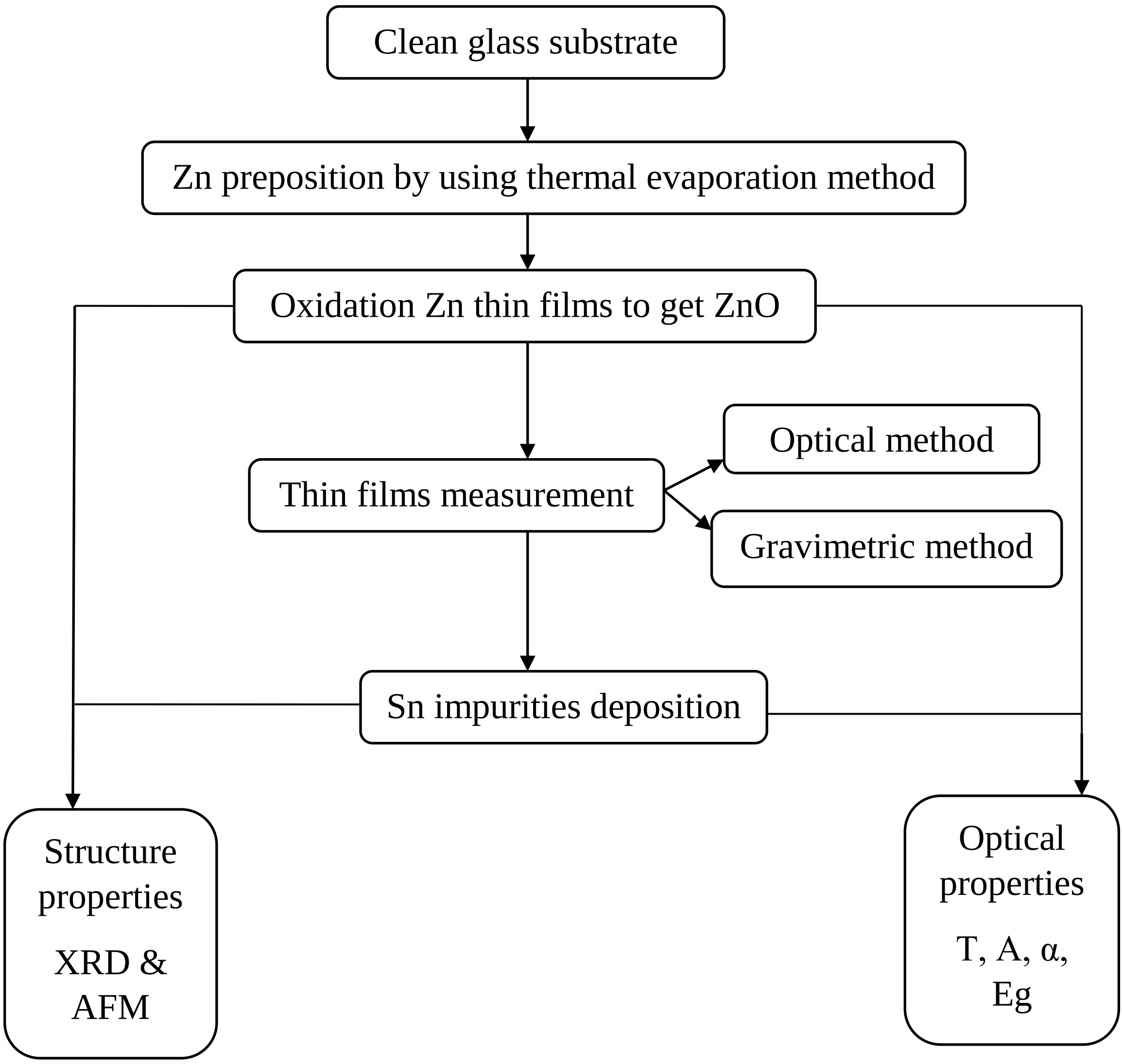

Figure (3-1) diagram the practical side for preparing ZnO thin films and measurements.

3.2 Thermal Evaporation Techniques

This method is one of the most common methods and adopted in the evaporation of material to prepare thin film under very low pressure sometimes reaches to (10^{-6}mbar) pressure varies depending on the materials used [102].

To get the thin films by this method we can follow sequential processes which are represented:

1- The material to be deposited is turned (convert)into steam.

2- Adhesion of the vapor of the material from the source of evaporation to the substrate with help of vacuum.

3- Deposition of the material on the substrate in the form of thin films.

The material will be placed in a boat and its melting point will be higher than the melting point of the material and will not react with it. The boat is heated by the flow of an electric current to the degree of melting of the material that evaporates and then deposited on the substrate. This method is suitable for evaporation of more metals and semiconductors but seems inappropriate to evaporate some alloys. thermal evaporation shown in figure (3-2).

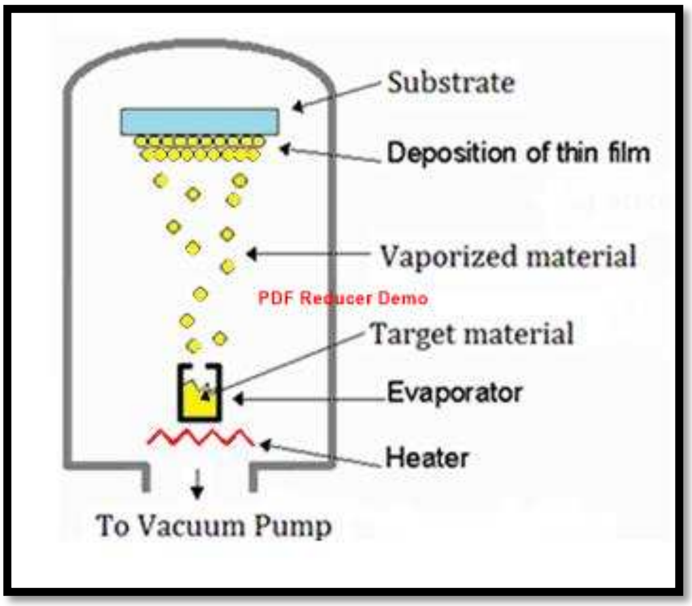

Figure (3-2) demonstration diagram of the thermal evaporation system.

the advantage of thermal evaporation method is highly efficient in obtaining excellent purity thin film with the least number of stress or internal tension, Easy preparation, absence of ionizing radiation and can the possibility of completing multiple samples with uniform conditions at the same time, on other hand the possibility of pollution from the heater or so-called (boat) and limited method of evaporation of low melting element or compounds such as Al،Cd,Sn،Pb،In،Zn،Cu [103,104].

The vacuum system model (Edward A) is used to evaporation (ZnO) thin films. Two parts consist of the vacuum system unit, the first stage is the chamber, and the pumping system represents the second part. The pumping system included two evaporation pumping (rotary pump and diffusion pump). The material will vaporize or sublimed into a gaseous state, then it will modify on the surface of the substrate. The Parameters that Influence on the Prepared Films Homogeneity [103].

1- Air pressure in evaporation chamber

2- The vertical distance between the evaporation bowl and the substrate.

3- Substrate temperature & deposition rate.

4- The shape of a boat and the type of material manufactured.

3.3 Substrate preparation

ZnO thin films have been prepared in several sequential stages and all stages have been carefully working to get pure ZnO thin films and doped.

Thin film has been prepared on a glass substrate with thickness (1 mm) and dimensions (25.4 x 76.2 mm^2) were used. The glass substrate is cleaned using soap and then leave under running water for (15) min.To remove surface contaminants glass substrate was cleaned with distilled water by ultrasonic for (15) min. The last stage using ethanol by ultrasonic for (15) min and allowed to dry completely. The purpose of using all these stages to ensure the accuracy of cleaning, this important because it affects the quality of the films.

3.4 Preparation of Zinc Oxide (ZnO/Sn) thin films

Zinc oxide has a high melting point of about (2243K), this point is great compared to the melting point of pure Zinc element (Zn), therefore Zinc was chosen for deposition on glass substrate, because it has a low melting point (680K), it evaporates easily and does not require a catalyst to produce ZnO thin film, therefore we get Zn thin film by thermal evaporation method.

The process of preparation of thin films consist of the following steps:

1- Prepare the appropriate mass of Zinc material to be evaporated under vacuum to have the desired thickness. This mass is placed in the molybdenum boat that made in size (1 cm^3).

2- special masks were made for deposition of Zinc metal on a glass substrate that has been cleaned than prove well on the sample holder. Masks are also used to determine the geometry shape of the thin film, the appropriate dimension was selected between boat and sample holder for the deposition of thin films with greater adhesion to the substrate.

3- The evacuation of chamber from the air and reduction the pressure inside the chamber until stabilized into ($4x10^{-5}$ Torr). The process of heating the boat begins by raising the electric current gradually and slowly. The material will evaporate from the boat and during this process, the material is monitored through the chamber.

4- After the evaporation process had been completed, the samples were left in the chamber until reaches room temperature in order to ensure the deposition of Zinc metal on the substrate with good adhesion without creaks or defects. The samples are removed accurately and carefully to avoid scratch the films.The samples are placed in special dried cans to keep them from external conditions that exposed until the next step.

5- Zinc thin films are oxidized by placing the thin film in an electric oven (vectoreen) at (680K) for two hours, during thermal oxidation air is pumped out and after (24) hours the sample are removed from the oven to ensure gradual cooling of the samples.

6- Finally, Sn thin film was a deposit on ZnO thin films by evaporating Sn under vacuum. The ratio of Sn to ZnO was precise to weight (3 to 9 step 2)wt%.

3.5 Film Thickness Measurement

3.5.1 Gravimetric method

In this method is used a sensitive electronic balance is used (Precisa-Swiss) which is sensitive (10^{-4} g), By the equation, the thin film thickness can be calculated:

$$t = \frac{m}{4\pi\rho . h^2} \quad \text{.........................(3-1)}$$

Where:

t: The thickness (nm).

m: is the mass evaporated (mass difference in the pellet) (g).

p: is the material density (Zn= 5.67g/cm^3) and (h) is the height from the source (boat) to the substrate (slides) (h= 18 cm) [105]. The resulting errors in calculating the thickness of the materials in this method are due to the following reasons:

a- Consider the density of the thin film equal to the density of the material in size.

b- Loss part of the material during deposition by volatilization or recoil from the surface of the substrate, therefore, it is preferable to calculate an error ratio (2%) of the weight of the material to ensure the required thickness.

3.5.2 Optical Interference Method

This method is standard and very accurate in measuring the thickness of thin films. (Tolansky, 1948; Wiener, 1887) were the first to use this method though the interference system in figure (3-3) .the thickness of the thin film can be calculated according to the following equation:-

$T=\frac{\lambda}{2}\times\frac{\Delta x}{x}$……………………….(3-2)

Where:

XΔ: Fringe of width.

X: the distance between the two consecutive directions.

λ: wavelength of light used (sodium 589.3nm).

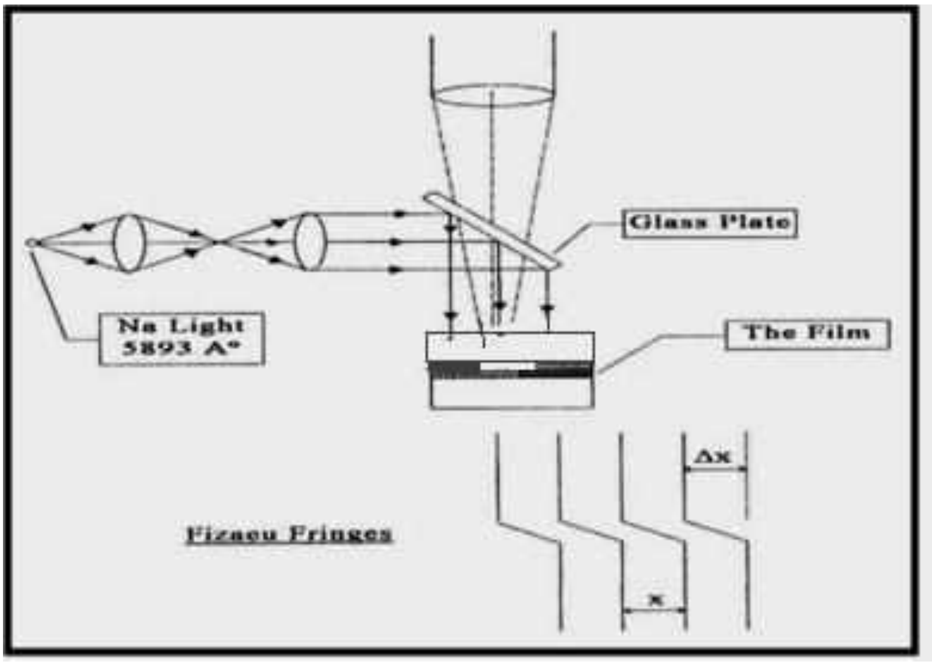

Figure (3-3) Optical interference fringes method.

3.6 Characterization of ZnO films

The Characteristic measurements of this technique is used to investigate the thickness, the structural features of the films were X-ray diffraction (XRD) and atomic force microscope (AFM). The optical features of the films were investigated by transmission through UV-Vis absorption spectroscopy.

3.7 Investigation the Structural of Prepared Films by (XRD) Technique

The structure of the prepared thin films is defined through studying X-ray diffraction output. The other variables of the thin films which they are examined through X-ray are:

1- The type of structure (crystalline or amorphous).

2- The appearance of doping with Sn.

3- The annealing effects.

4- Calculating the lattice constant and the average volume of the crystal.

(x-rat instrument)

(XRD 600 SHIMADZU JAPAN)

(X-ray) diffraction technique type (Shimadzu XRD-6000) that had been used to investigation (ZnO) thin film crystal structure and crystallite size as well as knowledge of the addition of Tin impurities (3 to 9 step2)wt% with thickness (200 nm) under the following conditions:-

X-Ray Tube: (CuKα) radiation of wavelength (1.541A^o), Current (20 mA), Voltage (40kV), Range (20000) counts/s, 10-80 (deg); Scan Mode: continuous scan, scanning speed: (5 deg /min).

3.8 Atomic Force Microscope Measurements (AFM)

(AFM) technique is used to study the topography of the sample (SPM-AA3000 contact mode spectrometer, Angstrom) to obtain two-dimensional and three-dimensional images that describe the surface in terms of roughness and grain size that have high resolution values.

3.9 Optical Measurements

The measurement of the transmission (T) and absorption (A) spectrum of the thin films on the glass substrate using a spectrometer (UV-Visible) (1800 Spectra Photometer), the transmission and absorption values are measured as a function of incident wavelength (λ) within the wavelength range (300-1100)nm, as well as finding optical constants (Absorption coefficient, optical energy gap) calculated from equations (2-10), (2-13), (2-15) and (2-16).

Part two

Image Processing Procedure

3.10 Introduction

The second section included an explanation of how to prepared, acquisition and analysis images and a procedure of many enhancements on an image. there are many packages (software) that deal with image process and (CVIPtools) is one of them. This software has been used because of its maximal applications which include everything we desire to complete this work. Digital images of thin films are studied in several stages as shown in this section and could be summarized in the following diagram.

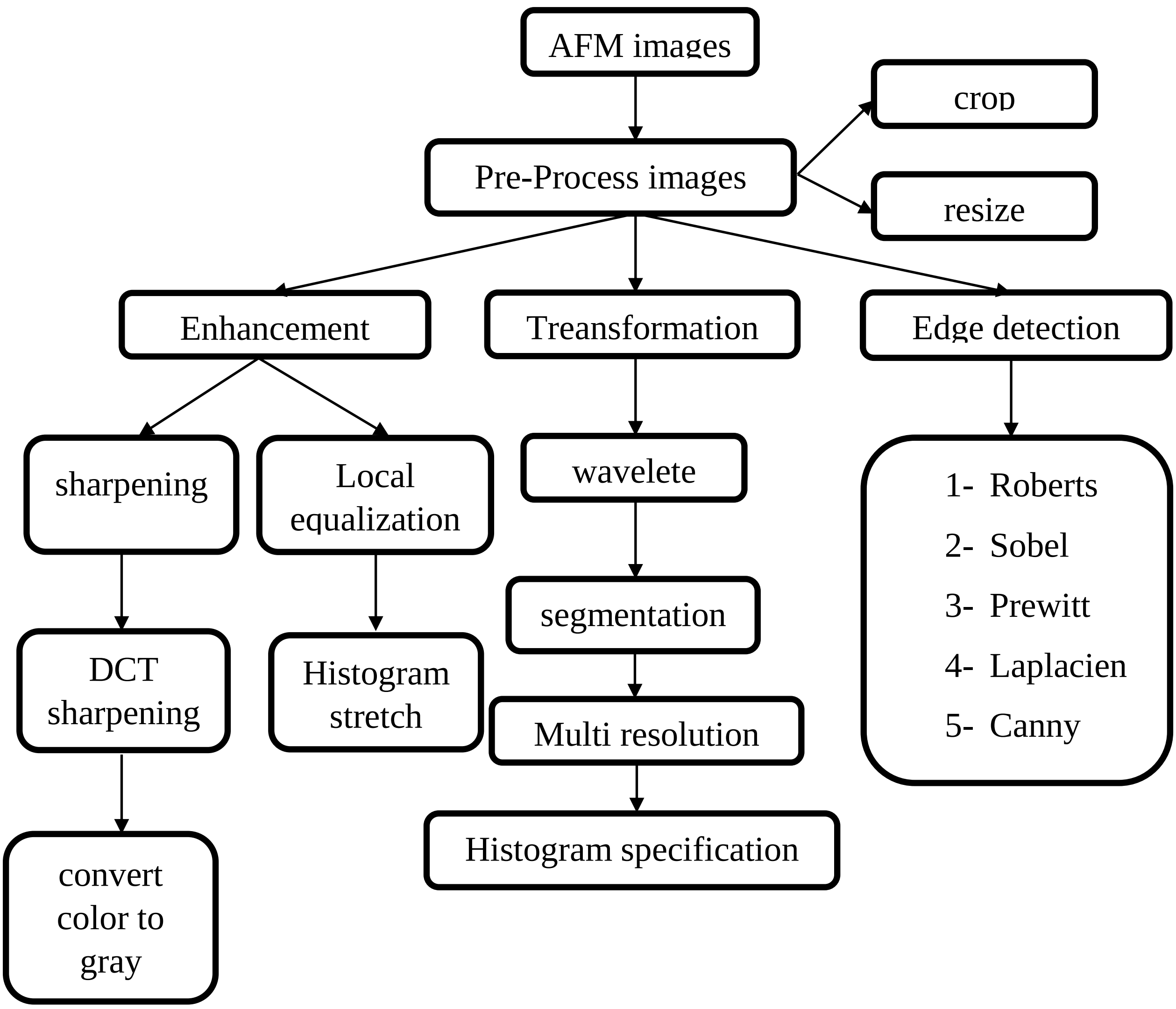

Figure (3-4) Diagram for image processing procedure.

After collecting the (AFM) images, the following steps and methods were used to manipulate the digital images:

3.11 Pre – process:

The pre-process steps which were applied to the images could be summarized in these steps:

1- Crop the digital images of prepared thin films from upper left corner to (10x100) pixels with a width and height according to pixels of images.
2- Resize the resulting images from the crop with width and height (400x400) pixels using zero order hold.

3.12 Enhancement

The following steps explain the procedure that had been applied in this research. The first step was using histogram contrast then local equalization. After that the listed application applied to get the enhanced images.

1- Histogram contrast application followed by histogram stretch.
2- Starting again with the original image and using histogram contrast then histogram specification.
3- Applying sharpening techniques then DCT sharpening.
4- Cropped and resized digital images.
5- Applying histogram contrast then local equalization.
6- Applying histogram contrast then histogram stretch.
7- Using digital images (step 5) to convert from color to gray.

3.13 Transformation

1- Using the orginal digital images to transform by wavelet.
2- Analyzed the output images by using multiresolution segmentation.

3- Cropped the digital images with a width and height (400x400) to exclude the undesired parts of the gained images.
4- Using histogram contrast then histogram specification.

3.14 Edge detection

The images are analyzed with edge/line detection by using the following parameters sequentially:

- Roberts
- Sobel
- Prewitt
- Laplacian
- Canny

1- Enhancement digital images that resulting from the step using histogram contrast after applying the Laplacian detection then histogram stretch.
2- Using histogram contrast then histogram specification.

Chapter Four

Results And Discussion

Results and discussions

4.1 Introduction

This chapter includes presentation and discussion of the results achieved through pure and doped (ZnO) thin films prepared by thermal evaporation with thickness (200±10) nm. The study of the structure and optical properties for ZnO thin films was determined. The results will be discussed widely in this chapter.

4.2 Pure ZnO thin films

The first step of preparing the thin films,is deposit the (Zn) on glass substrate by thermal evaporation. The next step is oxidation the thin films to have (ZnO) thin films.

4.2.1 Structural Properties

- **X-Ray Diffraction(XRD)**

Figure (4-1) shows the X-ray diffraction for pure ZnO thin film at thicknesses (200±10)nm prepared by simple evaporation technique. The structure appears to be polycrystalline of (hexagonal Wurtzite). This figure illustrated the structural growth with crystal directions (100), (002) and (101) at the angles (2θ) (31.69), (34.36) and (36.23) respectively [106,107]. The preferred orientation is (100) with respect to the deposition method.

The results gained from (XRD) matches the (JCPDS) cards (joint committee on powder diffraction standards) for d_{hkl} and diffractions angles as shown in table (4-1). (JCPDS) cards was (00-036-145).

The crystal growth of this thin films in that direction refers to (van der drift) model (Survival of the fastest). This model called survival of the fastest, whereas the nucleation takes many directions at first steps of growth, then they will compete between these direction of grows. The fastest in growth will domain the process and let the other directions of growth to eliminate, and that results matches with [108]. The main domain of crystal direction is

(100). The increase in the values of the intensity indicates the increasing of crystallization at that direction.

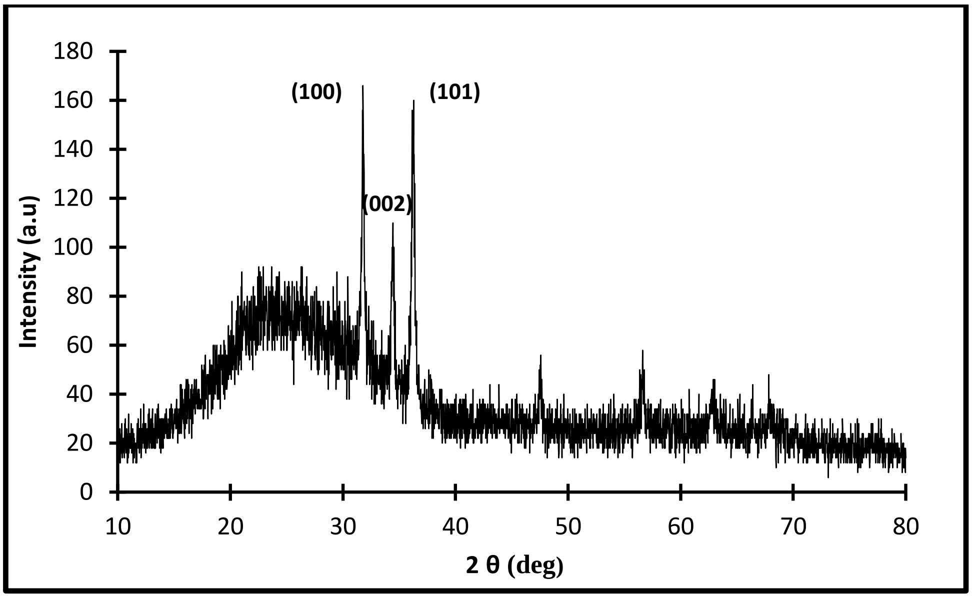

Figure (4-1) X-ray diffraction for ZnO thin film.

The X-ray diffraction charts will gives many variables that presents in table (4-1). The values of the distance between the atomic levels (d_{hkl}) and the diffraction angles (2θ), which corresponding to the peaks of the x-ray diagram. The displacement of the sits of peaks is due to the preparation conditions.

Table (4-1): XRD and JCPDS for ZnO thin films.[00-036-145]

2Θ(deg) (JCPDS)	2Θ(deg) observed	d(A^o) (JCPDS)	d(A^o) observed	hkl planes (JCPDS)
36.2521	36.23	2.4759	2.47	101
34.4211	34.36	2.6033	2.60	002
31.7694	31.69	2.8143	2.82	100

The other parameters that been studied through X-ray diffraction are, full width at half maximum (FWHM), crystallite size (D) and dislocation density (δ), and that agree with equations (2-3) and (2-4). These results were listed in table (4-2).

Table (4-2): X-ray diffraction parameters for prepared ZnO thin films.

FWHM (deg)	C.S (nm)	δ x10^{14} lines .m^{-2}
0.27	29.9	11.3

- **The Atomic Force Microscope (AFM)**

The atomic force microscopy is used to determine the morphology of the prepared thin films. The other reason for using (AFM) are to shows the effect of doping, average grain size, distribution, and surface roughness on the properties of thin films and to obtain high-resolution images, as shown in figure (4-2).

The most common observations on the ZnO thin films surface are the homogeneity and well distribution on the substrate. The very low peaks that move upwards in spherical or hemispherical shape separated by Nano scale distances indicate that particle walls are very small. The image shows the good surface uniformity and without cracks or gaps. These results of the good uniformity makes this thin films a good choice to be used in solar cells and semiconductors devices applications.

Figure (4-2) illustrates AFM images, the survey of the surface of ZnO thin films prepared at thickness (200) nm in (3D).

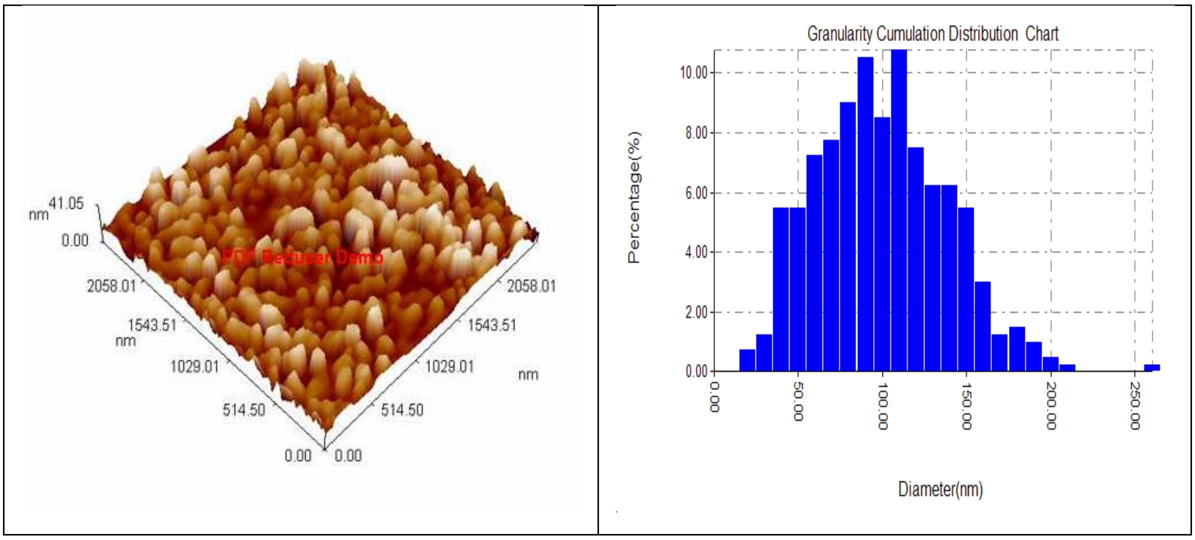

Figure (4-2) AFM images of ZnO thin film.

Table (4-3) shows the average grain size, distribution and the surface roughness based on the root mean square (RMS).

Table (4-3): average grain size, root mean square and roughness density.

Average grain size (nm)	(RMS) (nm)	Roughness density (nm)
94.82	7.38	6.04

4.3 Doping ZnO thin films with Sn

Thin films was doped (3 to 9 step 2) wt% with Tin, after Measurements were done for pure thin films. Doping was done by thermal evaporation followed by thermal diffusion at (413k) for (one hour). We will show the results that obtained from the measurements:

4.3.1 Structural Properties

- **X-Ray Diffraction(XRD)**

Figures (4-3) illustrate X-ray diffraction of doping Zinc Oxide thin films with Tin at different percentages. This figure shows the peaks in the pattern of (100), (002) and (101). The XRD results indicated all films are (polycrystalline) structure of (hexagonal Wurtzite) agree with [34, 40] comparing with (JCPDS) cards.

Table (4-5) shows the variation of intensity is depend on the rate of the Sn impurities. The preferred orientation direction is depend on Sn content, the value of pure ZnO films I(100) is a high intensity compared to both I(002) and I(101). At doping (3%) the value of I(100) is reducing until we reach (7%) compared to pure ZnO. the value of I(101) for doping (5%) continues to increase and the domain orientation become (101). At doping (7%) the value of I(002) is increased compared to (5%) and the value of I(101) decrease, therefore, the preferred orientation is (002) agree with researcher[34]. At doping (9%) the value of (002) decrease compared to (7%) while I(100) increased then the value of I(002), I(101), therefore again a preferred orientation along I(100) similar to pure ZnO. It is clearly noticed that was a peak appeared for Sn at (7%) and this peak increased at (9%). These results match the (JCPDS) cards (00-019-1365) for Sn. The prepared thin films have the same hexagonal structure for all samples without any other patterns.

Table (4-4) illustrated the (d_{hkl}) and (2θ) for the measured samples and the corresponding data from (JCPDS) cards. The results were matched with a little displacement for the doped thin films than the undoped . This result may be explained that Sn can easily substitute for Zn due to their similar ionic radii (0.074 nm for Zn^{+2} and 0.069 nm for Sn^{+4}) resulting in a small latticE distortion and great more electron vacancies[44].

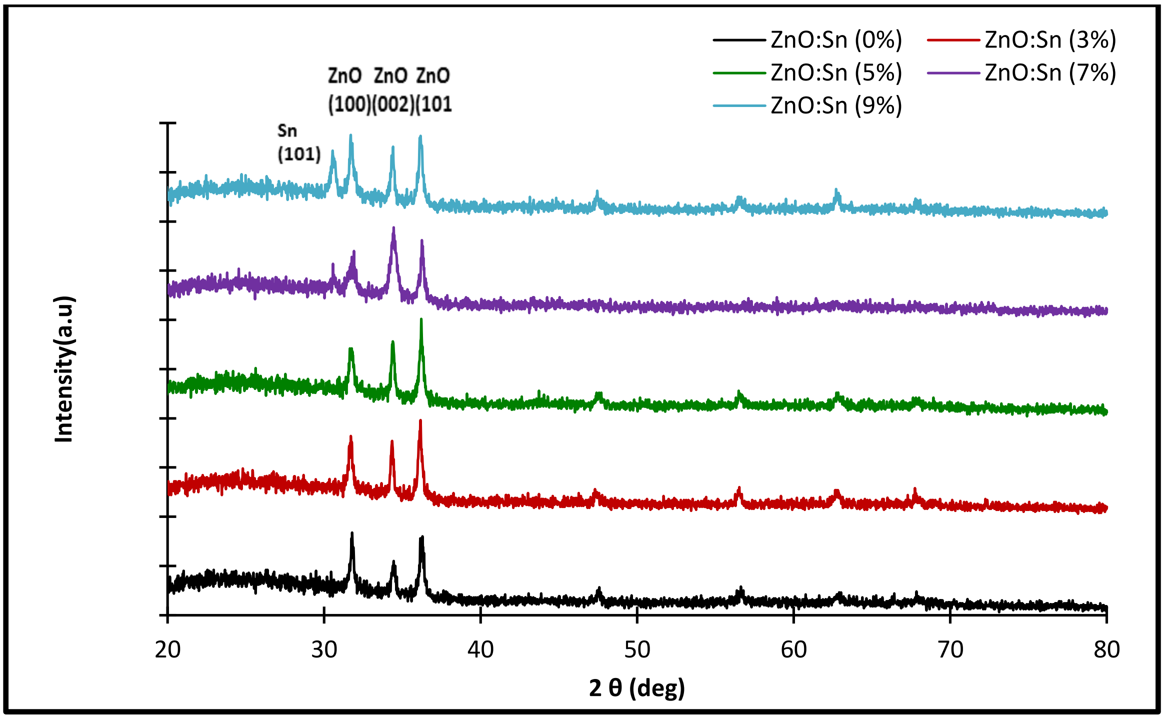

Figure (4-3) X-ray diffraction for pure and doped ZnO:Sn thin films with different doping (3 to 9 step 2)wt%.

Table (4-4) indicates the comparison of X-ray diffraction results. The values of the distance between the atomic levels (d_{hkl}) of the diffraction angles and their surfaces 2θ corresponding to the sites of the peaks of the thin films prepared for the distinctive models correspond to the values in [JCPDS] numbered [00-036-145].

Table (4-4): XRD and JCDPS for pure and doped ZnO:Sn [00-036-145].

Doping Ratio	2Θ(deg) (JCPDS)	2Θ(deg) observed	d(A^o) (JCPDS)	d(A^o) observed	hkl (JCPDS)
ZnO:Sn (0%)	36.2521	36.2373	2.4759	2.4769	101
	34.4211	34.4309	2.6033	2.6026	002
	31.7694	31.8029	2.8143	2.8114	100
ZnO:Sn (3%)	36.2521	36.1414	2.4759	2.48331	101
	34.4211	34.3494	2.6033	2.60866	002
	31.7694	31.7009	2.8143	2.82030	100
ZnO:Sn (5%)	36.2521	36.1248	2.4759	2.47845	101
	34.4211	34.4026	2.6033	2.60474	002
	31.7694	31.7524	2.8143	2.81584	100
ZnO:Sn (7%)	36.2521	36.2711	2.4759	2.47473	101
	34.4211	34.4464	2.6033	2.60153	002
	31.7694	31.7945	2.8143	2.81221	100
ZnO:Sn (9%)	36.2521	36.1703	2.4759	2.48140	101
	34.4211	34.3761	2.6033	2.60669	002
	31.7694	31.7454	2.8143	2.81644	100

Table (4-5) illustrate the variation of integrated intensity of (100), (002) and (101) different peaks

Table (4-6) indicates the diffraction angle (2θ), full width at half maximum (FWHM) and crystalline size (C.S) was obtained by x-ray diffraction for all peaks.

Table (4-5) The variation of intensity of XRD doping thin films.

Sn content %	$I_{(100)}$	$I_{(002)}$	$I_{(101)}$	Domain	Sn $I_{(101)}$
ZnO:Sn (o%)	166	110	156	100	_
ZnO:Sn (3%)	164	154	194	101	_
ZnO:Sn (5%)	140	150	202	101	_
ZnO:Sn (7%)	140	188	162	002	114
ZnO:Sn (9%)	176	152	174	100	144

Table (4-6) X-ray diffraction of the peaks of ZnO thin films.

Sample	FWHM (deg)	C.S (nm)	$\delta * 10^{14}$ (line.m^{-2})
ZnO:Sn (0%)	0.27	29.91	11.3
ZnO:Sn (3%)	0.27	31.2	11.09
ZnO:Sn (5%)	0.27	30.4	11.5
ZnO:Sn(7%)	0.28	29.3	11.7
ZnO:Sn(9%)	0.44	19.1	30.1

The crystal size was decreased with increasing impurities and increasing of dislocation (δ) [109, 110] disagree with [34, 40, 42, 46]. When the Sn is insert in to lattice ZnO it impedes growth of grains causing a decrease in a crystalline size for thin films. Increase in dislocation due to saturation of substitution sites, forcing the ions (Sn) to occupy the interstitial sites [44]. Crystallization in the direction (101) increase with doping (3&5)% indicate improvement thin films at (5%) have good Crystallization compared with other percentage, this result was reflected in other properties. Degradation of other thin films (7&9)% because there is a great value for percent doping with Sn beyond it cause deterioration of the properties of thin films [34]. The dislocation is an indication on the crystals quality and Crystallization Level.

The relation between dislocations and square volume is ($\delta \propto C.S^{-2}$). and through table (4-6) appears an increasing of layers with increasing impurities.

- **The Atomic Force Microscope (AFM)**

Table (4-7) indicate the possibility of the effect doping (5%) on the properties of ZnO thin films.it was measured one sample doping (5%) figure (4-4) show the (3D) AFM image and the result of measuring shown in the table (4-7).

Table (4-7) average grain size, (RMS) and roughness with doping (5%).

Average grain size (nm)	Root mean square (RMS) (nm)	Roughness density (nm)
51.27	5.21	4.4

Figure (4-4) illustrate AFM image, the survey of the surface of thin films prepared at doping (5%) in (3D).

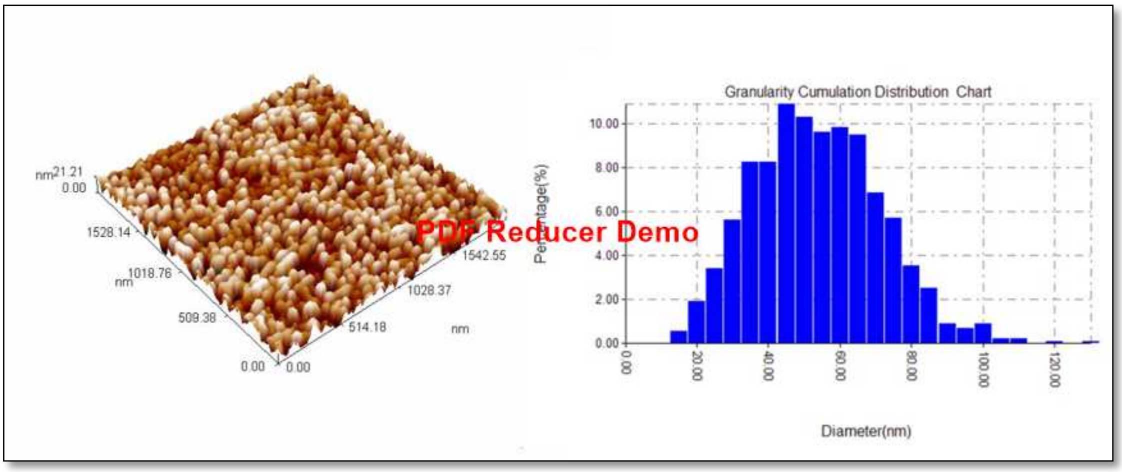

Figure (4-4) AFM image of thin film with doping ZnO:Sn (5%).

4.3.2 Optical properties

Figure (4-5) illustrated the transmittance spectra with respect to wavelength for ZnO:Sn thin films. The figure shows the transmittance appear at cut off wave length that separate it with absorption spectra, then the transmittance increase with increasing wavelength for the electromagnetic wave.The transmittance of ZnO thin films change with increasing doping percentages. This behavior happened because of the creation of local states, gained from the impurities, at energy gap between valance and conduction bands, Another reason is the creation of crystal defects tends to increase photon scattering, which agrees with [38, 40, 46] but disagree with [37, 43, 44]. Another reason for the change in the transmittance is due to increase in dislocation (δ) with increase doping. The transmittance increase at (5%) due to reduction of the voids in the sample and improvement of the homogeneous structure with uniformly distribution particles (good incorporation of the dopant in the ZnO lattice structure), this corresponds to the structure properties observed decrease the dislocation density at (5%).

It is also shown from the figure that the highest transmittance was for Zinc Oxide thin films, reaching Its transmittance is about (90%) of the wavelengths within the infrared region (800-900) nm and this is the least absorption, which matches [37].the change in the transmittance is due to increase in dislocation (δ) with increase doping. The previous behavior makes the ability to use the properties of ZnO thin film as transparent material for vehicles and airplanes windows, also as IR detector shields.

The transmittion and absorption spectrum was measured as a function of wavelength in the range (350-950) nm. Figure (4-5) illustrated transmittance spectra for doping Zinc Oxide thin films with different doping percentages.

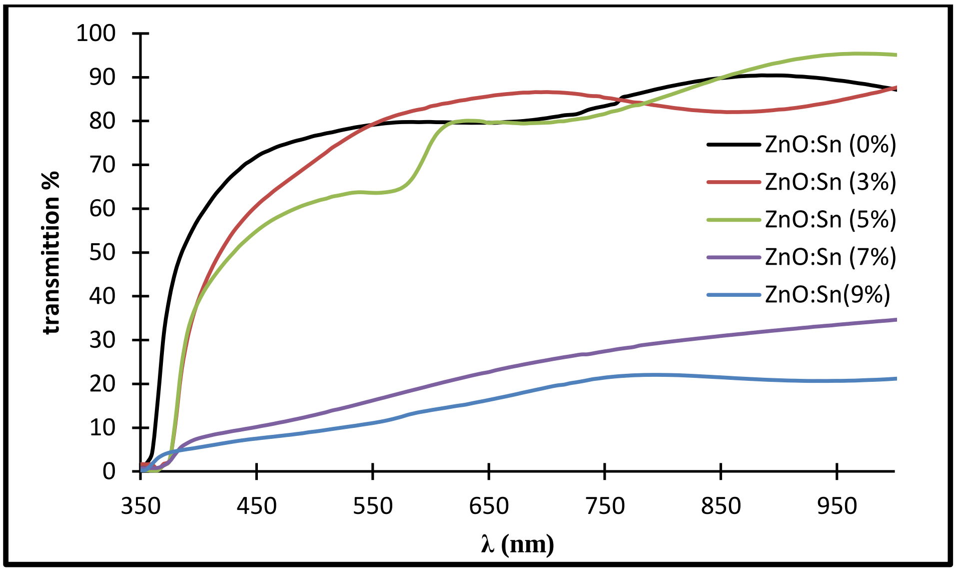

Figure (4-5) transmittance spectra for pure and doped ZnO thin films as a function of wavelength.

Figure (4-6) illustrated the increasing of absorption curve with increasing doping percentages. The reason for this behavior is the increasing of local states at forbidden region. This local states play as a step to transmit the absorbed electrons that have less energy than energy gap.

Doping thin films were recorded with a precipitation rate of (9)% in the study that showed higher absorption compared to the absorption of the thin films prepared from pure and doping.

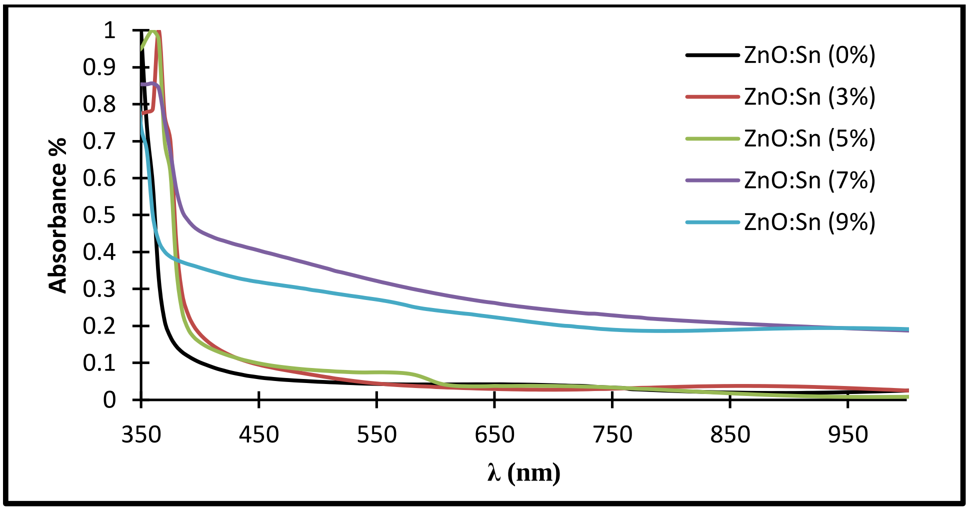

Figure (4-6) absorbance spectrum for pure and doped ZnO thin films as a function of wavelength.

Figure (4-7) illustrates the changes in the absorption coefficient as a function of the photon energy.

Figure (4-7) illustrated the absorption coefficient behaves in a similar to the absorbance spectrum. The absorption coefficient generally begins a gradual increase as photon energy increases at ranges (2.2-2.9) eV for doping thin films. By increasing doping rate the absorption coefficient increases at low photonic energy. The higher value of absorption coefficient is greater than (10^4) cm^{-1}, indicate to direct electronic transitions between the valence and conduction bands at these energies. The absorption coefficient has a maximum value at ($11x10^4$)cm^{-1}. These results obey the equation (2-15).

At the energy range (2.85-3.3) eV, the absorption coefficient remains almost constant. The stability of absorption values at that range of energies, because they are the most effective range to transmit the free direct electrons, then it will appear as almost constant absorption coefficients.

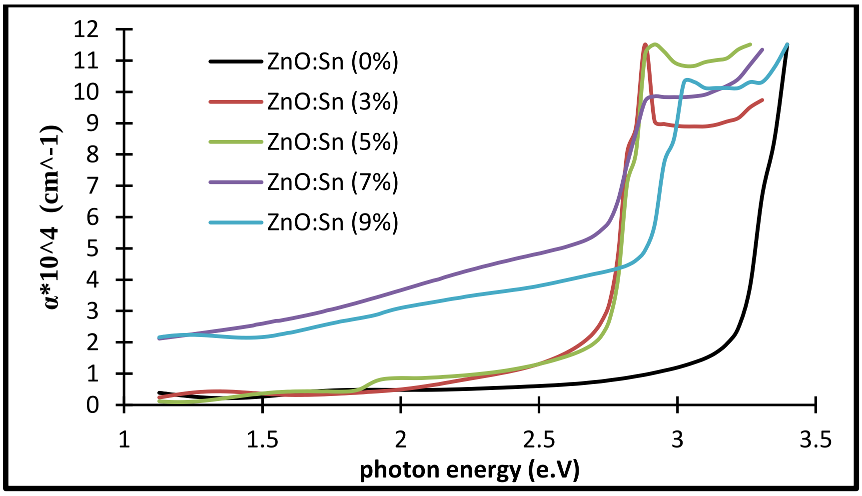

Figure (4-7) absorption coefficient for ZnO:Sn thin films with different percentages.

The optical energy gap of the thin films material is the standard path to use these materials in industries, such as solar cells, photovoltaic cells, optical diodes, electromagnetic radiation detectors، Figure (4-7) shows that the absorption coefficient values for all doped thin films are ($\alpha > 10^4$) cm^{-1} indicate that the electronic transition is a direct type. figures (4-8) illustrated the relation between (hν) and $(\alpha h\nu)^2$ and the modification process to achieve the intercept with X-axis. The achieved opinion is at the visible electromagnetic waves the relation is linear. The optical energy gap for doped ZnO thin films decrease with increase impurities and reach its lowest value at (7%). The energy gap at this rate is (2.72) eV mean decrease about (0.53) eV as shown in table (4-8). The appropriate reason for this contradiction is the donor density of state which made by Sn impurities, it raised the Fermi level. The raise of Fermi level makes the absorption decrease to (2.72 eV) for (7%) dopant, which agrees with [33, 40, 42]. The doping at (3, 5, 7)% makes an increase in absorption region for visible and the absorption edge tends to low energy region.The doping with 9% shows an increasing for energy gap, the widened of optical energy gap attributed to (Burstein-moss shift) , and that matches with [34, 38, 37, 39, 43, 46,38]. The other reason is the creation of crystal defects inside the crystal structure. Table (4-8) illustrates the values of energy gap. Figure (4-8) shows changes of energy gap with different doping.

Table (4-8) illustrate the change of energy gap with different doping.

sample	Energy gap (e.V)
ZnO:Sn (0%)	3.24
ZnO:Sn (3%)	3.21
ZnO:Sn (5%)	3.2
ZnO:Sn (7%)	2.72
ZnO:Sn (9%)	2.88

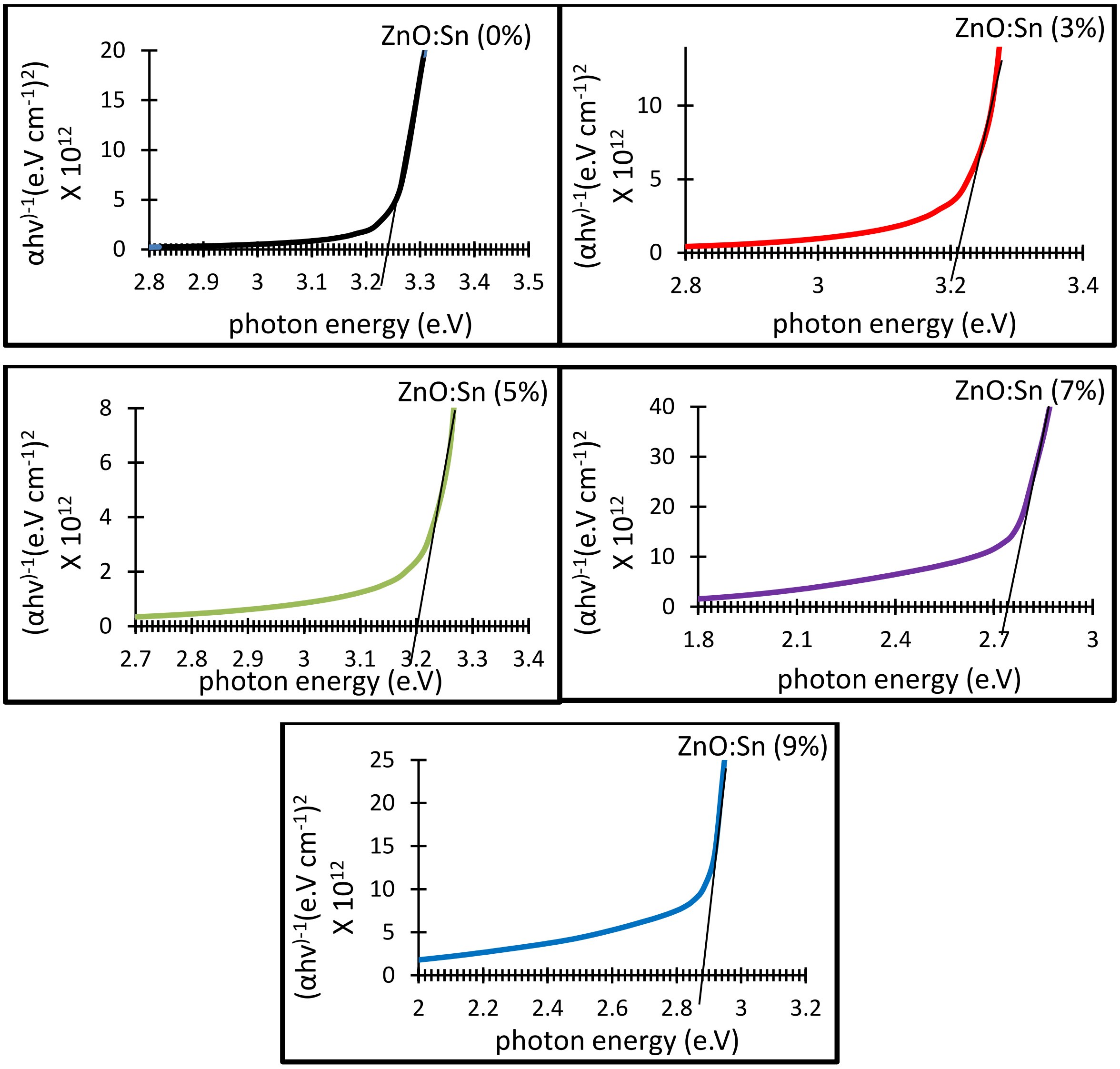

Figure (4-8) energy gap for pure and doped ZnO thin films.

4.4 Annealing (ZnO:Sn) thin films

The annealing process was applied to ZnO:Sn thin films at (473K) for one hour. The results at this stage will be illustrated consequently.

4.4.1 Structural Properties

- **X-Ray Diffraction(XRD)**

Figures (4-9) illustrate X-ray diffraction of doping Zinc Oxide thin films after annealing. Comparing the results between (XRD) and (JCDPS). Table (4-9) shows the comparing values. This behavior gained from annealing process which makes the atoms with bigger energies and reorders the structure.

The reason behind reduce the peaks, except the domain one, is the reorder process done with the domain direction. So the peak of Sn disappeared after annealing.

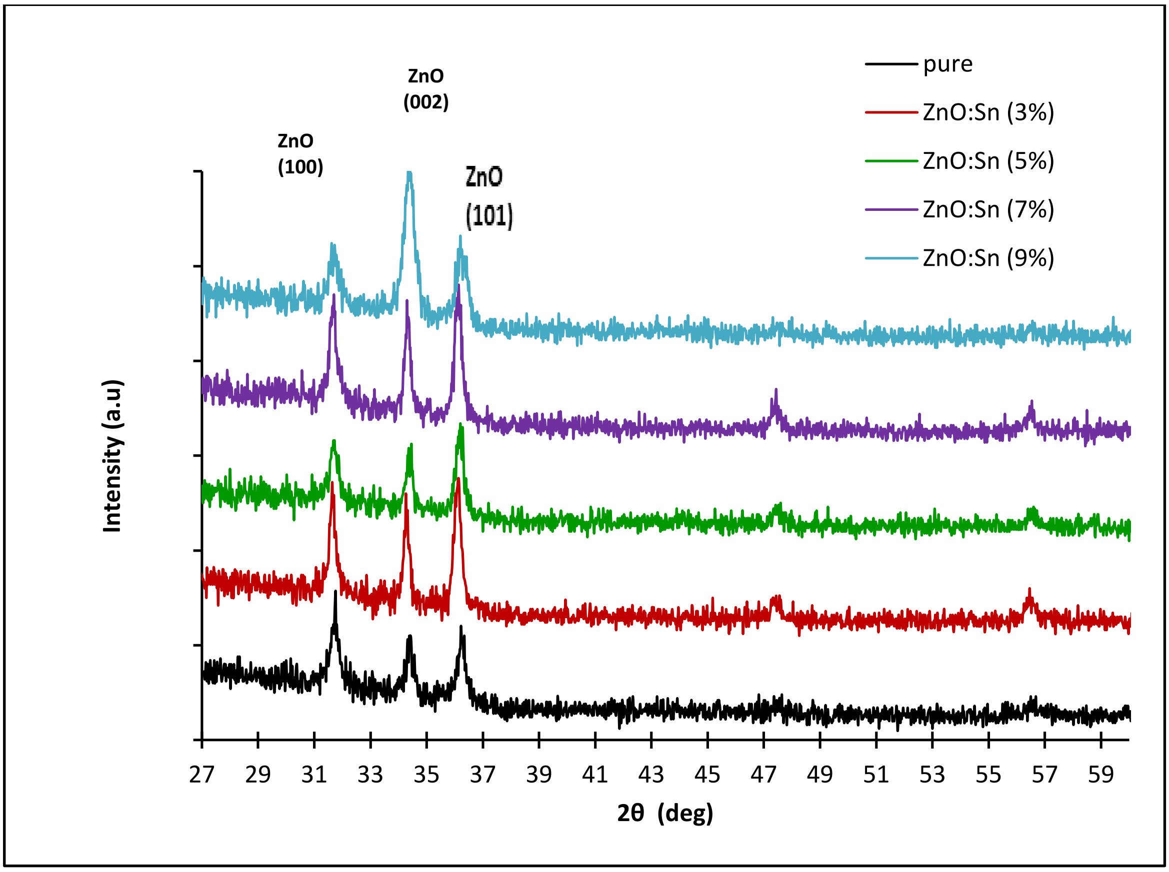

Figure(4-9) X-ray diffraction for ZnO thin films after annealing.

Figure (4-9) illustrated the annealing effects on the domain peak which make it decrease the intensity of peaks due to increase the defects and irregularity of thin films . Table (4-9) indicate the comparison the result of X-ray diffraction, that the values of the distance between the atomic levels (d_{hkl}) of the diffraction angles and their surfaces (2θ) corresponding to the sites of the peaks of the thin films prepared for the distinctive models correspond to the values in [JCDPS] numbered [00-036-145].

Table (4-9) XRD & for JCDPS pure & doped ZnO with Tin [00-036-145]

Doping of ZnO thin films	2Ө(deg) (JCDPS)	2Ө(deg) observed	d(°A) (JCDPS)	d(°A) observed	hkl (JCDPS)
ZnO:Sn (0%)	36.2521 34.4211 31.7694	36.25 34.40 31.75	2.4759 2.6033 2.8143	2.476 2.604 2.815	101 002 100
ZnO:Sn (3%)	36.2521 34.4211 31.7694	36.10 34.29 31.66	2.4759 2.6033 2.8143	2.485 2.612 2.823	101 002 100
ZnO:Sn (5%)	36.2521 34.4211 31.7694	36.18 34.39 31.71	2.4759 2.6033 2.8143	2.480 2.605 2.819	101 002 100
ZnO:Sn (7%)	36.2521 34.4211 31.7694	36.12 34.60 31.68	2.4759 2.6033 2.8143	2.484 2.609 2.821	101 002 100
ZnO:Sn (9%)	36.2521 34.4211 31.7694	36.28 34.39 31.71	2.4759 2.6033 2.8143	2.474 2.605 2.819	101 002 100

Table (4-10) shows the diffraction angle (2θ), full width at half maximum (FWHM) and crystalline size (C.S) was obtained by x-ray diffraction for for all peaks.

Table (4-10) X-ray diffraction for doped ZnO:Sn thin films after annealing.

Samples	FWHM (deg)	C.S (nm)	$\delta * 10^{14}$ (line.m^{-2})
ZnO (pure)	0.33	24.9	16.1
ZnO:Sn (3%)	0.27	30.6	10.8
ZnO:Sn (5%)	0.31	26.3	15
ZnO:Sn (7%)	0.27	30.7	10.8
ZnO:Sn (9%)	0.45	18.02	30.8

Table (4-10) illustrated decrease in crystalline size this is due to the annealing did not improve the properties of thin films but reduced it which reduced the crystallization and increase irregularity. The (FWHM) curve is wider at the middle based on Scherer equation, dislocation increase, agrees with [39].

- **The Atomic Force Microscope (AFM)**

Figure (4-10) illustrated the (AFM) images for ZnO pure and doped thin films. The influence of doping with Sn and annealing on the surface structure had been studied through analyzing (AFM) images. The results gained are increasing of the average grain size with (3%) then decreasing gradually to (9%). The (RMS) was decreased from (18.4) for pure thin films to (3.9) for doped thin films at (5%). The roughness also decreases from (15.7) for pure thin films to (4.6) for (5%) the behavior of RMS and roughness disagree with [39].

ZnO:Sn (0%)

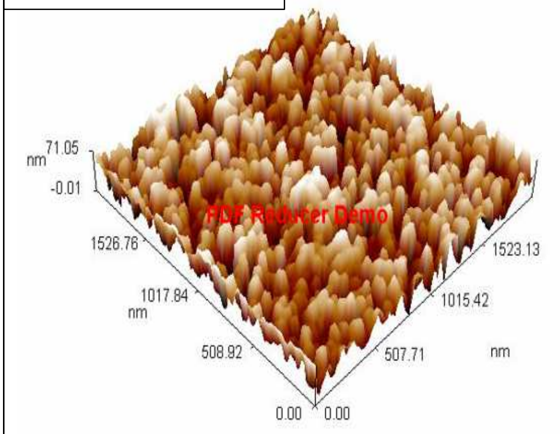

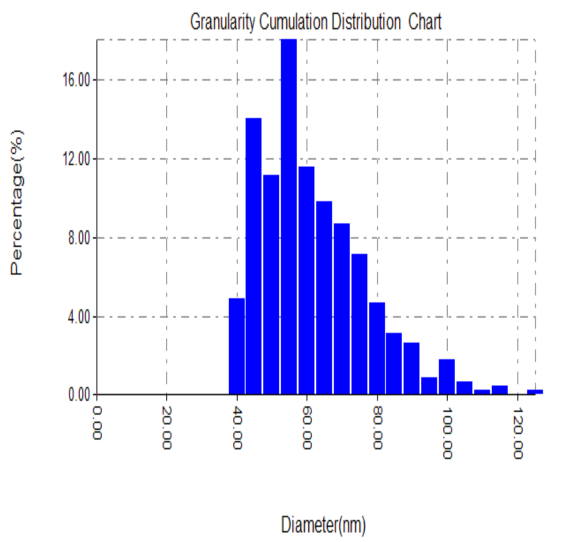

ZnO:Sn (3%)

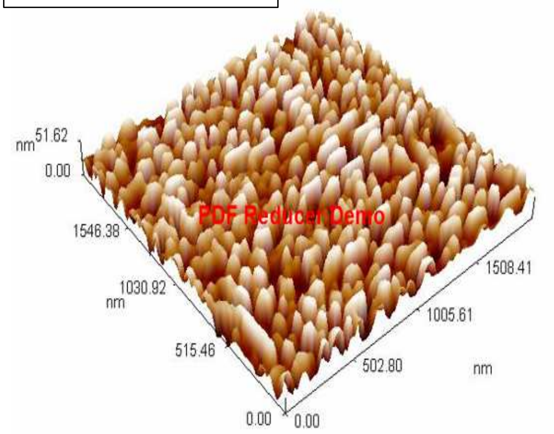

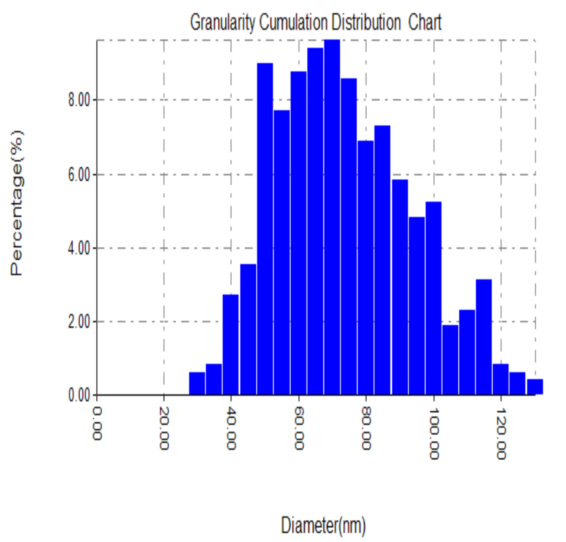

ZnO:Sn (5%)

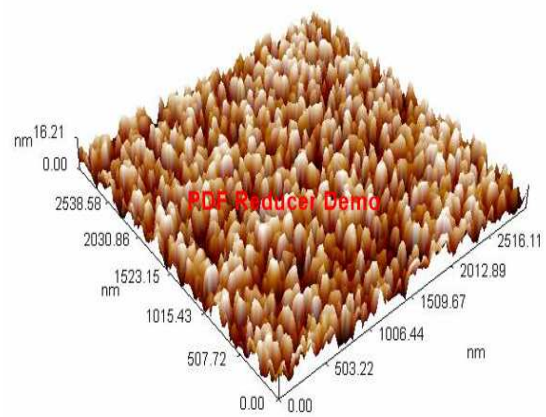

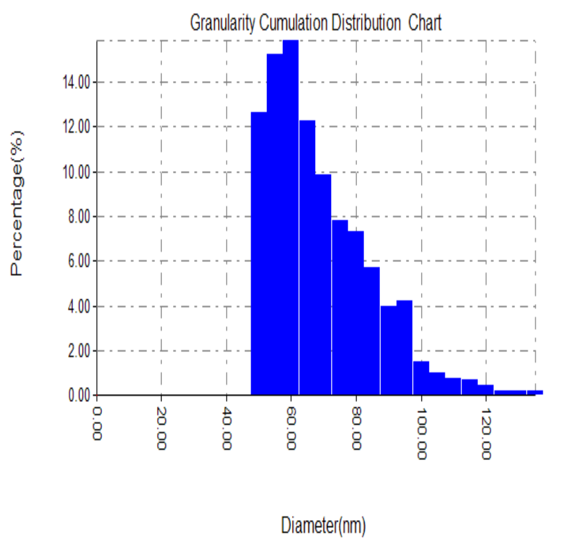

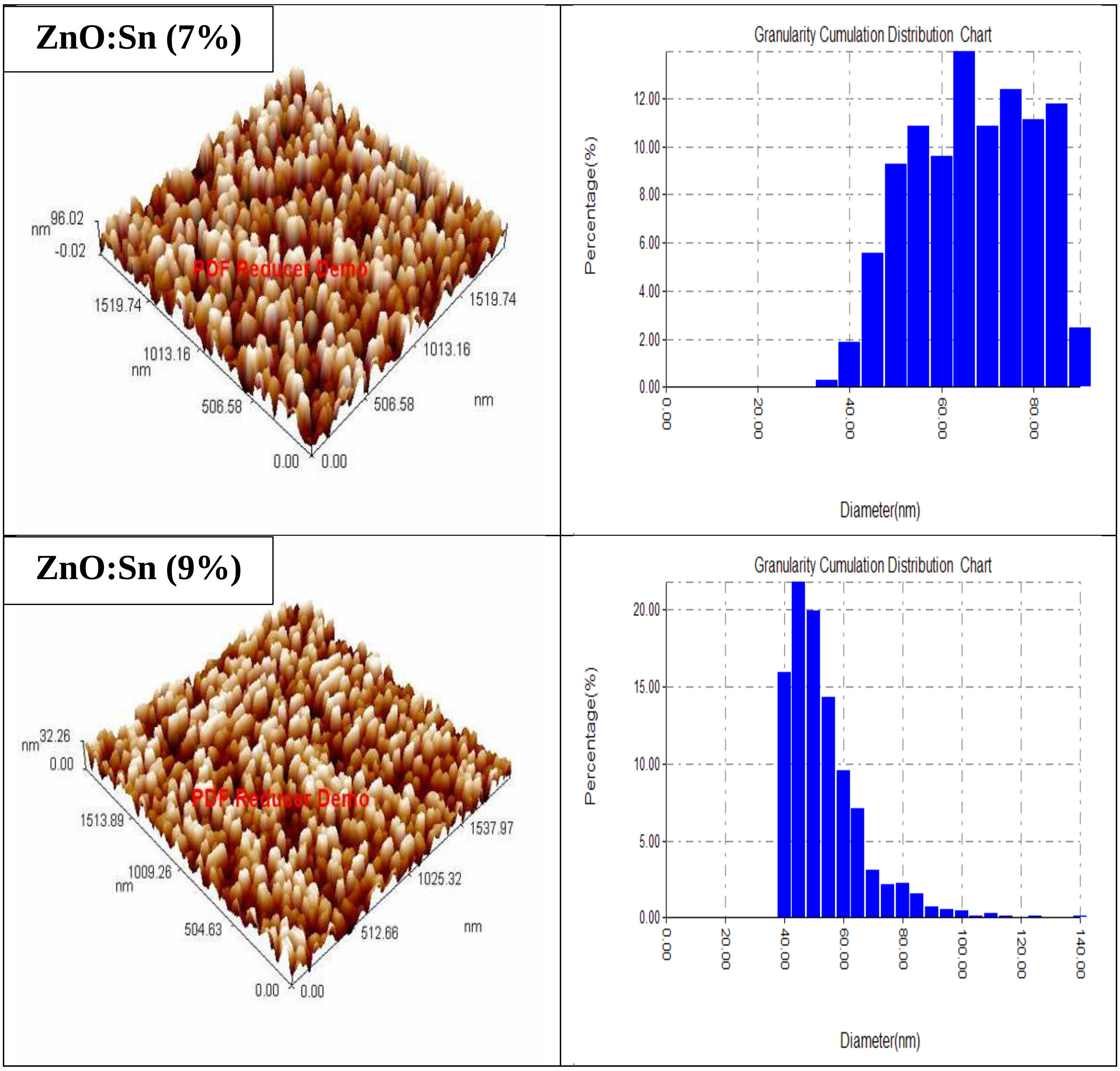

Figure (4-10) AFM images of ZnO:Sn films after annealing.

Table (4-11) indicates the possibility of the effect annealing of thin films on the properties of ZnO thinfilms. Figure (4-11) illustrate changes of roughness as a function of percentage doping.

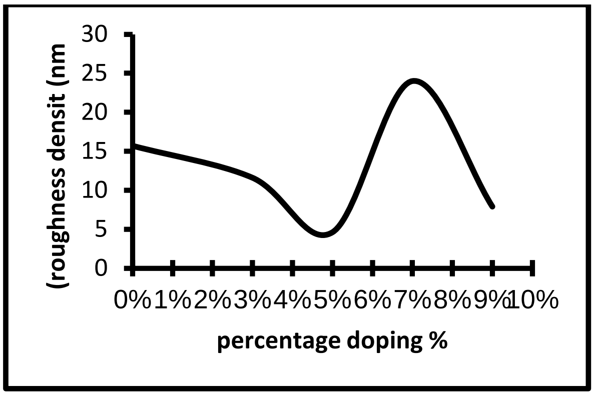

Figure (4-11) roughness density as a function of doping.

Table (4-11) Average grain size, (RMS), and roughness after annealing.

Sample	**Average grain size (nm)**	**Root mean square (RMS) (nm)**	**Roughness density (nm)**
ZnO:Sn (0%)	59.16	18.4	15.7
ZnO:Sn (3%)	71.13	13.6	11.6
ZnO:Sn (5%)	66.48	3.97	4.61
ZnO:Sn (7%)	64.34	27.7	24
ZnO:Sn (9%)	51.26	9.2	7.9

4.4.2 Optical properties

Optical measurements of doped thin films after annealing were performed. Figure (4-12) illustrated the transmittance spectra for ZnO thin films (pure and doped with Sn) and annealed with (473K). This figure shows the transmittance change with increasing wave length. The transmittance values decrease with increasing impurities. The annealing effects on the transmittance and makes ZnO thin films decrease than before annealing. therefore increase the dislocation mean increase irregular. While doped thin films increase in transmittance because the annealing makes the atoms with bigger energies and reorders slightly the structure.

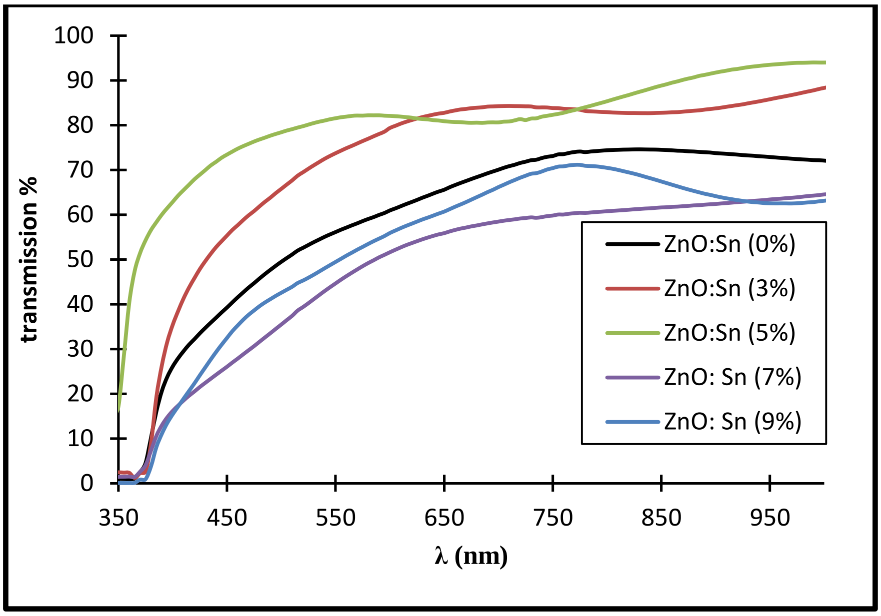

Figure (4-12) transmission spectra forZnO:Sn films after annealing.

Figure (4-13) illustrated the absorption spectra for ZnO pure and doped thin films after annealing with respect to wavelength. This figure shows the increase of absorption with annealing and displacement of optical absorption edge to the region of higher wave length. The absorption spectra for ZnO thin films gradually change with increasing impurities.

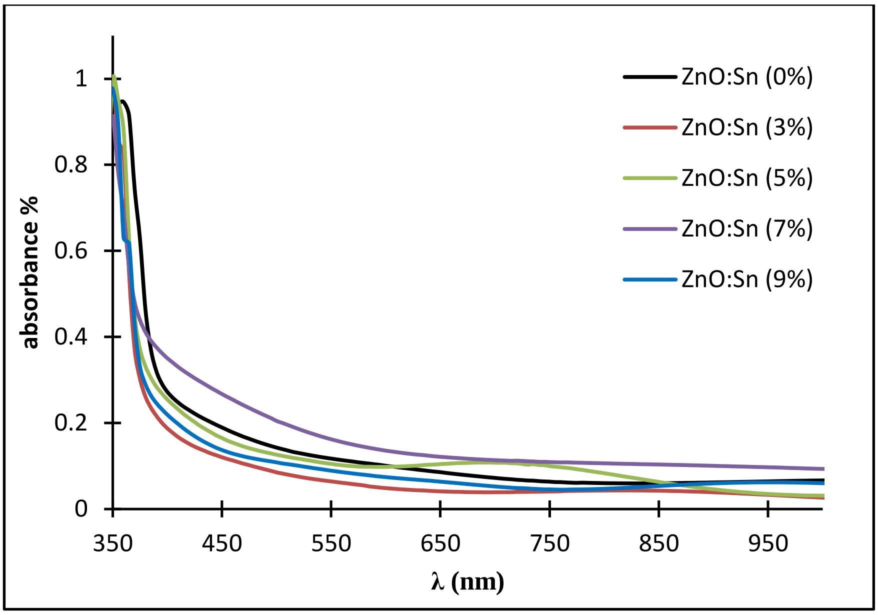

Figure (4-13) absorbance spectra for pure and doped ZnO films after annealing.

The absorption coefficient of doping thin films prepared after annealing from the absorbance spectrum. Figure (4-14) illustrates the changes in the absorption coefficient as a function of the photon energy.

The absorption coefficients appear to be increase gradually with increasing photon energy. The absorption coefficients reduce with increasing impurities. This figure shows that the absorbance coefficient values for pure and doped thin films after annealing is ($\alpha > 10^4$ cm^{-1}) indicate that the electronic transition is of the direct type.

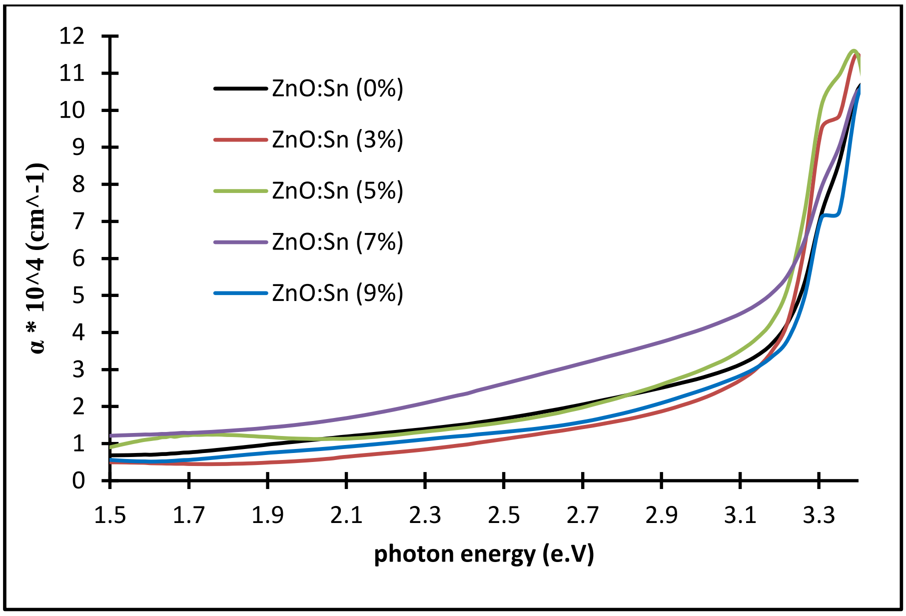

Figure (4-14) Absorption coefficient forZnO:Sn films after annealing.

Figure (4-15) illustrate the changes of energy gap for pure and doped thin films after annealing. That relation for $(\alpha h\nu)^2$ as a function of incident photon energy on ZnO thin films with different doping percentages after annealing, as shown in figure (4-15). The figure shows the decrease of energy gap directly with increasing impurities, agrees with [40] because of the replacement of (Zn^{+2}) by (Sn^{+4}). This process tends to increase of additional density of states which will reduce the energy gap.

Table (4-12) The change of energy gap after annealing.

sample	Energy gap (e.V)
pure	3.21
3%	3.19
5%	3.16
7%	2.7
9%	2.86

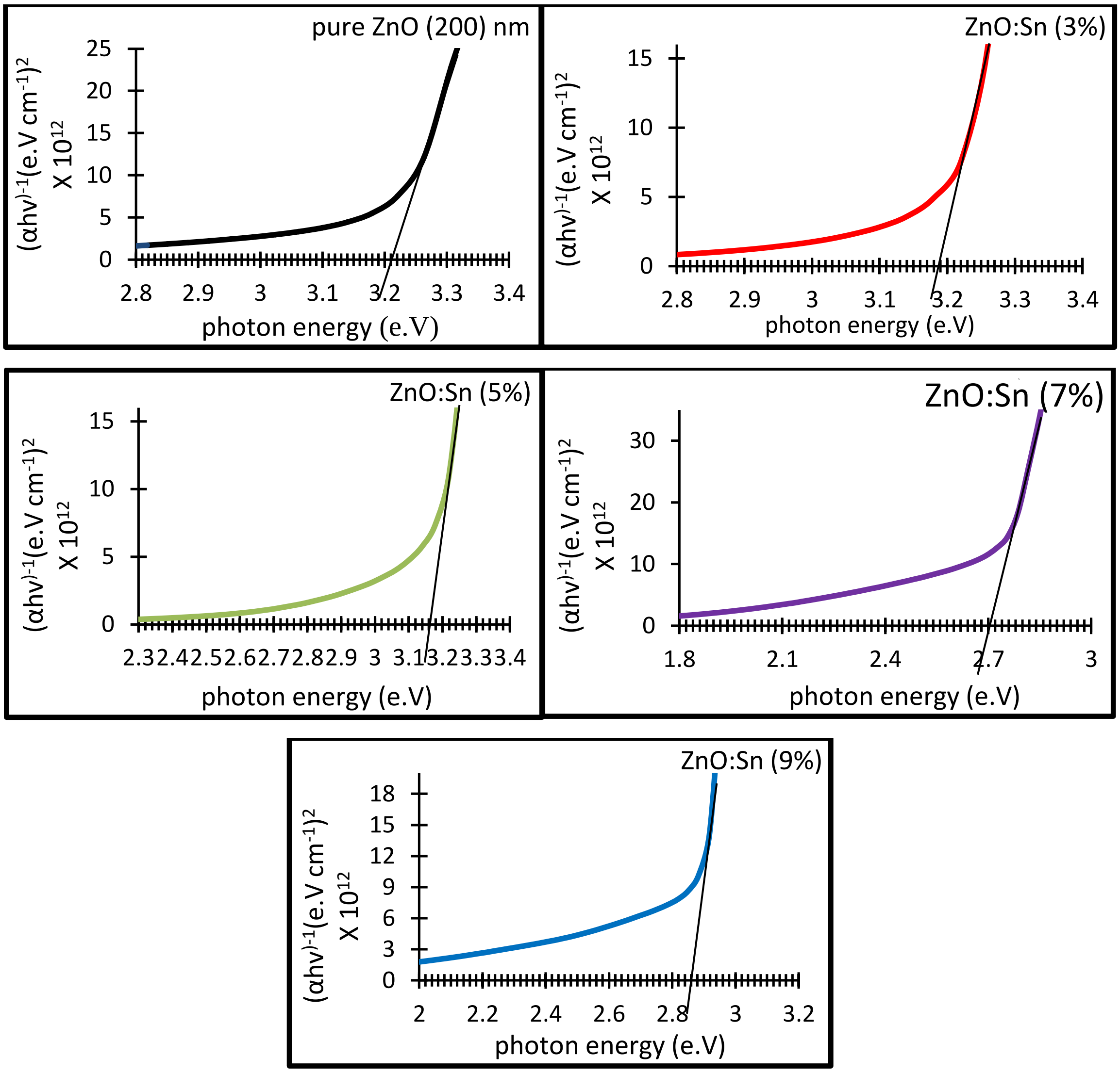

Figure (4-15) Energy gap for ZnO:Sn films after annealing.

Part Two

Image Processing

4.5 Introduction

The current section includes the presentation and discussion of the results of image processing techniques. This technique was applied to AFM images which were taken for pure and doped Zinc Oxide thin films. The diagram of this work consists of, doping, and annealing and their impact on the qualities surfaces of these films. The results that been obtained from structural and optical properties was compared with the results gained from image processing technology that been obtained from AFM.

4.6 Enhancement images for Pure thin films

After the pure thin films were obtained with thickness (200) nm, Figure (4-16) shows the number of digital images captured for the study samples obtained from the (AFM) measurement after the image were cropped then resized to (400x400) pixels.

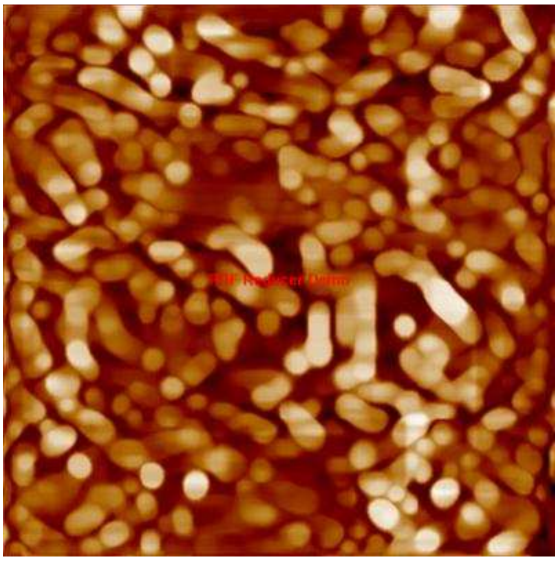

Figure (4-16) AFM image.

From the visual observation of the images shown in Figure (4-16), we notice that there is a clear heterogeneity in the color and nature of the granular distribution of the prepared (pure thin films with Different volume ratios).

4.6.1 Local equalization

This technique has been applied to the images representing thin films under study. It's an intermediate stage where the image is processed. Figure (4-17) shows the result of applying this technique to the image in Figure (4-16).

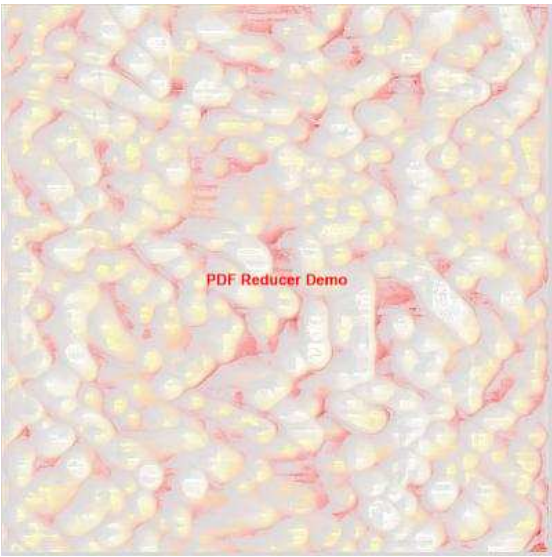

Figure (4-17) local equalization.

- ***Histogram stretch***

Figure (4-18) shows applied the (histogram stretch then histogram) technique to the images in Figure (4-17). The result obtained from this application that the sites of peaks and the grain size in white color. The ruggedness is clearly visible for the visual image. From histogram we notice a shift in blue color towards the right, while the distribution seems constant in green color within the same context, and the concentration of the red color and its shift towards the right.

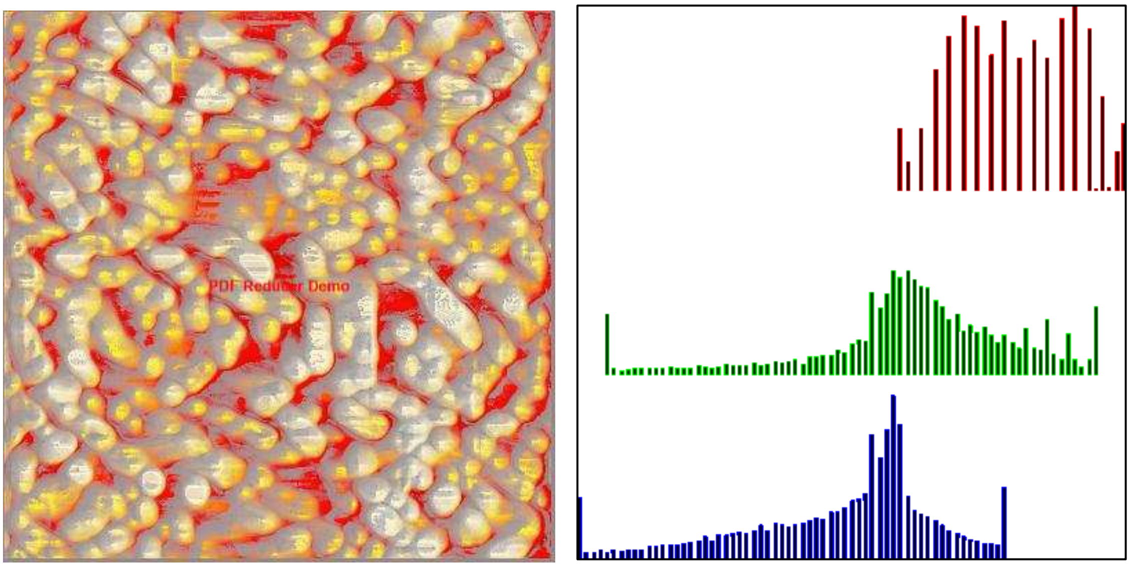

Figure (4-18) histogram stretch.

- ***Histogram specification***

Figure (4-19) illustrated the step of applied (histogram specification) technique to the image in Figure (4-16).This application was done to obtain one band within the gray level to reflective observation of peaks and distinguish them from the gaps.

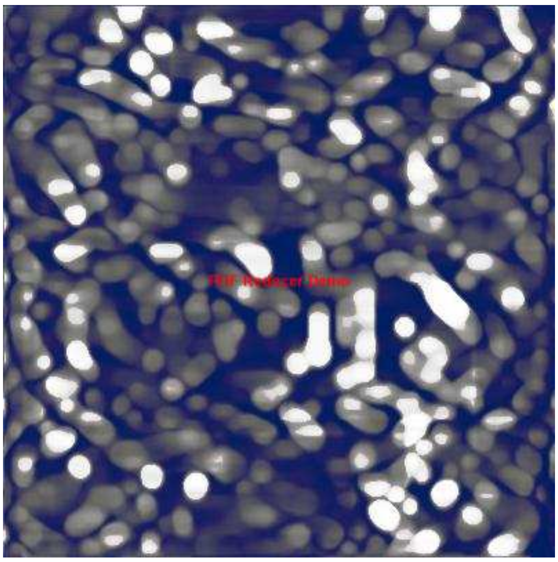

Figure (4-19) histogram specification.

4.6.2 DCT sharpening

Figure (4-20) shows the (DCT sharpening) technique when applied to the images in Figure (4-16) then cropped image (400x400) pixels. The result obtained from this application is to clarify the grain boundary and the differences are clear.

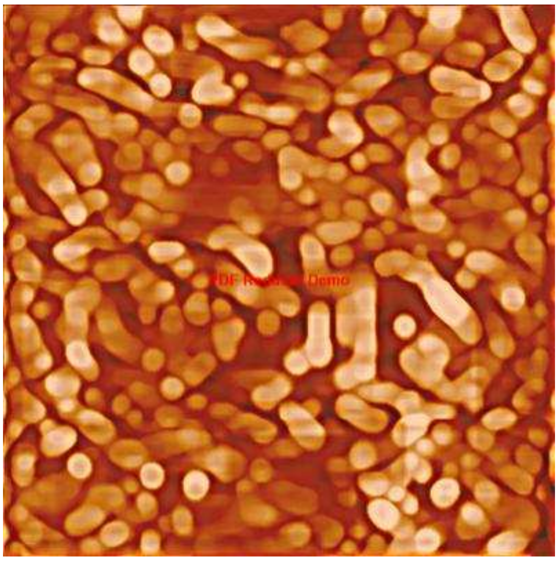

Figure (4-20) DCT sharpening technique.

- ***Local equalization for DCT sharpening images***

Figure (4-21) shows applied the (local equalization) technique to the image in Figure (4-20).

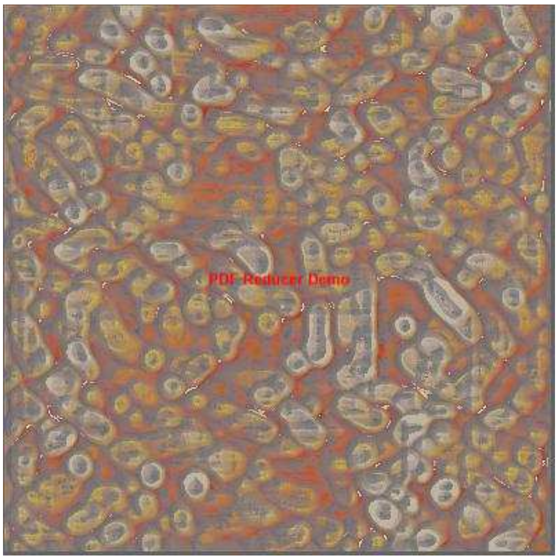

Figure (4-21) (local equalization) technique.

- ***Histogram stretch for DCT sharpening images***

Figure (4-22) shows the (histogram stretch then histogram) technique when applied to the image in Figure (4-21). The result of this application is a high clarity to the variation of elevations. From histogram we observe the increase of the green color concentrations at the minimum with the stability of distribution in red and blue.

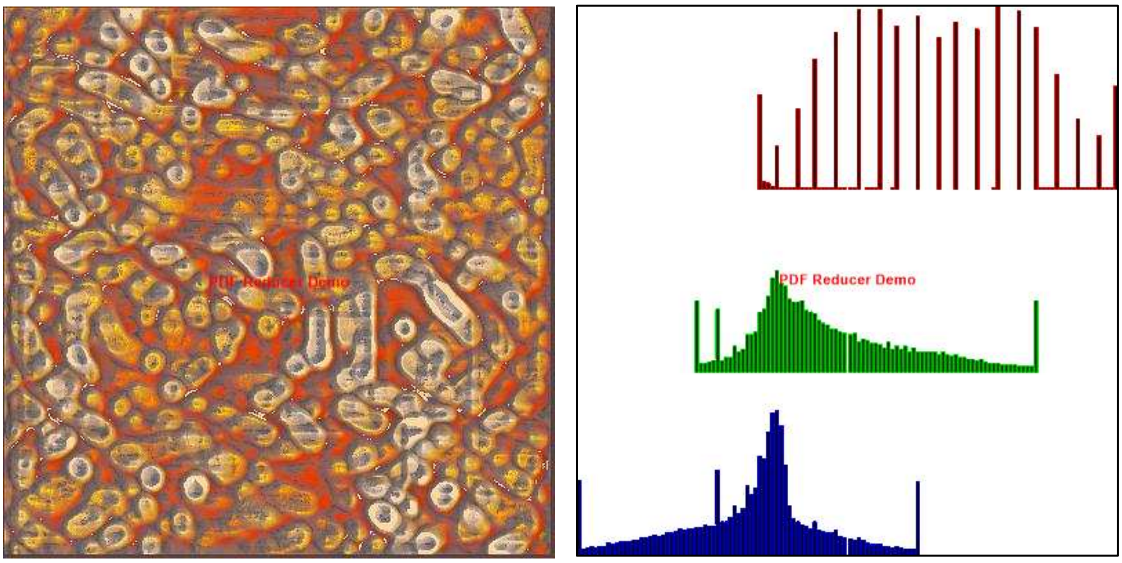

Figure (4-22) (histogram stretch) technique

4.6.3 Convert color to gray

Figure (4-23) shows applied the (convert color to gray then histogram) technique to the image in Figure (4-20).

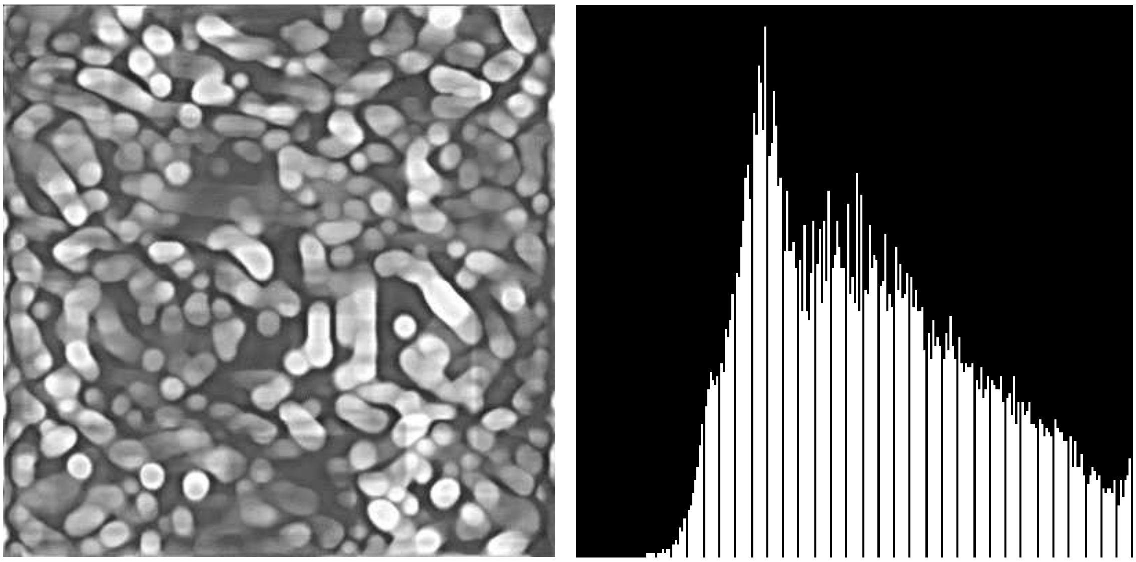

Figure (4-23) convert color to gray.

4.6.4 Transformation

Figure (4-24) shows the (transformation then histogram) technique by using wavelet to the image in Figure (4-16). The next step is segmentation technique by using multi-resolution to the image in above step. Finally cropped (400x400) pixels the result image from segmentation image. From histogram. It was observed that histogram has shifted to leftward to all bands.

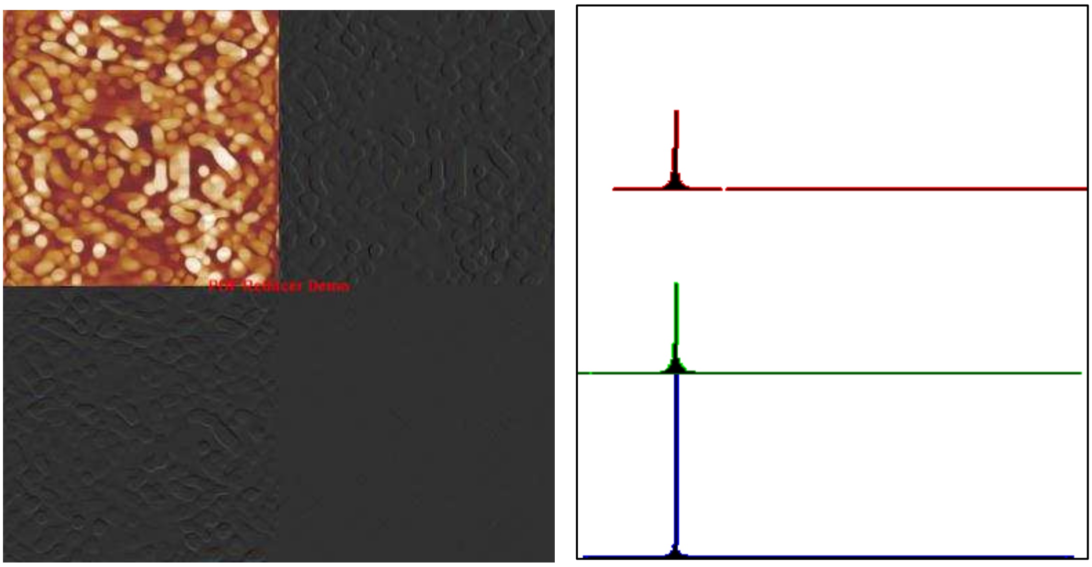

Figure (4-24) segmentation.

This method is used to work in the frequency domaine and is processed by segmentation and getting the figure listed in order to observe the change in histogram.

- ***Histogram specification***

Figure (4-25) shows applied the (histogram specification then histogram) technique to the image in Figure (4-24). Another method to determine the roughness and topography of the surface of thin films and the extent of regularity of this surface, where these results gave a distinct form of the following figure note that the elevation are opposite directions as they seen. From histogram notes Shift towards right.

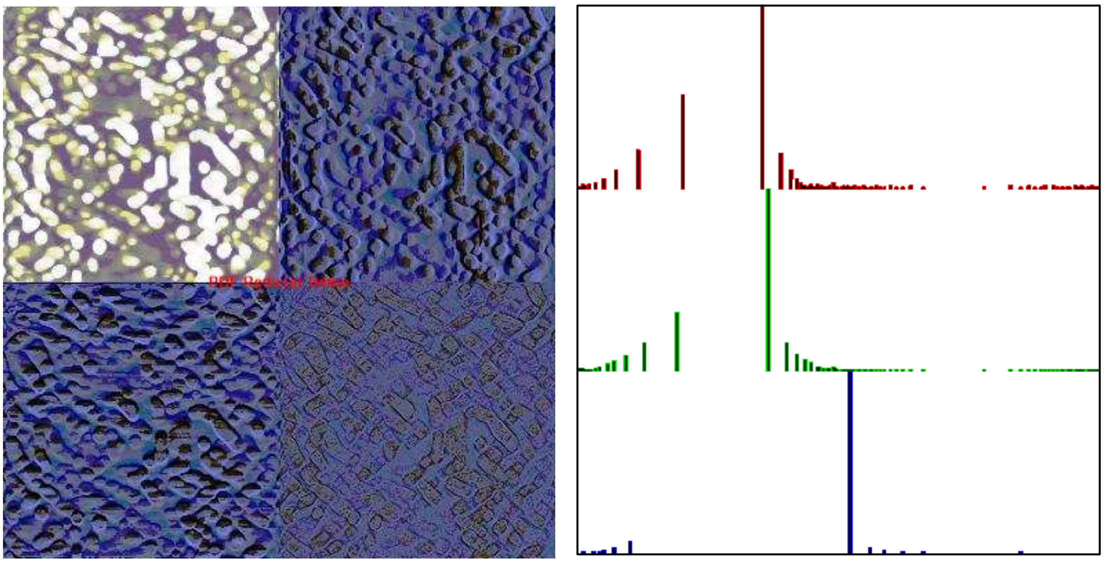

Figure (4-25) histogram specification.

4.6.5 Edge-detection

Figure (4-26) shows applied the (Roberts) operator to the image in Figure (4-16). This operater gives output in a three-dimensional between the roughness of the high and low surface of the thin films.

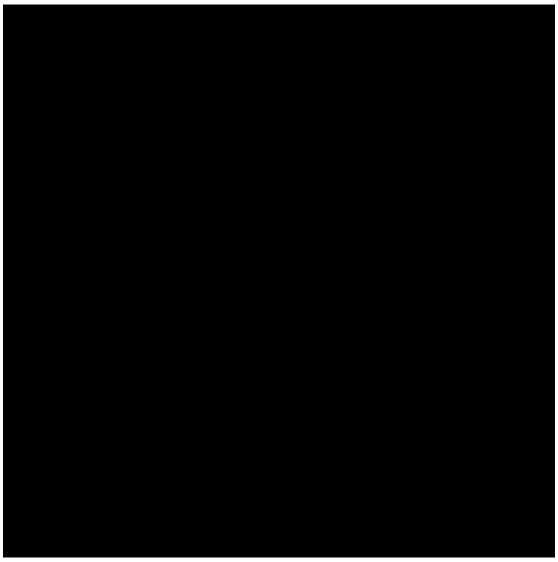

Figure (4-26) 'Roberts' edge detection.

Figure (4-27) shows the results from applying (sobel) operator to the image in Figure (4-16).

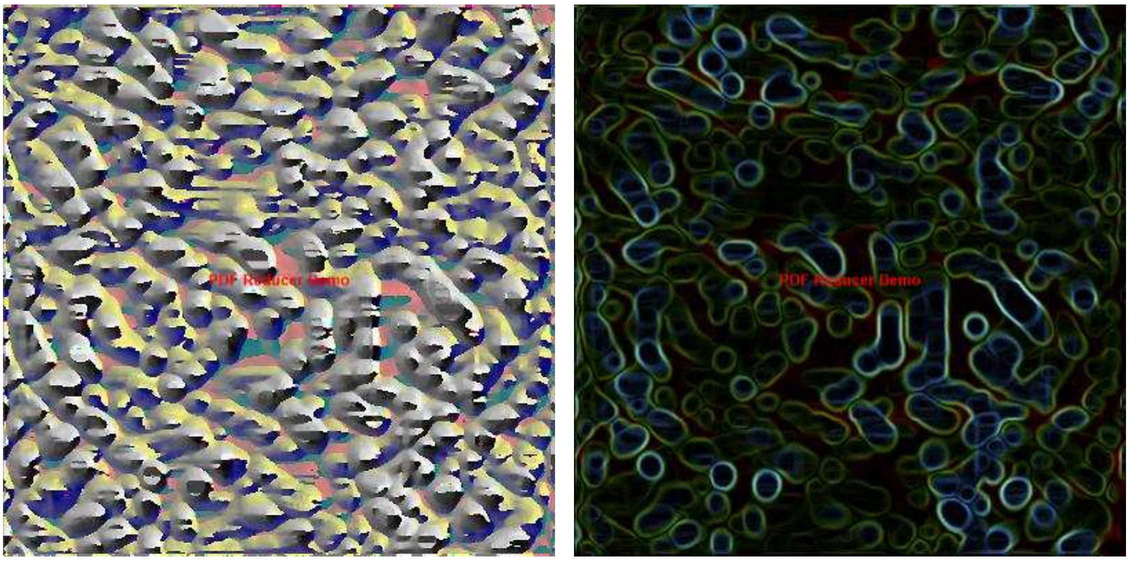

Figure (4-27) 'Sobel' edge detection.

Figure (4-28) show applied the (Prewitt) operator to the image in figure (4-16). This operater give a nagative direction of image.

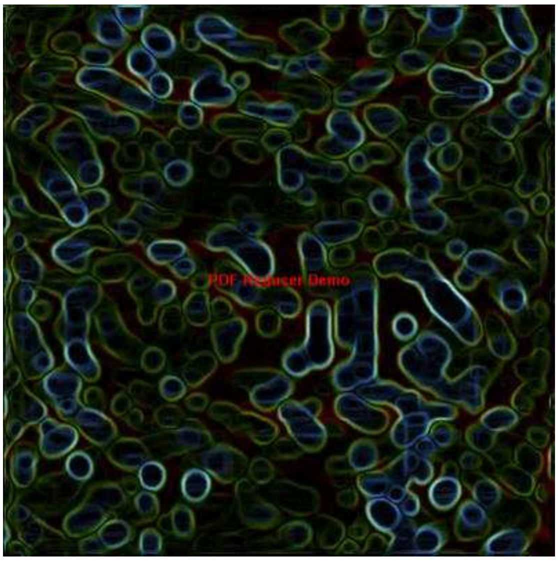

Figure (4-28) 'Prewitt' edge detection.

Figure (4-29) show applied the (Laplacian) operator to the image in figure (4-16).

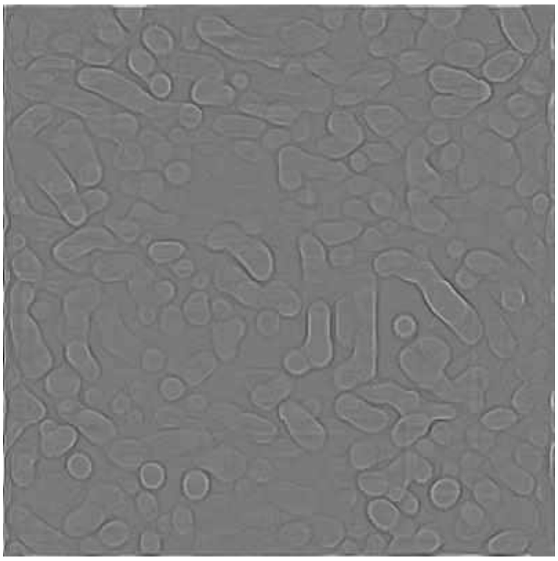

Figure (4-29) 'Laplacian' edge detection.

Figure (4-30) show applied the (histogram stretch) operator to the image in Figure (4-29). This operator gives the boundary of the topography to the surface of the thin film as shown in the image.

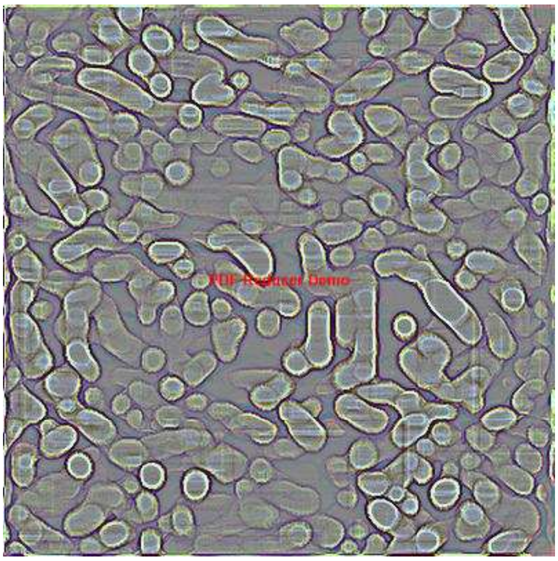

Figure (4-30) histogram stretch.

Figure (4-31) show applied the (Canny and historam specification) operator to the image in figure (4-16). This operater gives a boundaries in three bands. From historam specification the variation of the parameter is unclear.

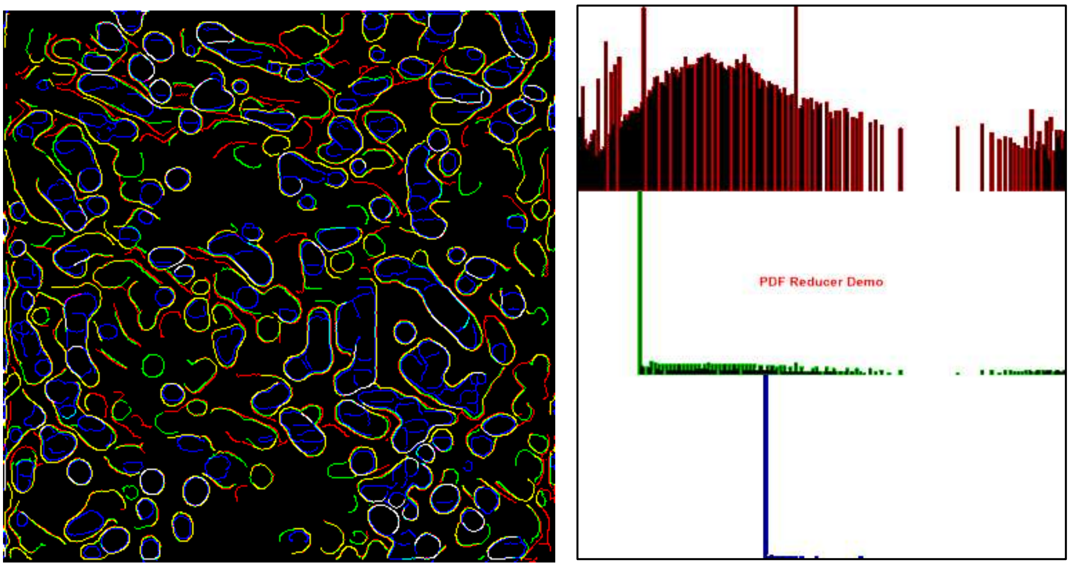

Figure (4-31) 'Canny' edge detection.

4.7 Comparing Images before and after annealing :

Thin films with percentage (5%) will be compared with thin film after annealing. Figure (4-32) shows digital images captured for the study samples obtained from the (AFM) measurement after the images were cropped then resized to (400x400) pixels.

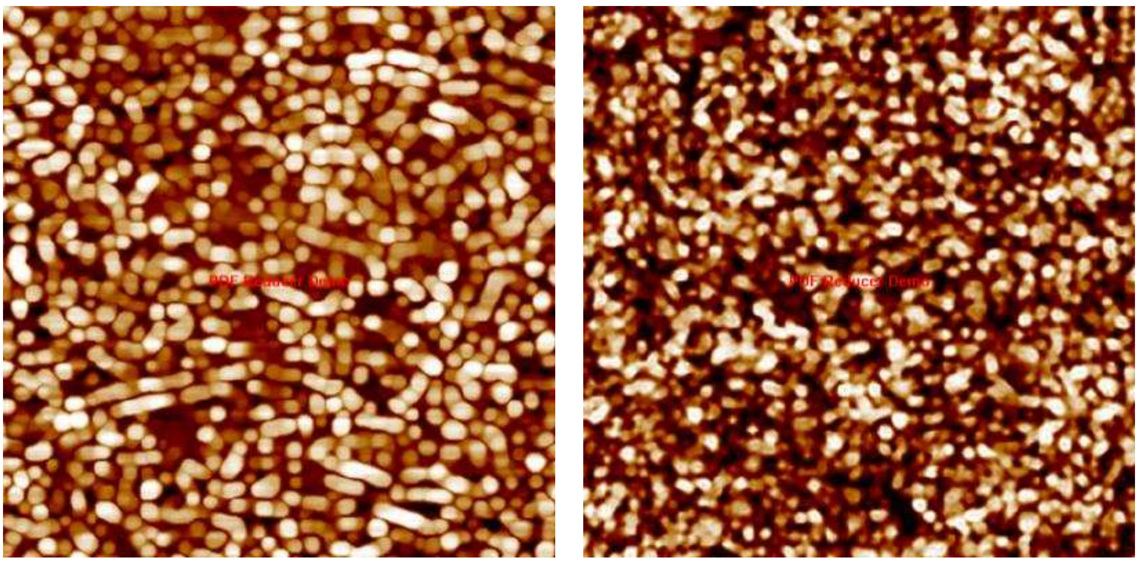

ZnO:Sn (5%) ZnO:Sn (5%) after annealing

Figure (4-32) AFM images for doping thin films.

4.7.1 Local equalization & Histogram stretch

This technique has been applied to the images representing thin films under study. Figure (4-33) shows the result of applying these two techniques then applied histogram to the images in Figure (4-32). The sites of peaks and the grain size in white color was observed before and after annealing. From histogram It is a clear from this figure the shift to right for all bands for thin films after annealing.

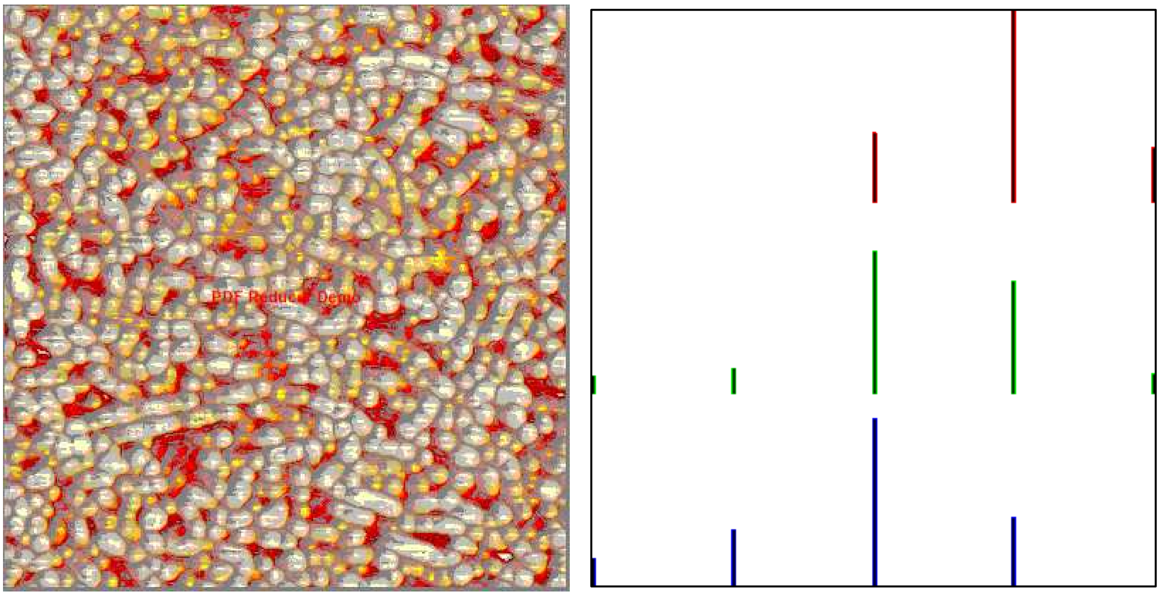

ZnO:Sn (5%)

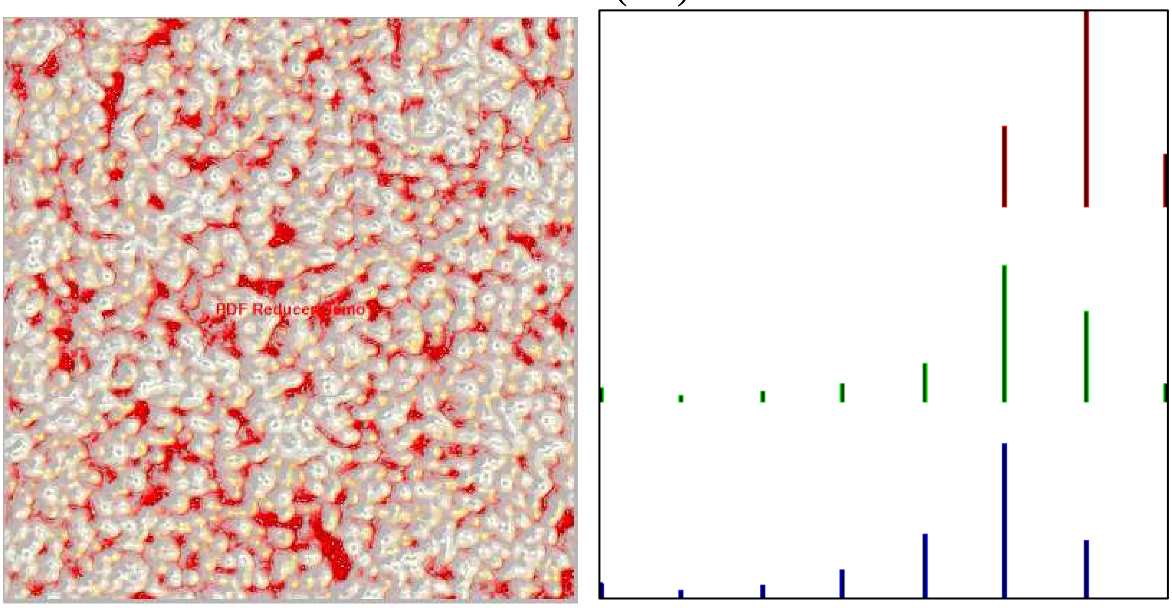

ZnO:Sn (5%) after annealing

Figure (4-33) local equalization and histogram stretch.

- ***Histogram specification***

Figure (4-34) shows applied the (histogram specification) technique to the images in figure (4-32). The figure shows the high differences appeared visually to be distinguished the surface variability.

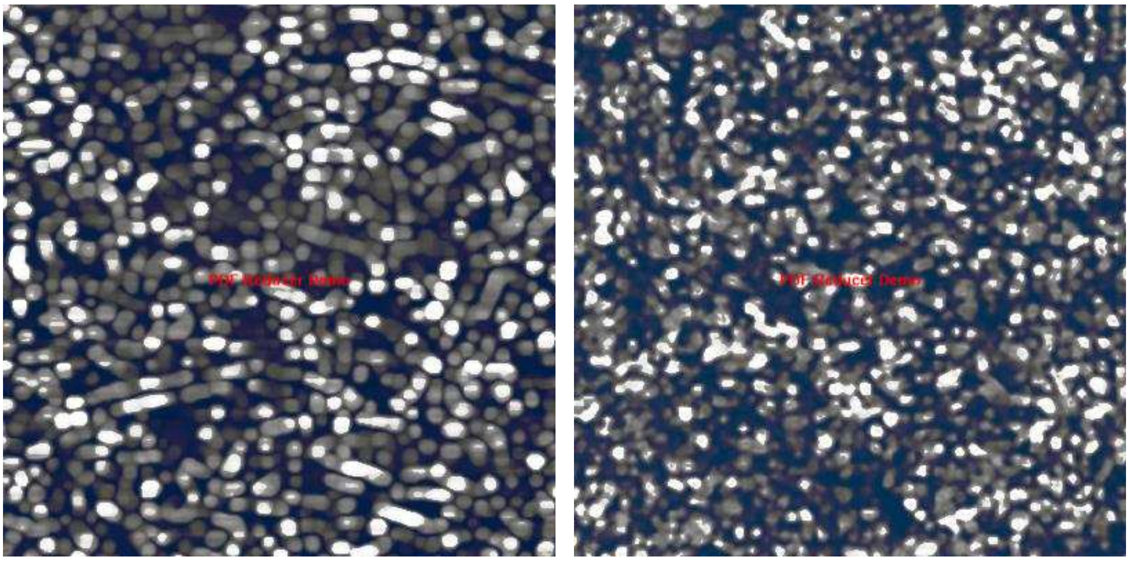

ZnO:Sn (5%) ZnO:Sn (5%) after annealing

Figure (4-34) histogram specification for doping thin films.

4.7.2 DCT sharpening

Figure (4-35) shows applied the (DCT sharpening) technique to the images in Figure (4-34) then cropped images (400x400) pixels. The variation of shape of the grain boundaries and the different are clear according to the before and after annealing.

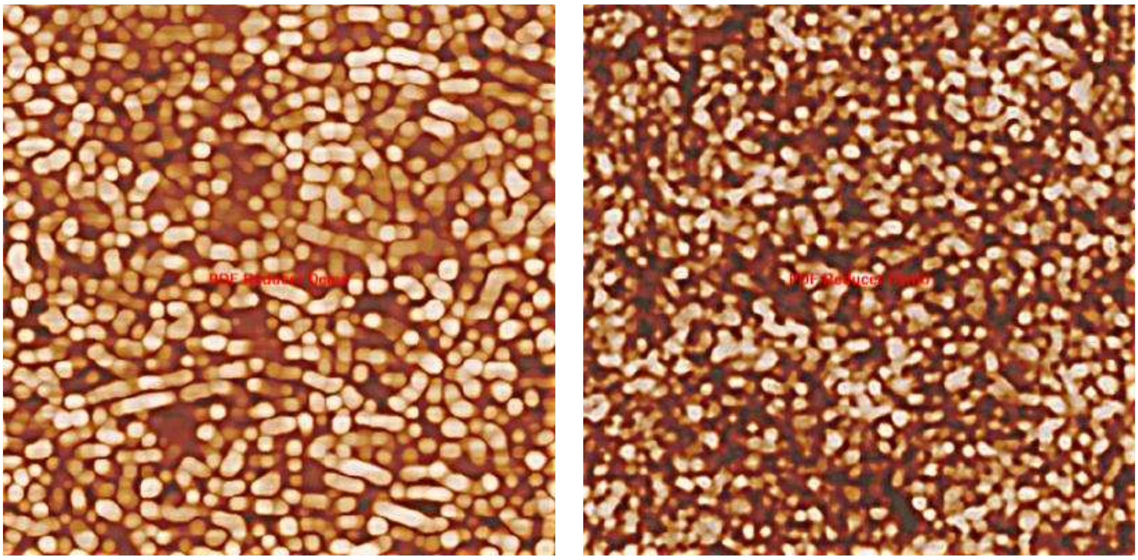

ZnO:Sn (5%) ZnO:Sn (5%) after annealing

Figure (4-35) (DCT sharpening) technique for doping thin films.

- ***Local equalization for DCT sharpening images***

Figure (4-36) shows applied the (local equalization) technique to the images in figure (4-35).

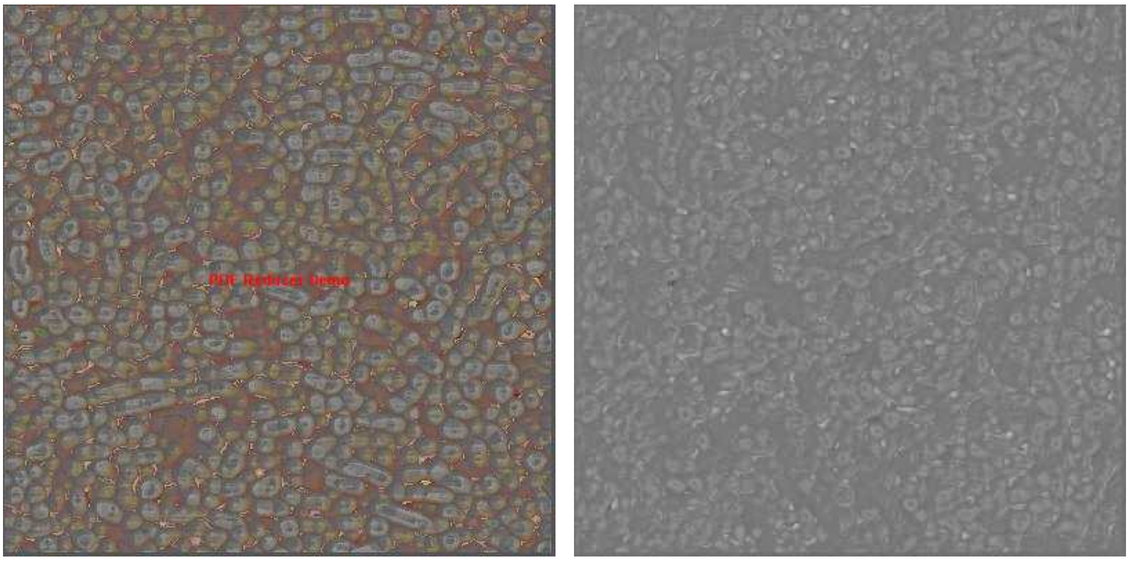

ZnO:Sn (5%) ZnO:Sn (5%) after annealing

Figure (4-36) (local equalization) technique for doping thin films.

- ***Histogram stretch for DCT sharpening images***

Figure (4-37) shows the (histogram stretch then histogram) technique when applied to the images in Figure (4-26). The roughness is clearly visible to the human eyes for doped thin films before and after annealing. From histogram The three bands behave as shrink histogram where the red band shrink and contrast to middle. The green and blue bands was concentrated at the peaks of each band and increase the intensity.

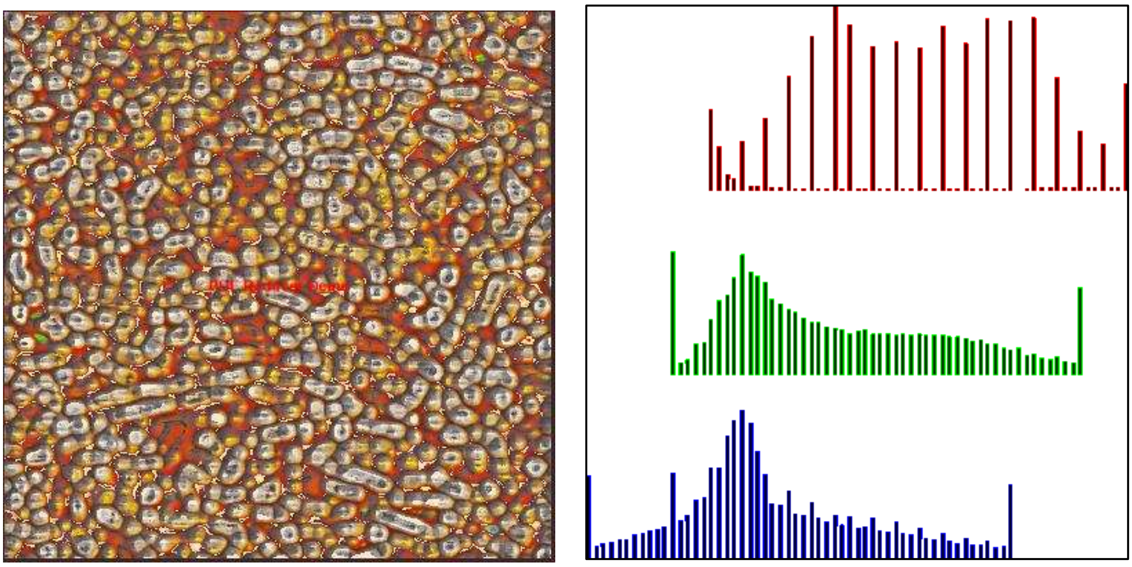

ZnO:Sn (5%)

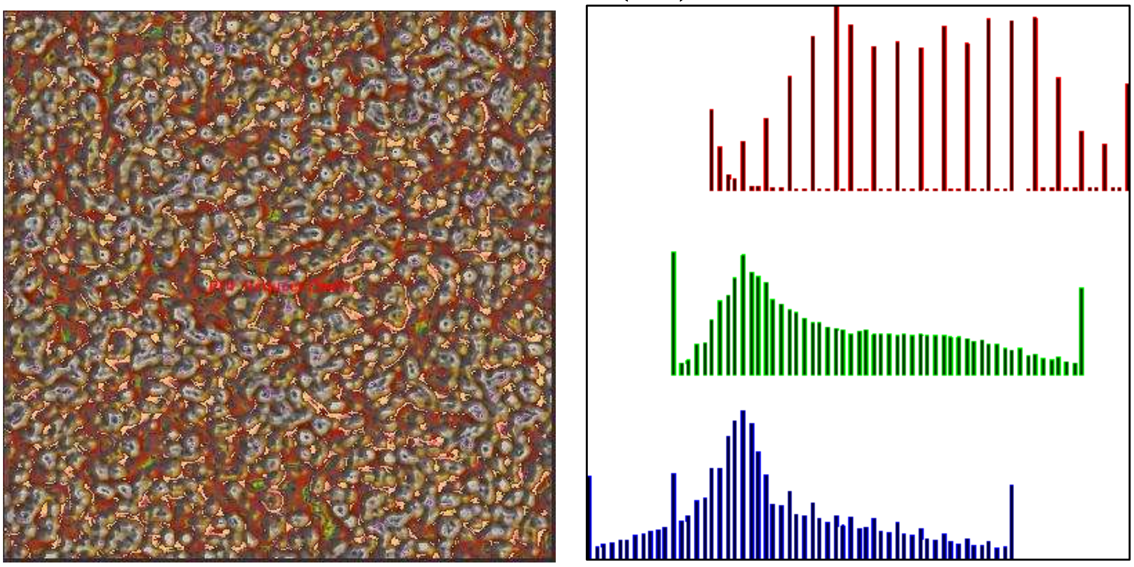

ZnO:Sn (5%) after annealing

Figure (4-37) (histogram stretch) technique for doping thin films.

4.7.3 Convert color to gray

Figure (4-38) illustrated the (color to gray conversion then histogram) technique when applied to the images in figure (4-36). This conversion depends on the reflectivity of the electromagnetic spectrum on each pixel. The output images show a good contrast between the two images where the annealing effects is the difference between these two images. From histogram the annealing affects the histogram to be concentrated and uniformed at a narrow range of the frequency. This changes to histogram happed because the annealing makes the structure more alignment and uniformity.

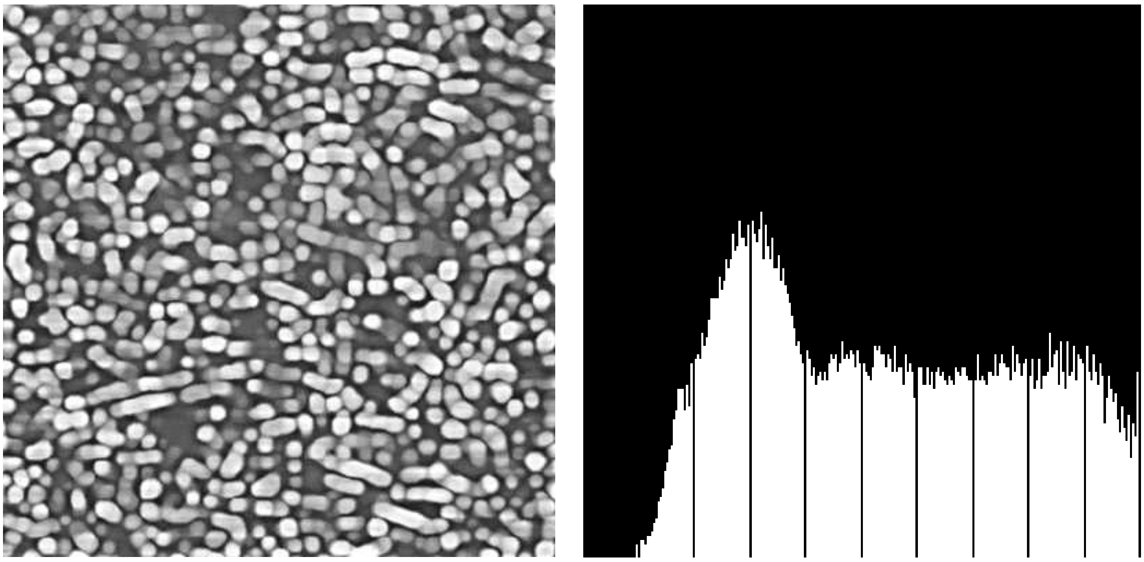

ZnO:Sn (5%)

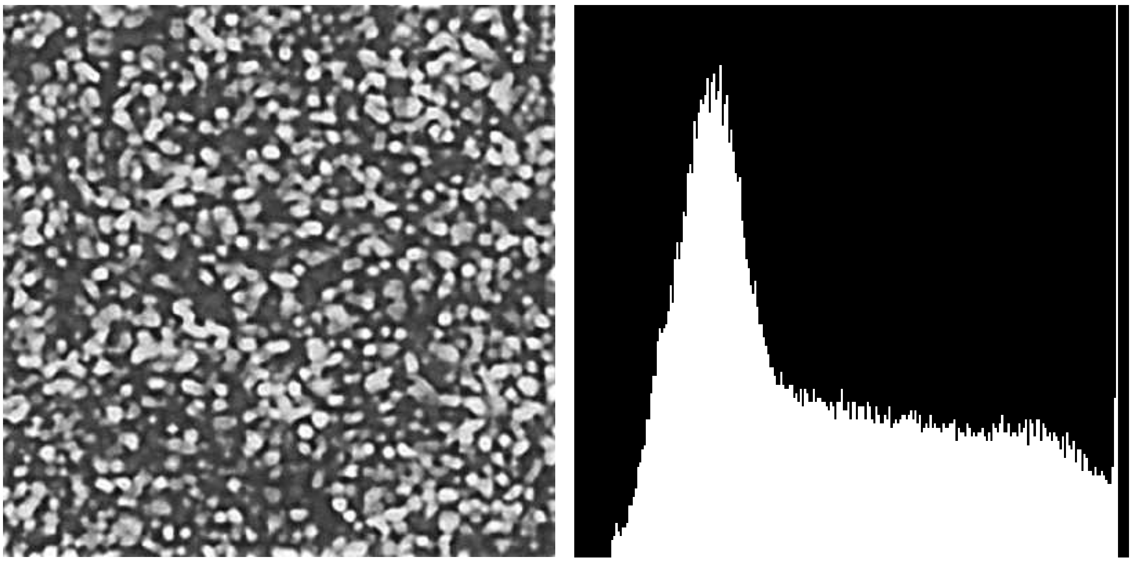

ZnO:Sn (5%) after annealing

Figure (4-38) (convert color to gray) for doping thin films.

4.7.4 transformation

Figure (4-39) shows the (transformation then histogram) technique by using wavelet to the images in Figure (4-34). Then segmentation technique by using multi-resolution to the image in above step. Finally cropped (400x400) pixels the result images from segmentation image.

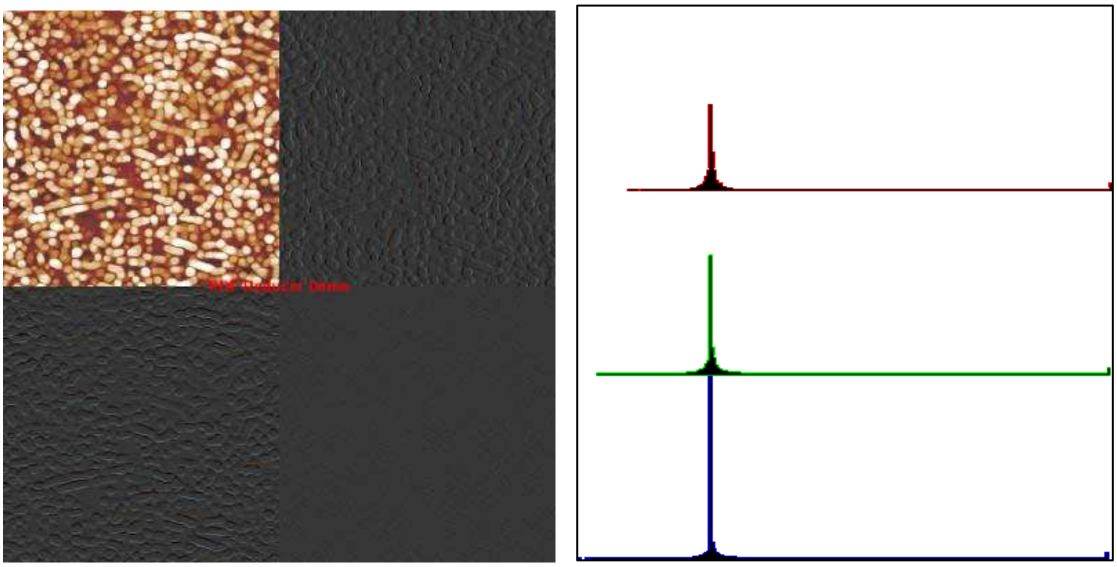

ZnO:Sn (5%)

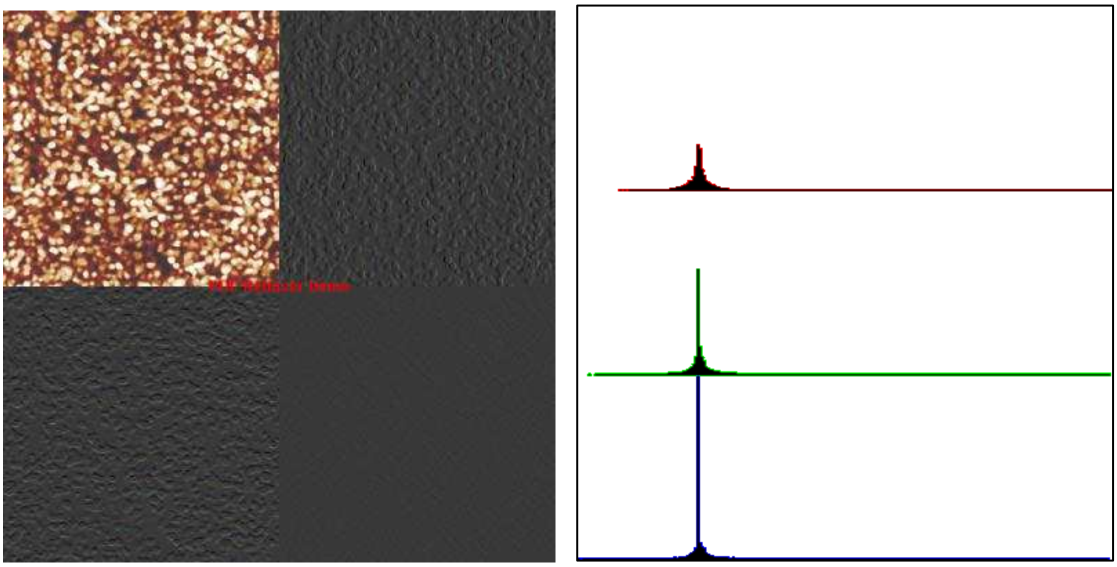

ZnO:Sn (5%) after annealing

Figure (4-39) (segmentation) for doping thin films.

- ***Histogram specification***

Figure (4-40) shows applied the (histogram specification) technique to the images in Figure (4-39). The roughness and topography of the surface of thin films is clear before and after annealing. From histogram after cropped to eliminate the echo images. The results are not exclusive to distinguish the differences between the surfaces for thin films, before and after annealing.

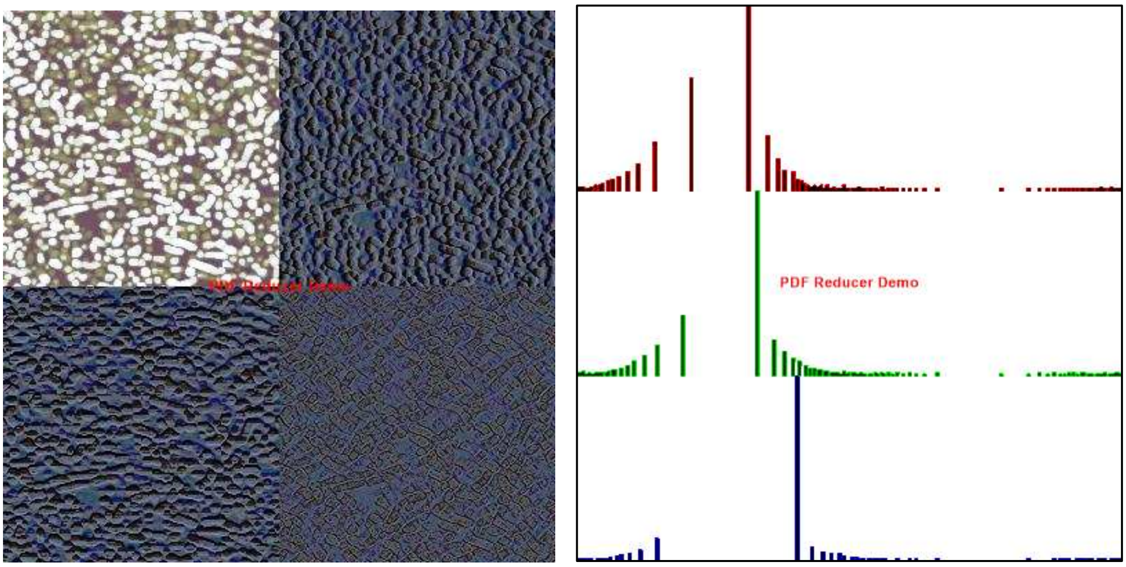

ZnO:Sn (5%)

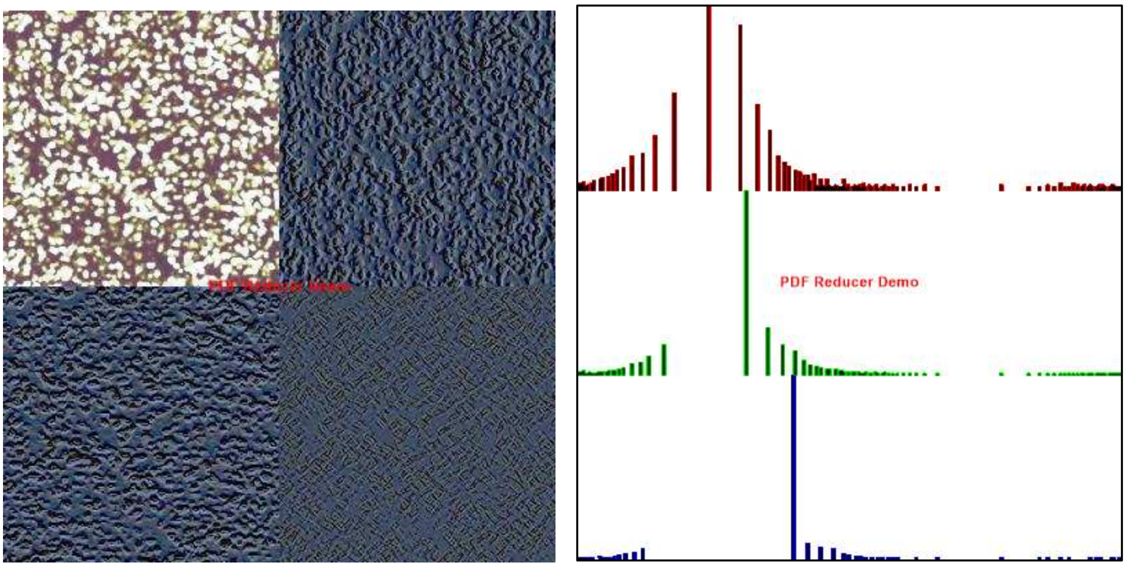

ZnO:Sn (5%) after annealing

Figure (4-39) (histogram specification) for doping thin films.

4.7.5 Edge-detection

Figure (4-41) shows applied the (Roberts) operator to the images in Figure (4-34).

Figure (4-42) shows applied the (sobel) operator to the images in Figure (4-34). This operater gives the output in three dimantion to explore the roughness and that application shows the diffrences for ZnO:Sn thin films before and after annealing.

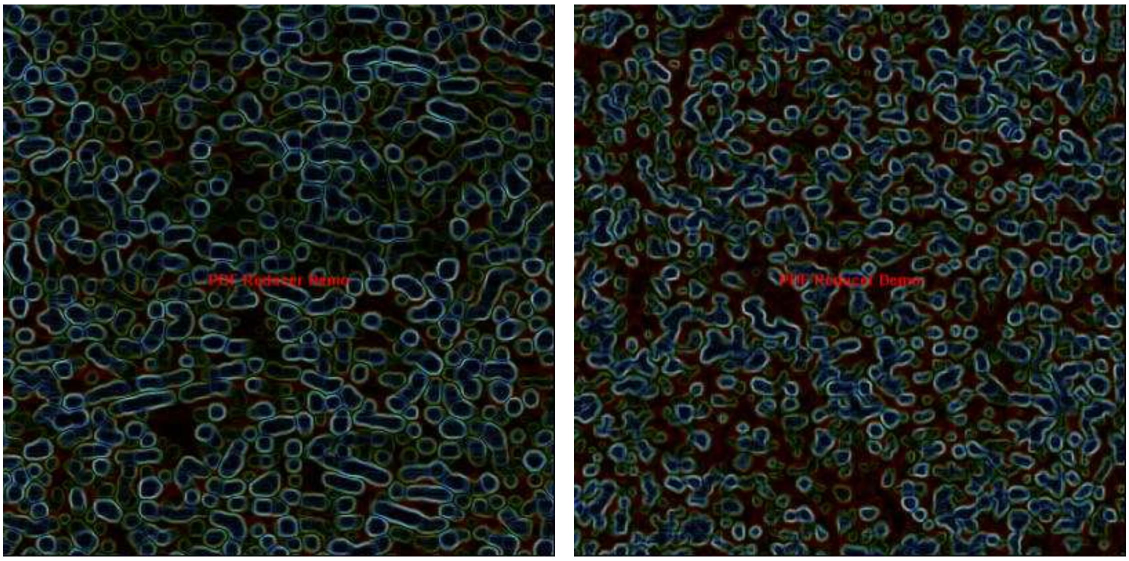

ZnO:Sn (5%) ZnO:Sn (5%) after annealing

Figure (4-41) 'Roberts' edge detection for doping thin films.

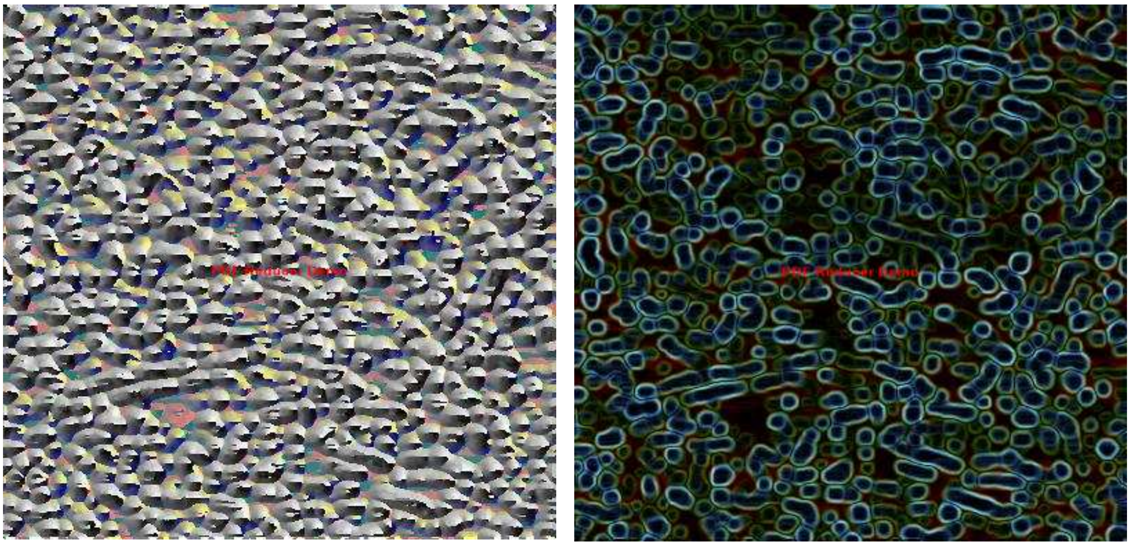

ZnO:Sn (5%)

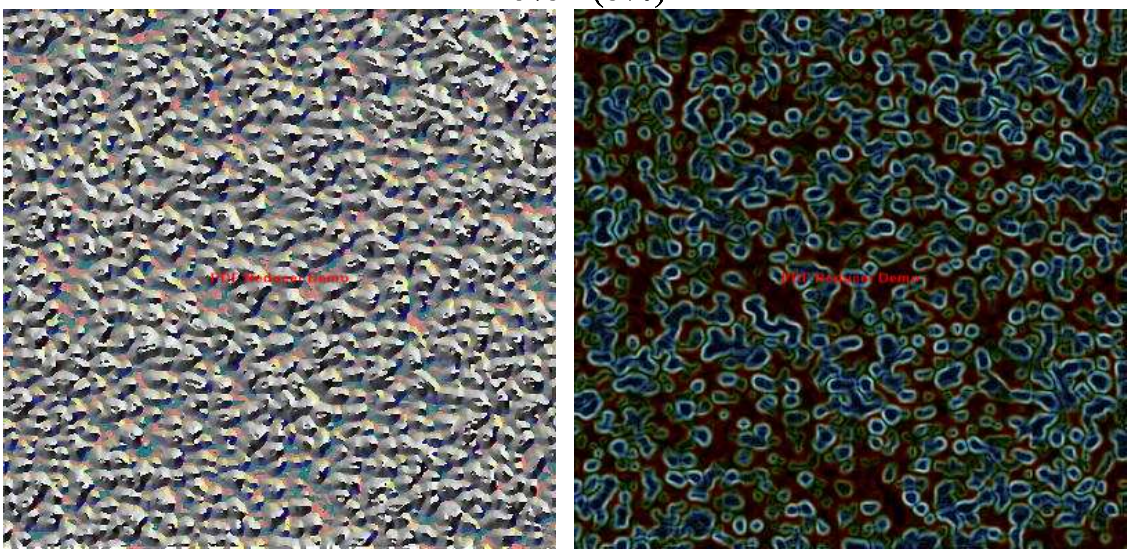

ZnO:Sn (5%) after annealing

Figure (4-42) 'Sobel' edge detection for doping thin films.

Figure (4-43) shows the output images when applied (Prewitt) operator to the images in Figure (4-34). This operator gives the nagative for images and the variation is clear before and after annealing.

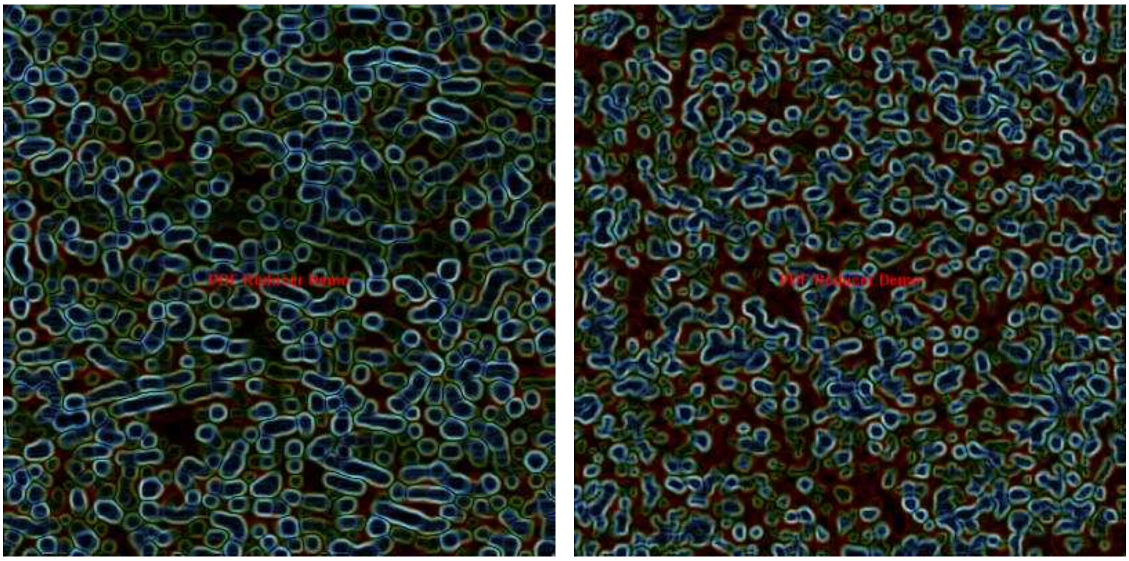

ZnO:Sn (5%) ZnO:Sn (5%) after annealing

Figure (4-43) 'Prewitt' edge detection for doping thin films.

Figure (4-44) shows applied the (Laplacian) operator to the images in figure (4-34).

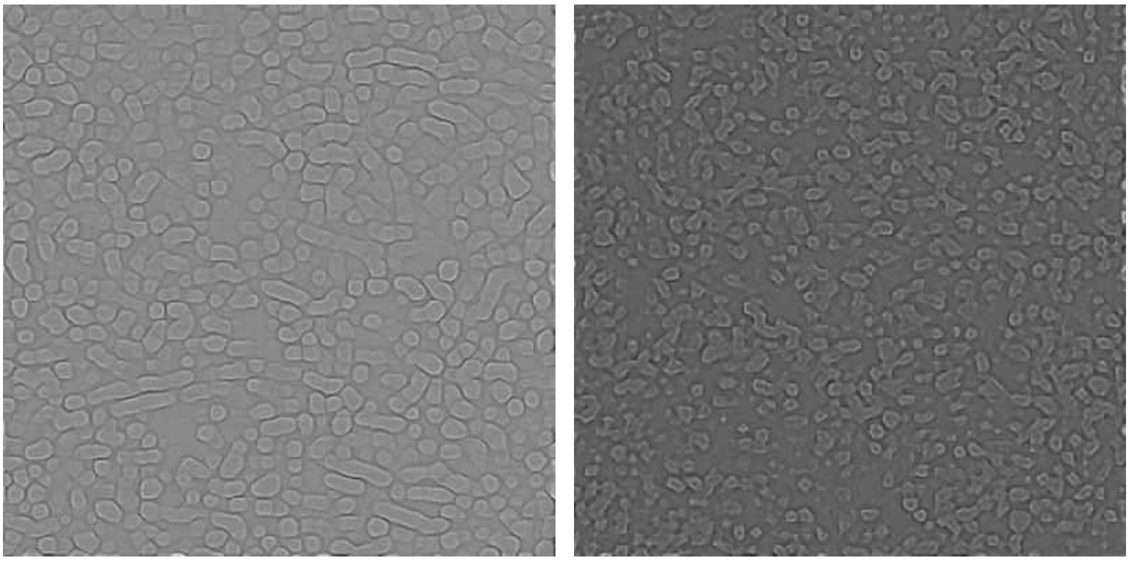

ZnO:Sn (5%) ZnO:Sn (5%) after annealing

Figure (4-44) 'Laplacian' edge detection for doping thin films.

Figure (4-45) shows applied the (histogram stretch) operator to the images in figure (4-44). The bounaries is clear before and after annealing.

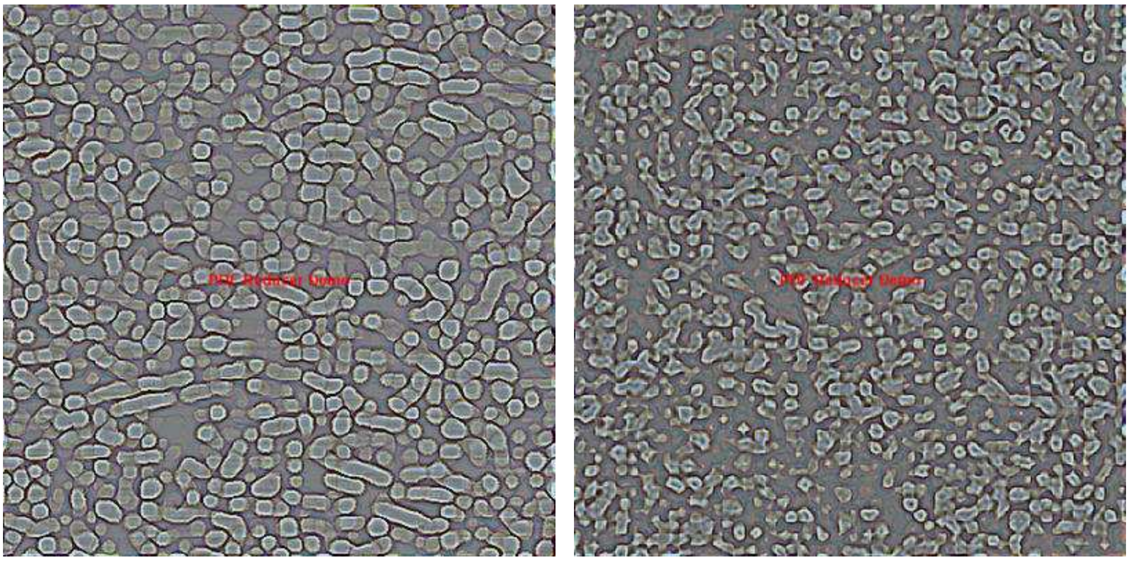

ZnO:Sn (5%) ZnO:Sn (5%) after annealing

Figure (4-45) histogram stretch for doping thin films.

Figure (4-46) shows the (Canny) operator when applied to the images in Figure (4-34) then applied histogram specifaction. The bounadies is clear in three bands bafore and after annealing. The three bands edge detection output refer to different elevation in the surface of the thin films.

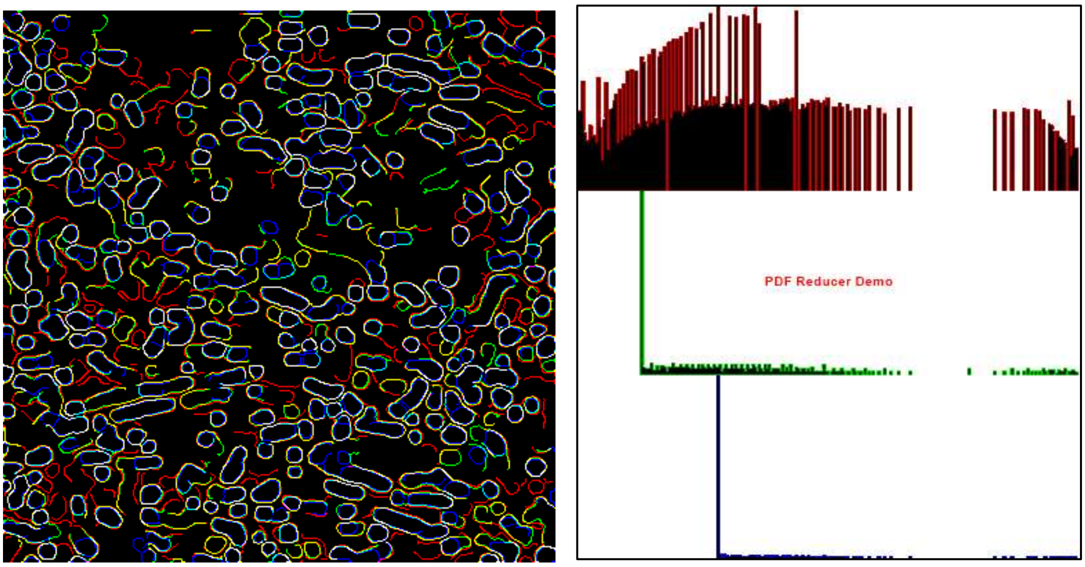

ZnO:Sn (5%)

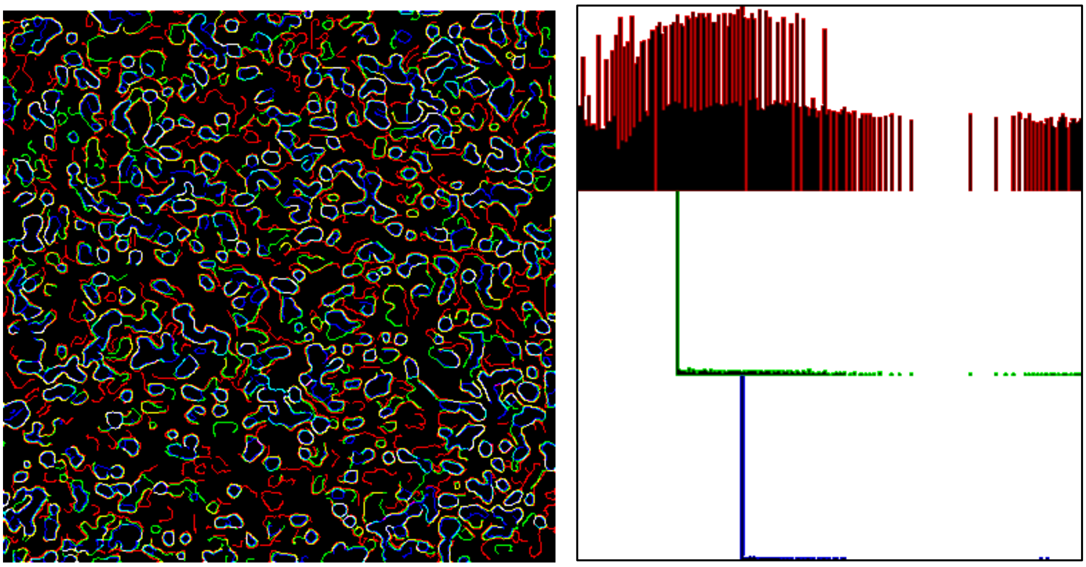

ZnO:Sn (5%) after annealing.

Figure (4-46) 'Canny' edge detection for doping thin films.

4.8 Images Enhancement for Doped and annealed thin films :

Thin films were doping with different percentage, the percentage doping will be compared with pure thin film. Figure (4-47) shows the number of digital images captured for the study samples obtained from the (AFM) measurement after the images were cropped then resized to (400x400) pixels.

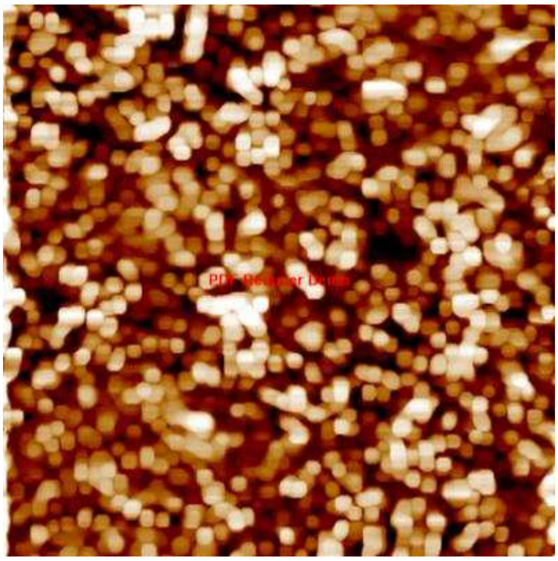

ZnO: Sn (0%) after annealing

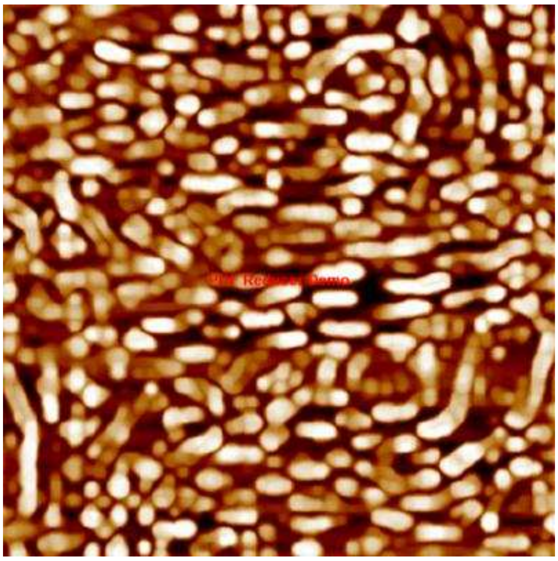

ZnO: Sn (3%) after annealing

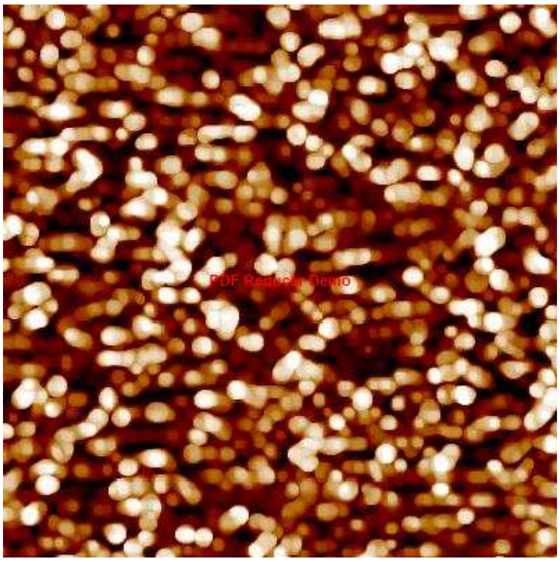

ZnO: Sn (7%) after annealing

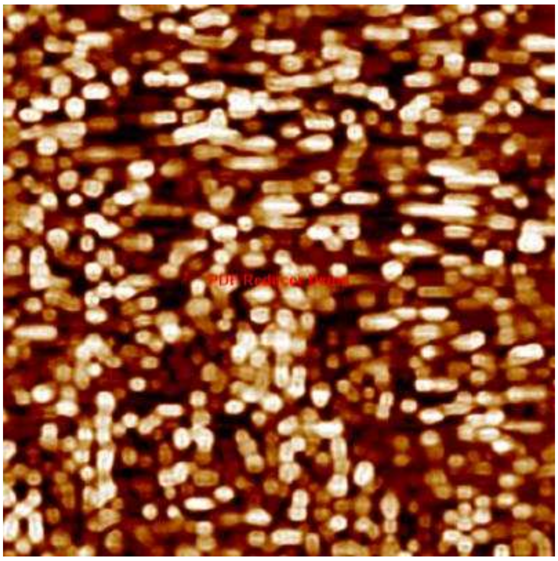

Zno: Sn (9%) after annealing

Figure (4-47) AFM images for pure and doping thin films.

4.8.1 Local equalization & Histogram stretch

This technique has been applied to the images representing thin films under study. Local equalization techniques was used and mentioned as median stage to be processed. Figure (4-48) shows applied the (histogram stretch) technique to the images gained from local equalization techniques. The variation of peaks sites and the grain size after annealing for thin films doping and the roughness is clear for visual viewer.

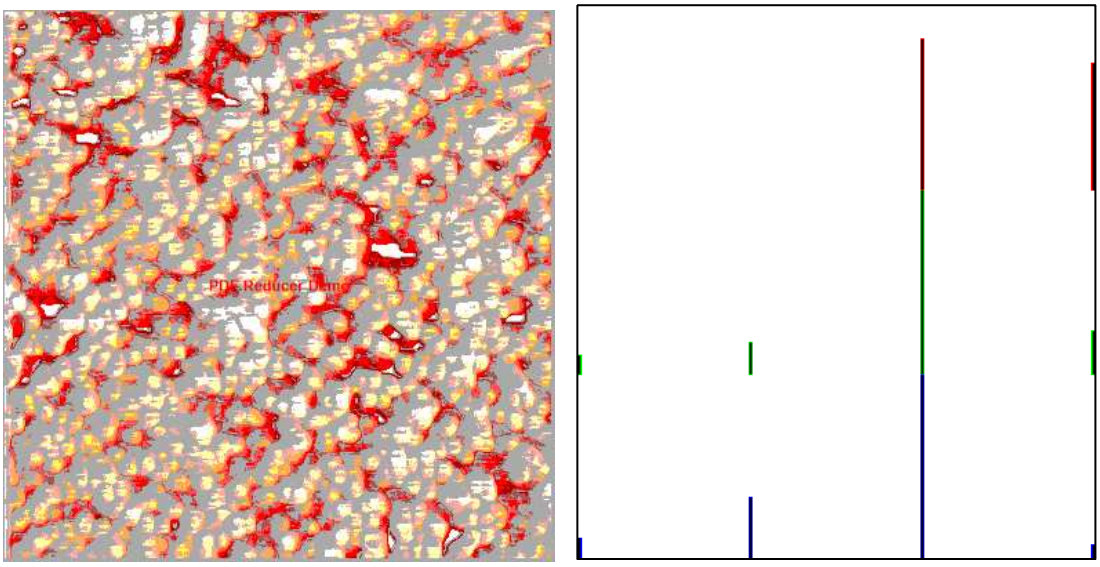

ZnO: Sn (0%) after annealing

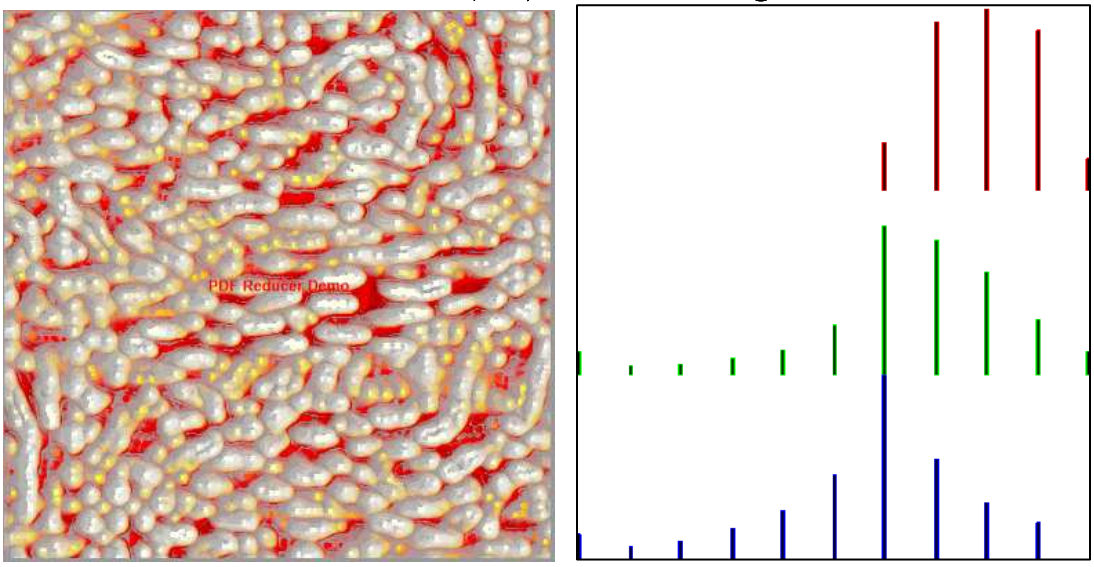

ZnO: Sn (3%) after annealing

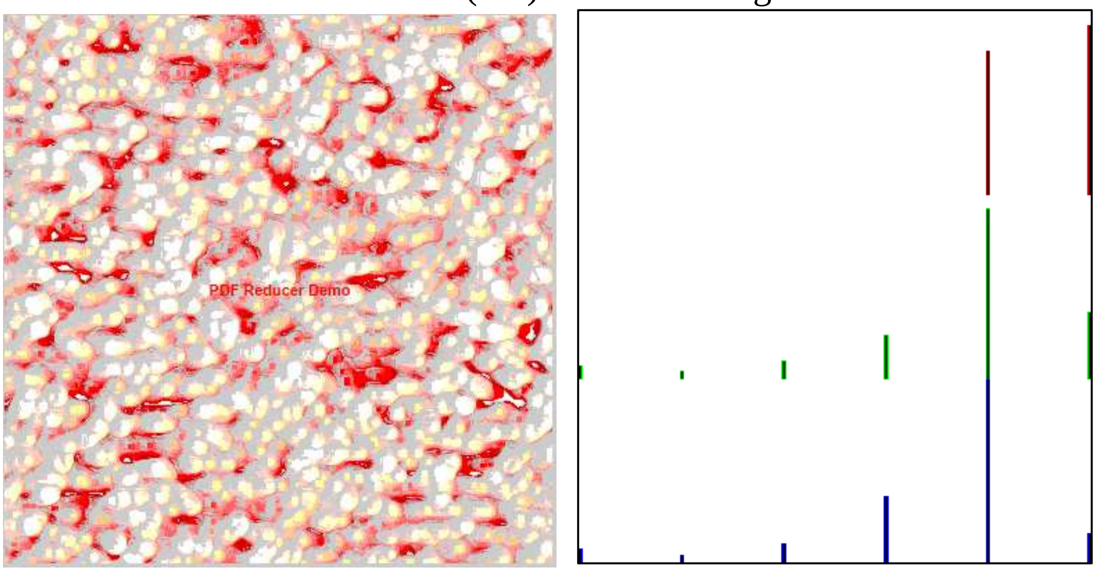

ZnO: Sn (7%) after annealing

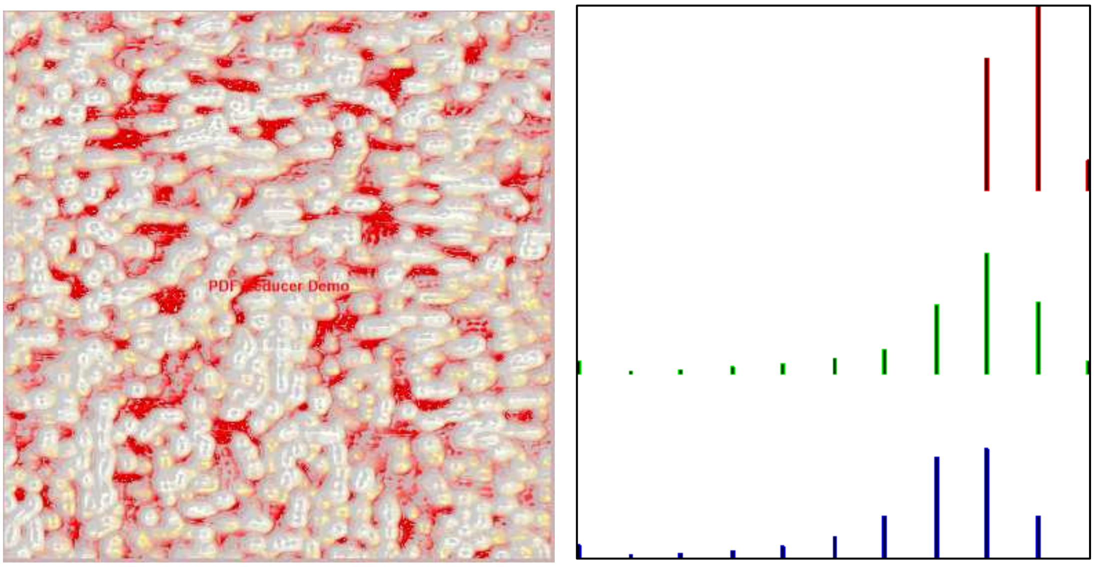

Zno: Sn (9%) after annealing

Figure (4-48) histogram stretch for pure and doping thin films.

- ***Histogram specification***

Figure (4-49) shows applied the (histogram specification) technique to the images in Figure (4-47). The reflective of peaks sites is clear and Differentiation from the gapes sites.

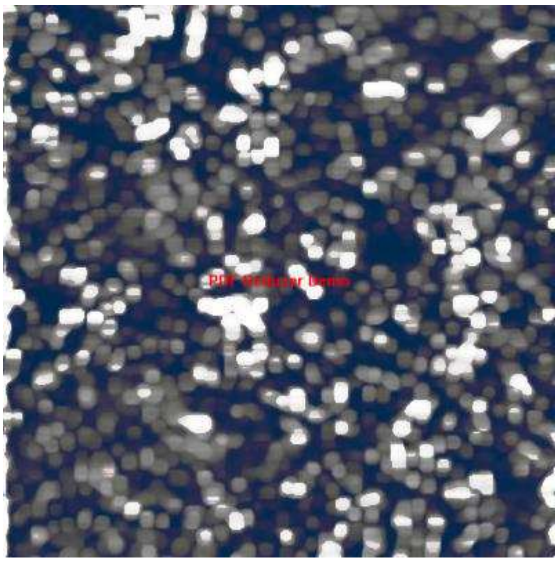

ZnO: Sn (0%) after annealing

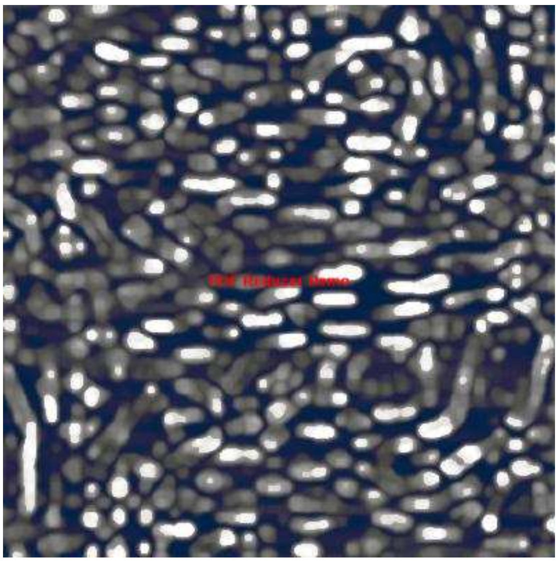

ZnO: Sn (3%) after annealing

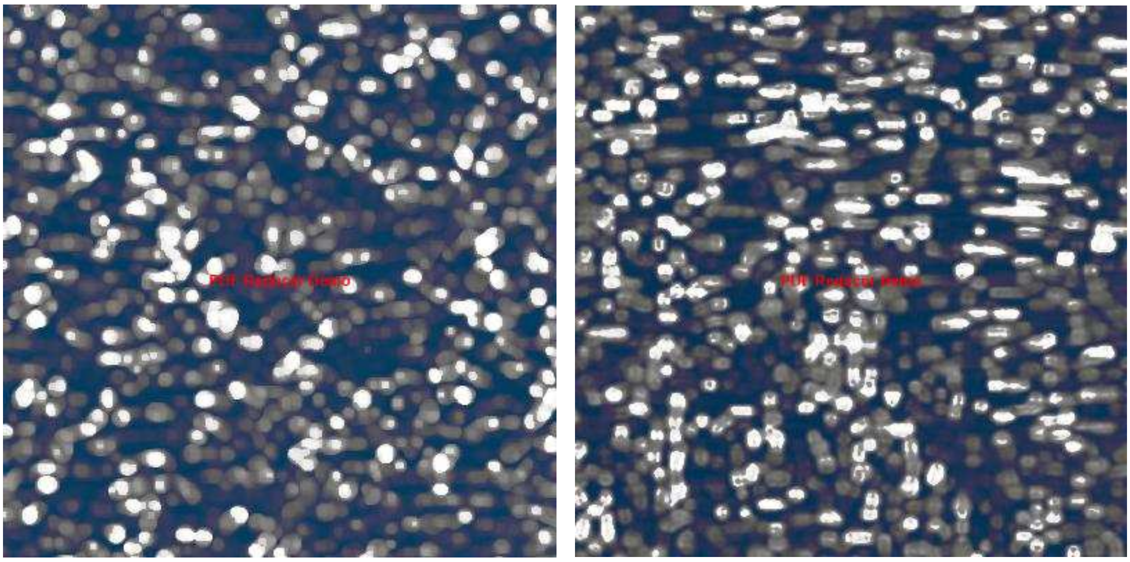

ZnO: Sn (7%) after annealing Zno: Sn (9%) after annealing

Figure (4-49) histogram specification for pure and doping thin films.

4.8.2 DCT sharpening

Figure (4-50) shows applied the (DCT sharpening) technique to the images in Figure (4-47) then cropped images (400x400) pixels. The variation of grain boundaries is clear for thin films doping after annealing.

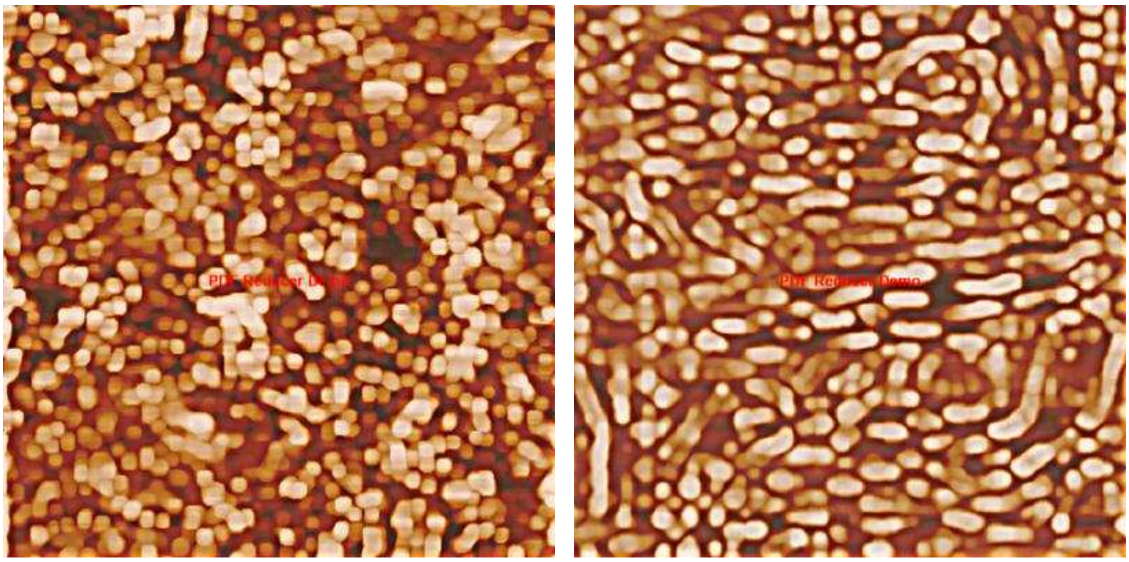

ZnO: Sn (0%) after annealing Zno: Sn (3%) after annealing

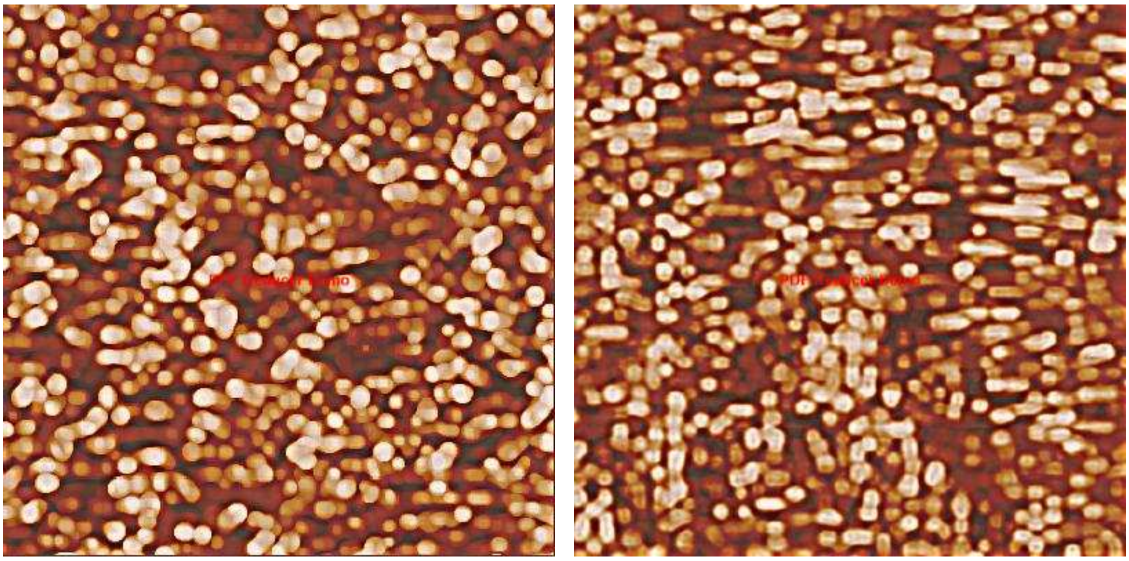

ZnO: Sn (7%) after annealing Zno: Sn (9%) after annealing

Figure (4-50) DCT sharpening technique for pure and doping thin films.

- ***Local equalization for DCT sharpening images***

Figure (4-51) shows applied the (local equalization) technique to the images in Figure (4-50).

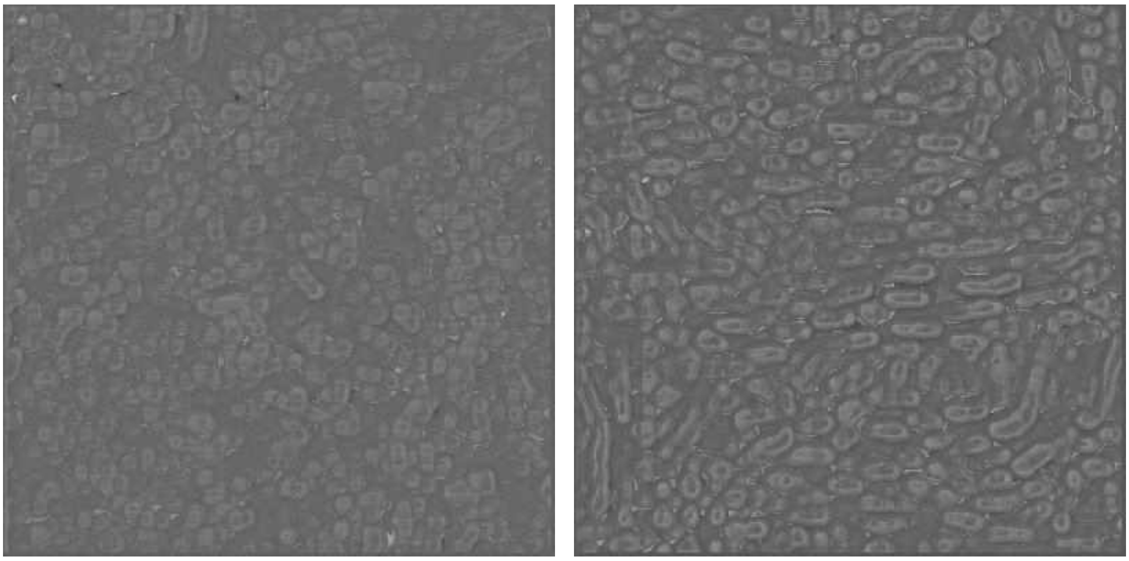

ZnO: Sn (0%) after annealing Zno: Sn (3%) after annealing

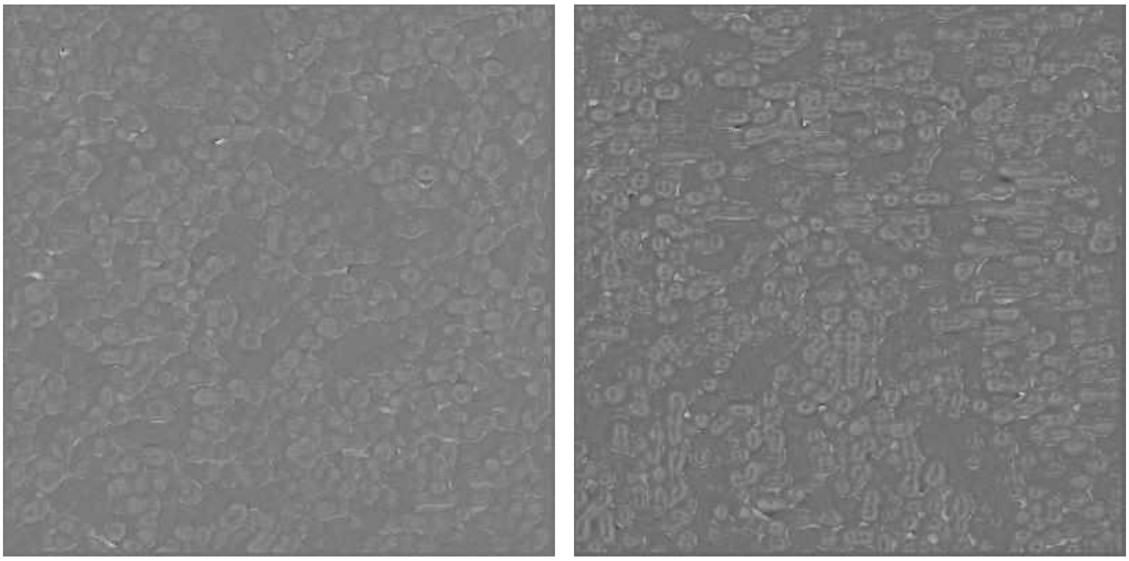

ZnO: Sn (7%) after annealing Zno: Sn (9%) after annealing

Figure (4-51) local equalization technique for pure and doping thin films.

- ***Histogram stretch for DCT sharpening images***

Figure (4-52) shows applied the (histogram stretch) technique to the images in Figure (4-51). The Clarity is extinguished between high and low area for all thin films after annealing. applied the histogram to the images. The variation in frequency is clear for red band and stable for green and blue color.

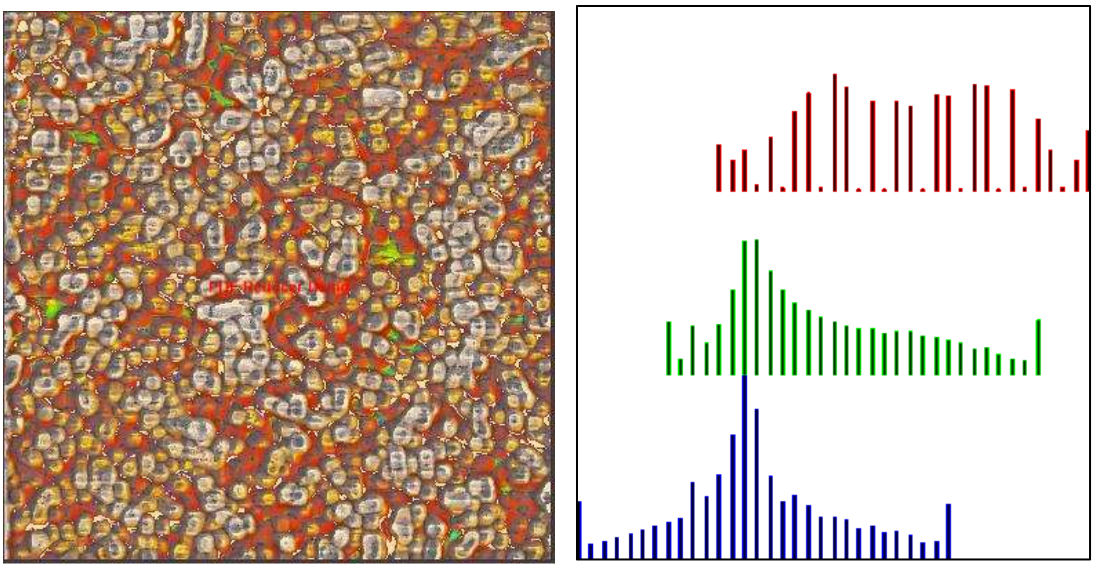

ZnO: Sn (0%) after annealing

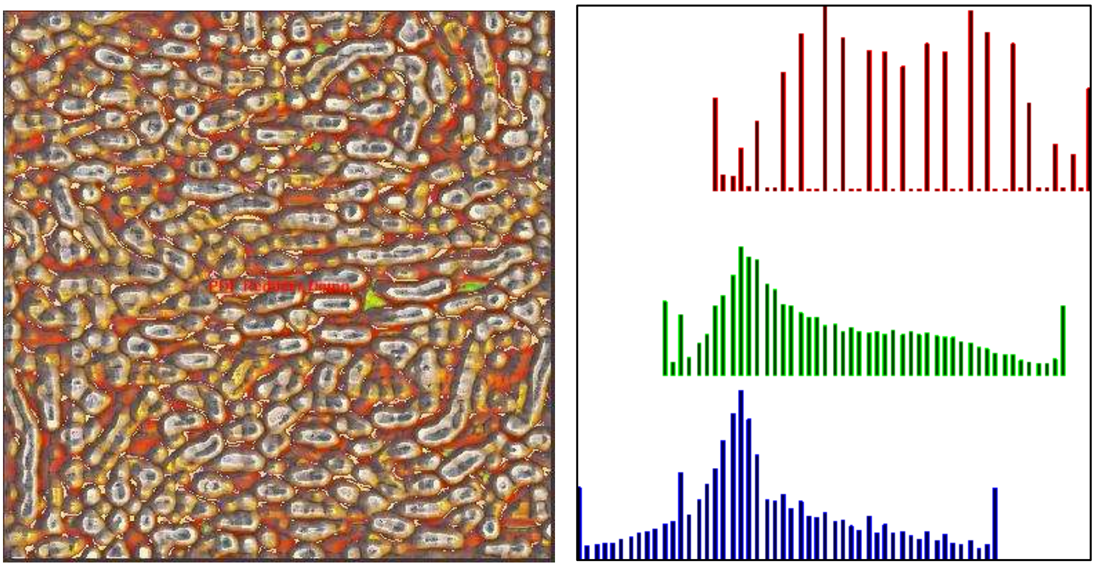

Zno: Sn (3%) after annealing

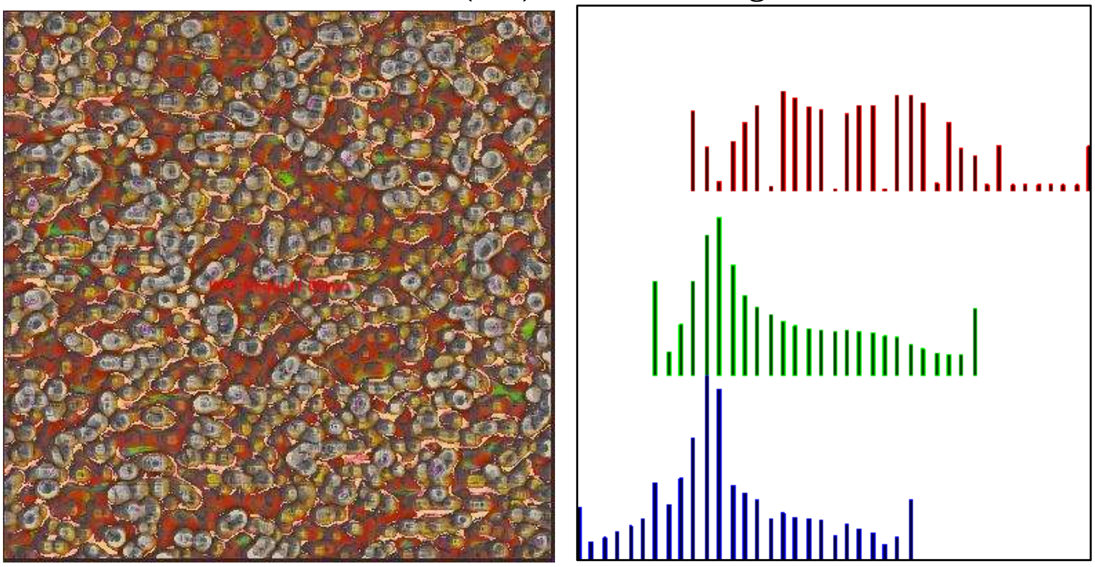

ZnO: Sn (7%) after annealing

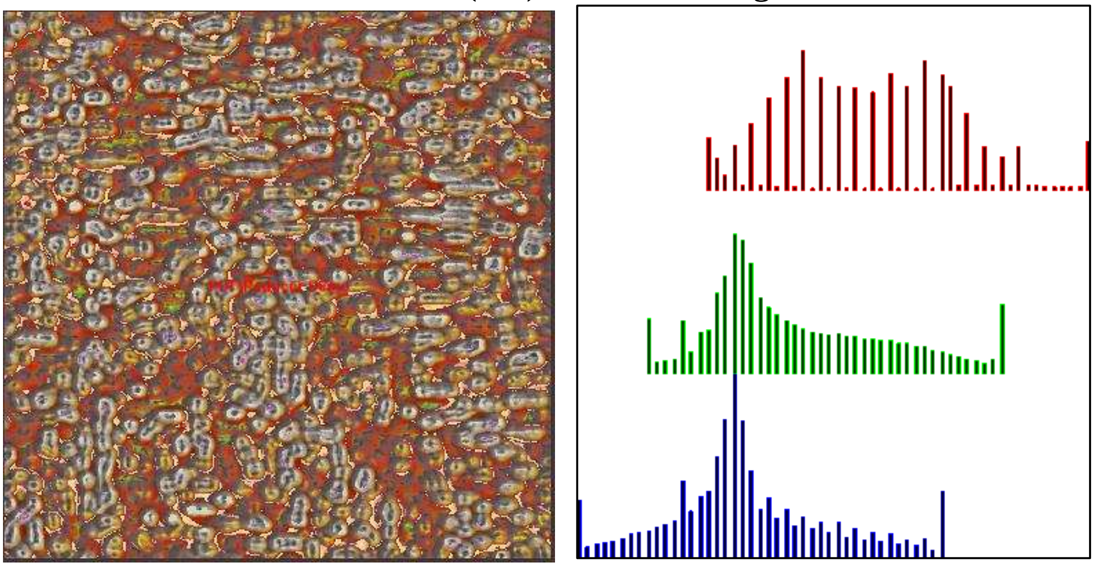

Zno: Sn (9%) after annealing.

Figure (4-52) histogram stretch technique for pure and doping thin films.

4.8.3 Convert color to gray

Figure (4-53) shows applied the (convert color to gray then histogram) technique to the images in Figure (4-50).

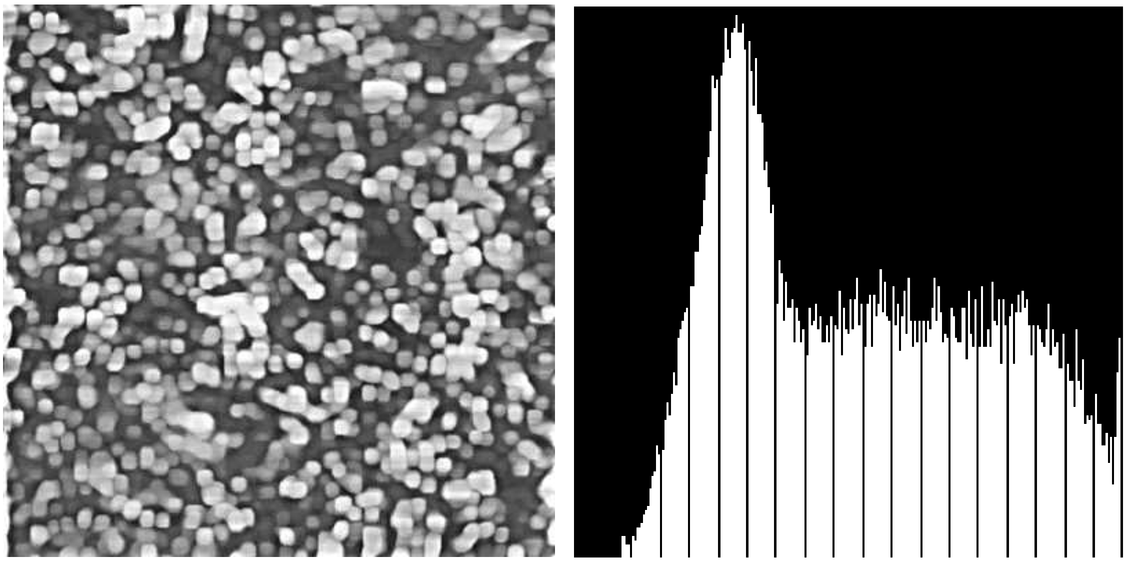

ZnO: Sn (0%) after annealing

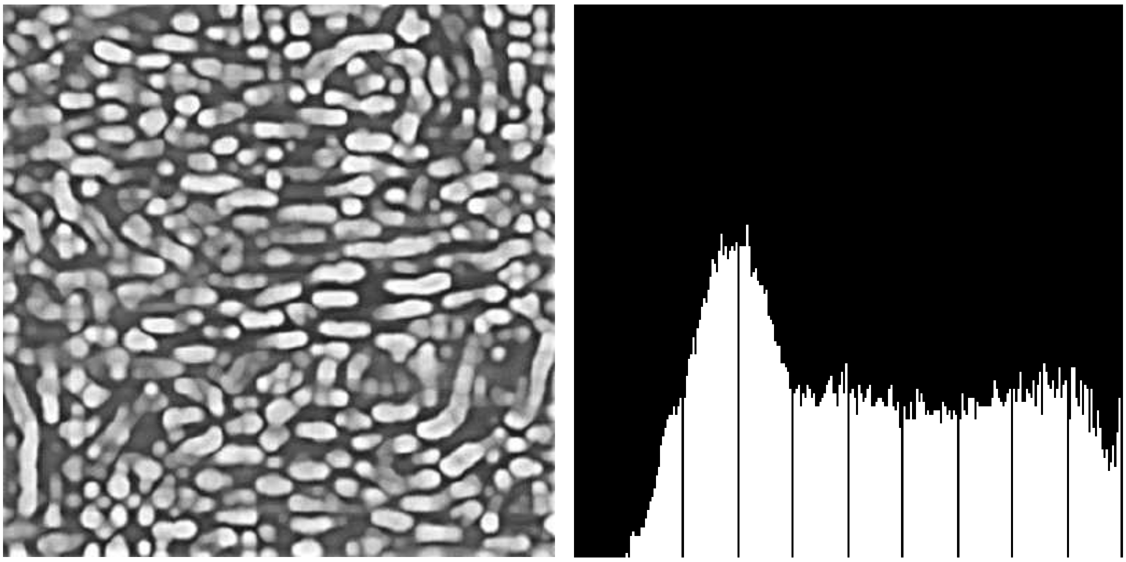

Zno: Sn (3%) after annealing

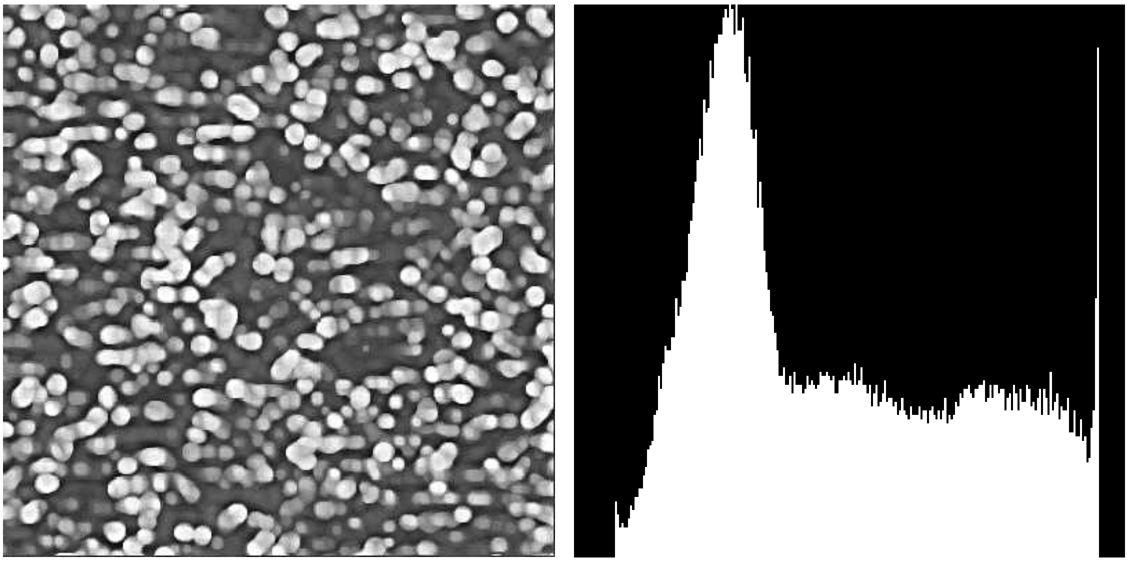

ZnO: Sn (7%) after annealing

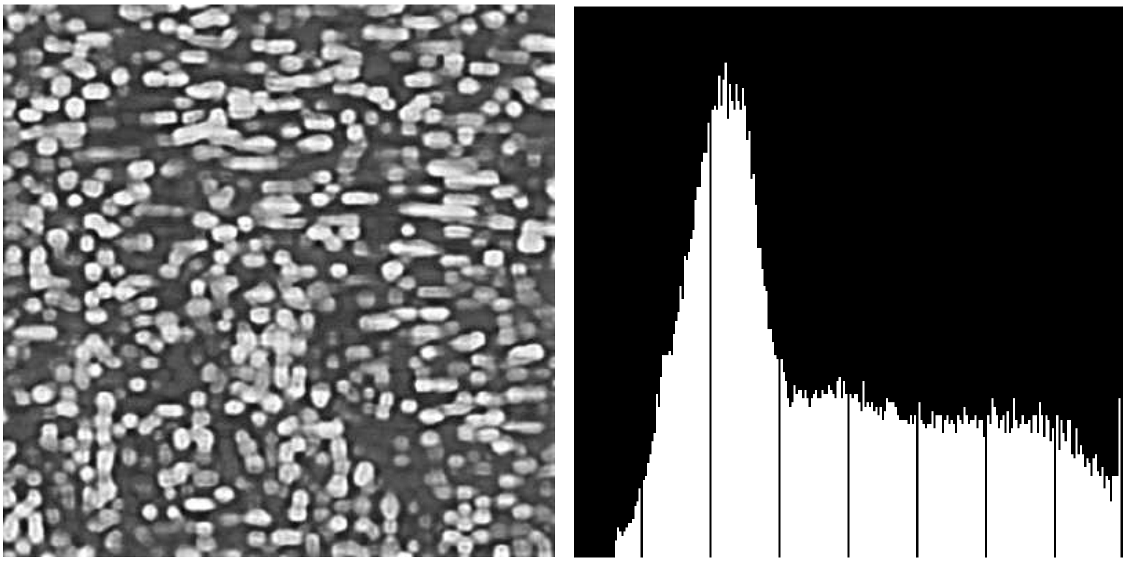

Zno: Sn (9%) after annealing

Figure (4-53) convert color to gray for pure and doping thin films.

4.8.4 Transformation

Figure (4-54) shows the (transformation) technique by using wavelet to the images in figure (4-47). Then segmentation technique by using multi-resolution to the image in above step. Finally cropped (400x400)pixels the result images from segmentation image. This method is used to work in the frequency domaine and is processed by segmentation and getting the figures listed in order to observe the change in histogram.

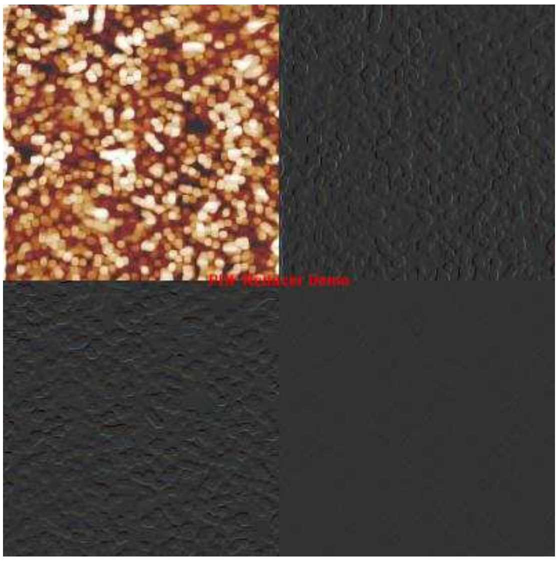

ZnO: Sn (0%) after annealing

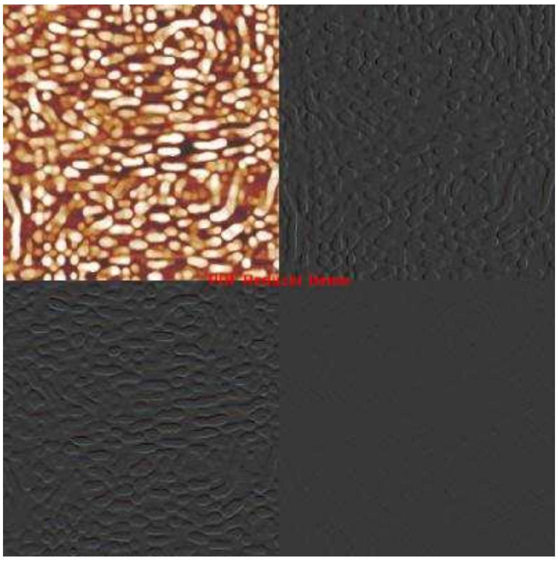

Zno: Sn (3%) after annealing

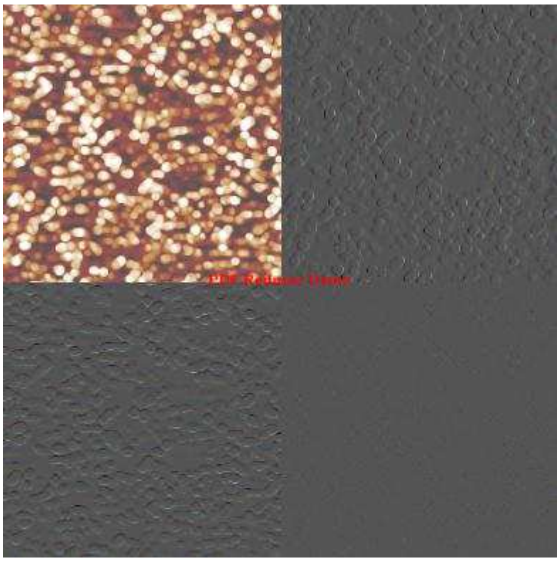

ZnO: Sn (7%) after annealing

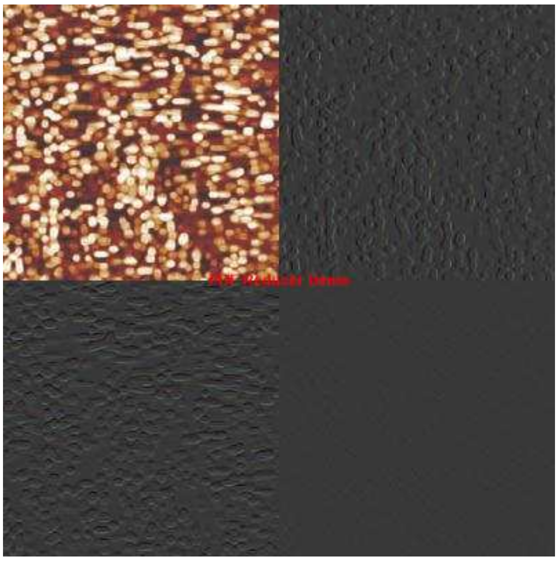

Zno: Sn (9%) after annealing

Figure (4-54) (segmentation) for pure and doping thin films.

- ***Histogram specification***

Figure (4-55) shows the (histogram specification) technique when applied to the images in Figure (4-54). This method used to determine the roughness and topography of the surface of thin films and the extent of regularity of this surface, where these results gave a distinct form of the following figures note that the values of high and low are negative direction.

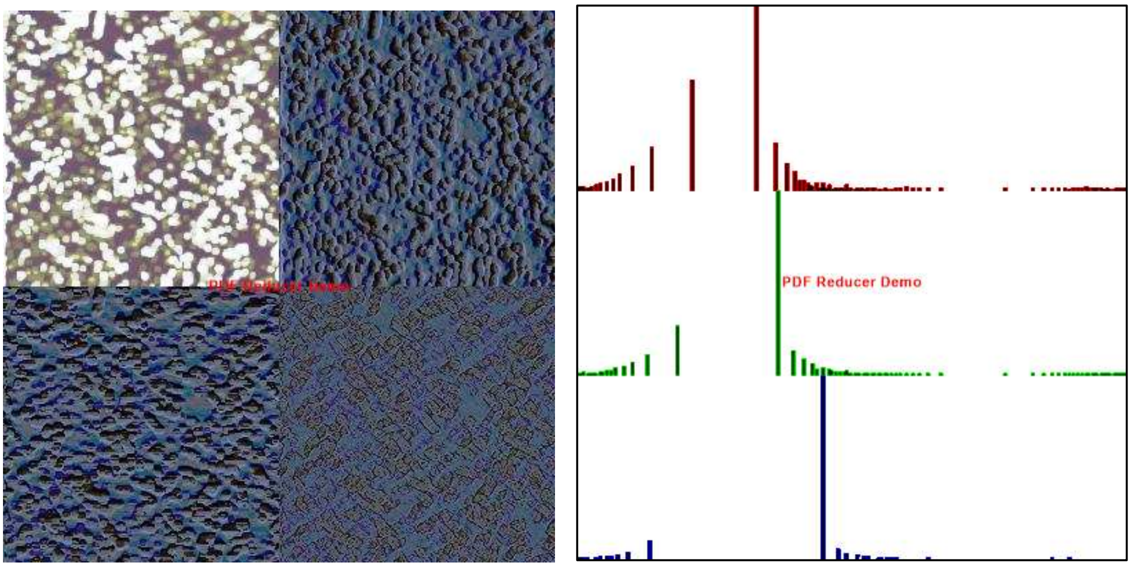

ZnO: Sn (0%) after annealing

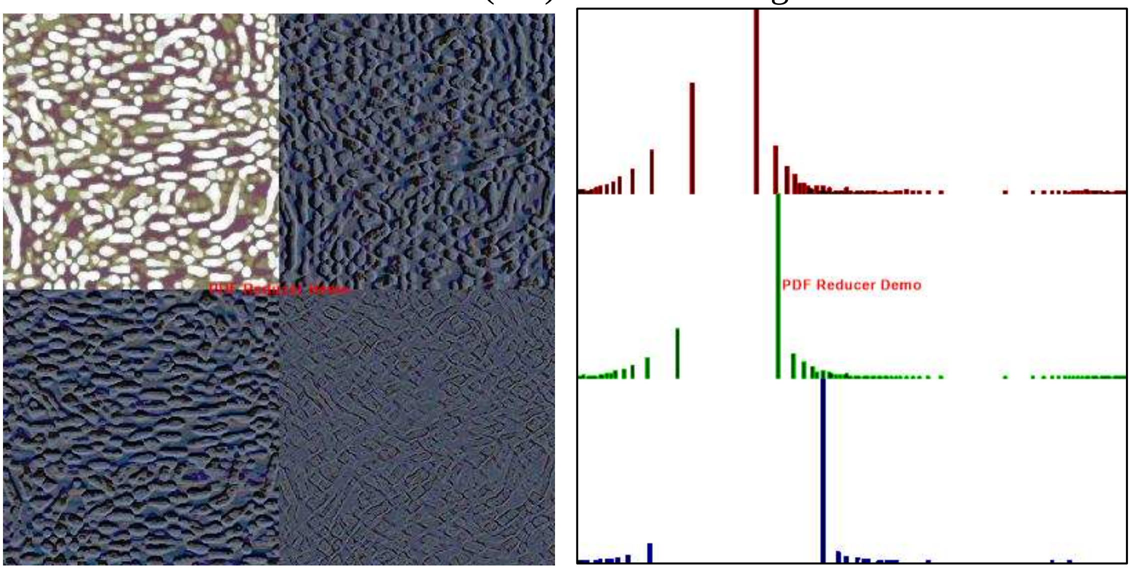

Zno: Sn (3%) after annealing

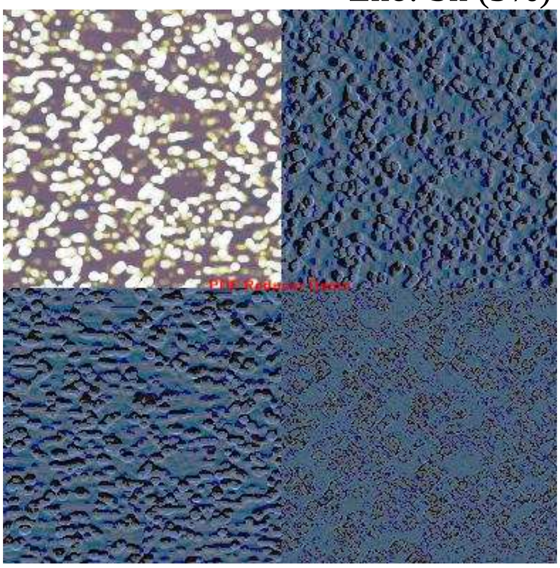

ZnO: Sn (7%) after annealing

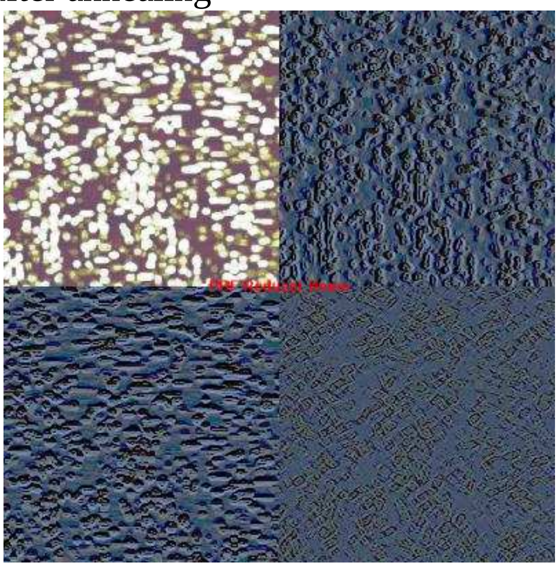

Zno: Sn (9%) after annealing

Figure (4-55) histogram specification for pure and doping thin films.

4.8.5 Edge-detection

Figure (4-56) shows the (Roberts) operator when applied to the images in Figure (4-47).

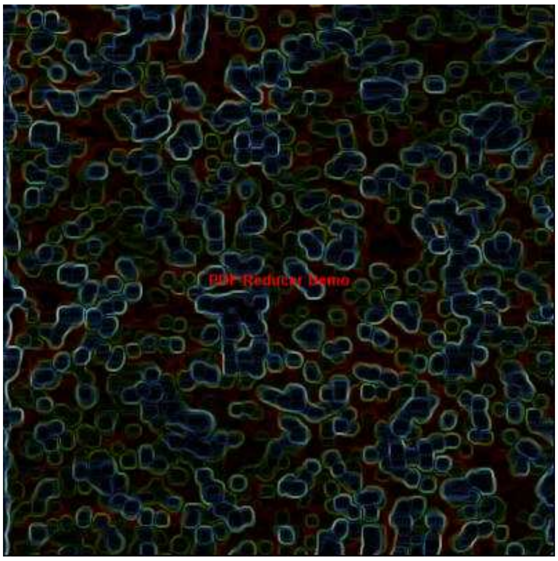

ZnO: Sn (0%) after annealing

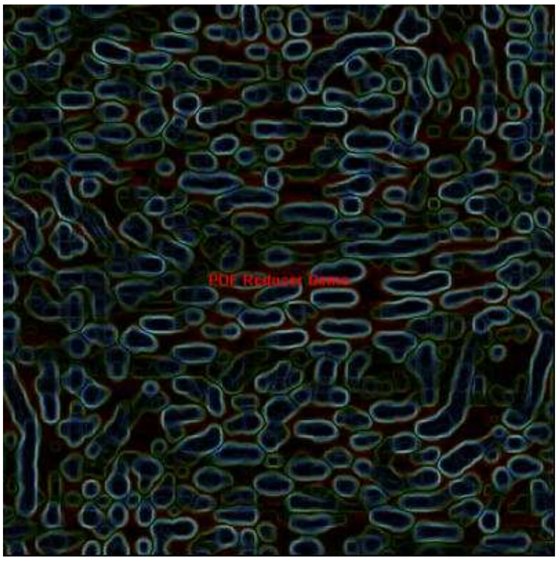

Zno: Sn (3%) after annealing

ZnO: Sn (7%) after annealing

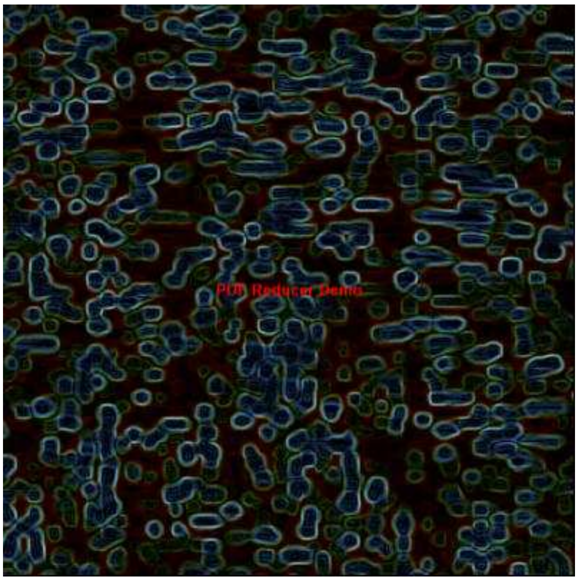

Zno: Sn (9%) after annealing

Figure (4-56) 'Roberts' edge detection for pure and doping thin films.

Figure (4-57) shows the (sobel) operator when applied to the images in Figure (4-47). This operater gives the output in two and three dimantion. The both output images can be a good choice to give a true reference to examine the roughness of the surfaces.

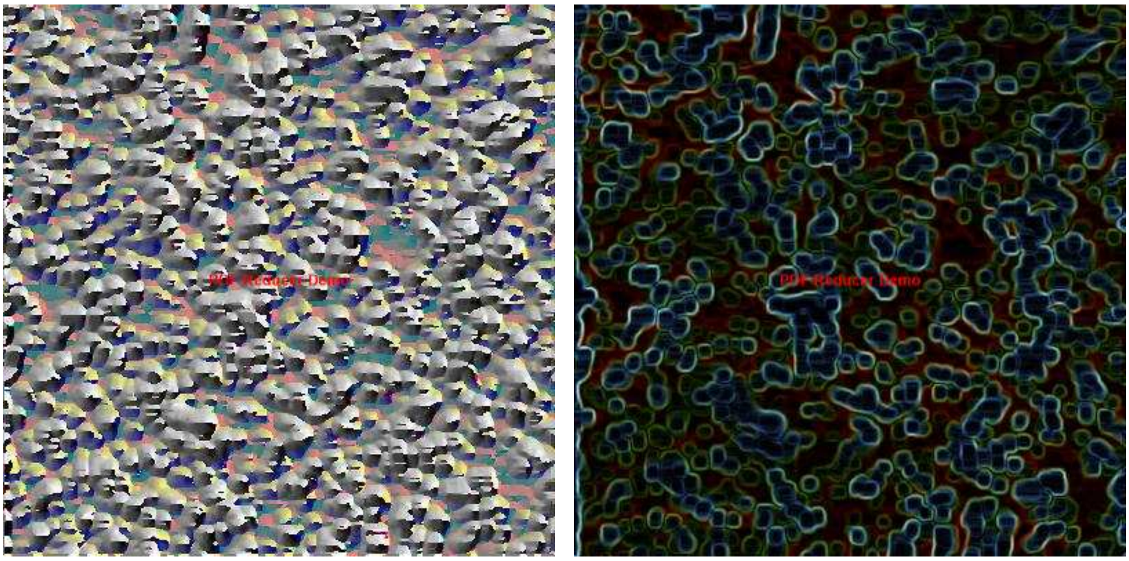

ZnO: Sn (0%) after annealing

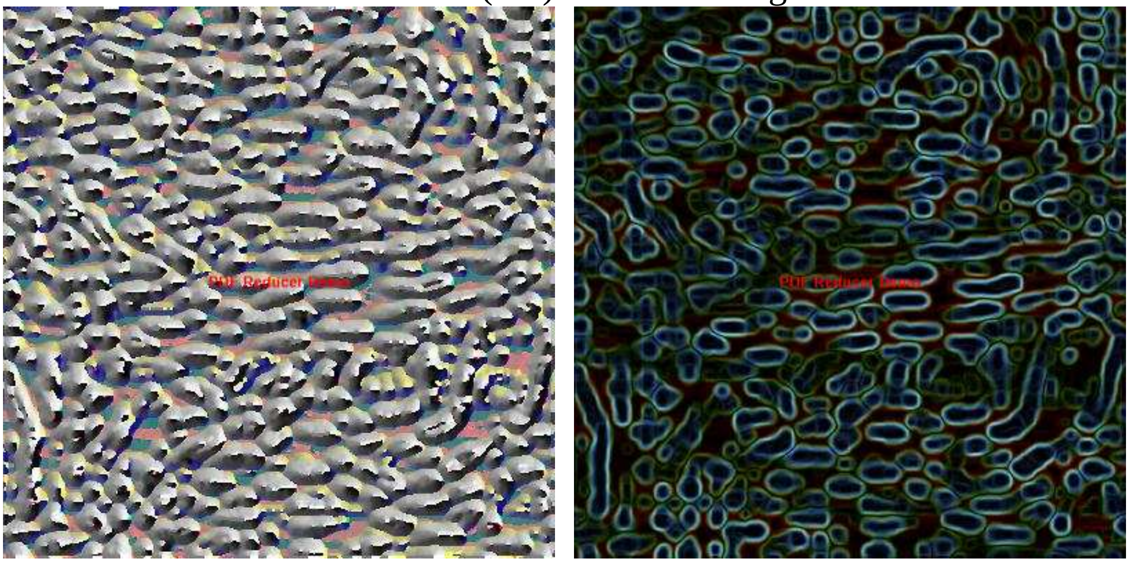

Zno: Sn (3%) after annealing

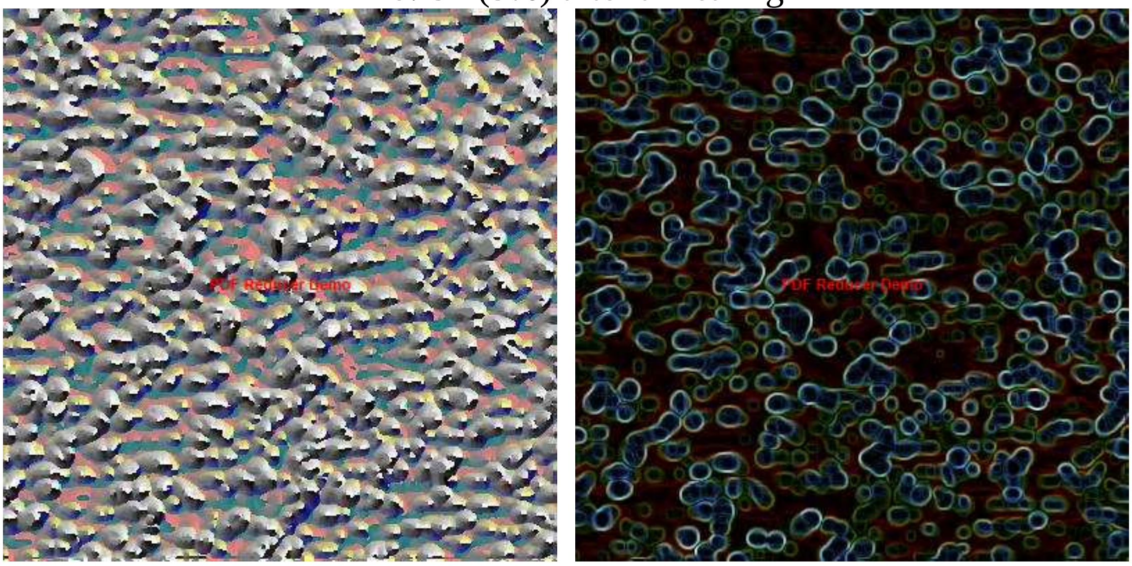

ZnO: Sn (7%) after annealing

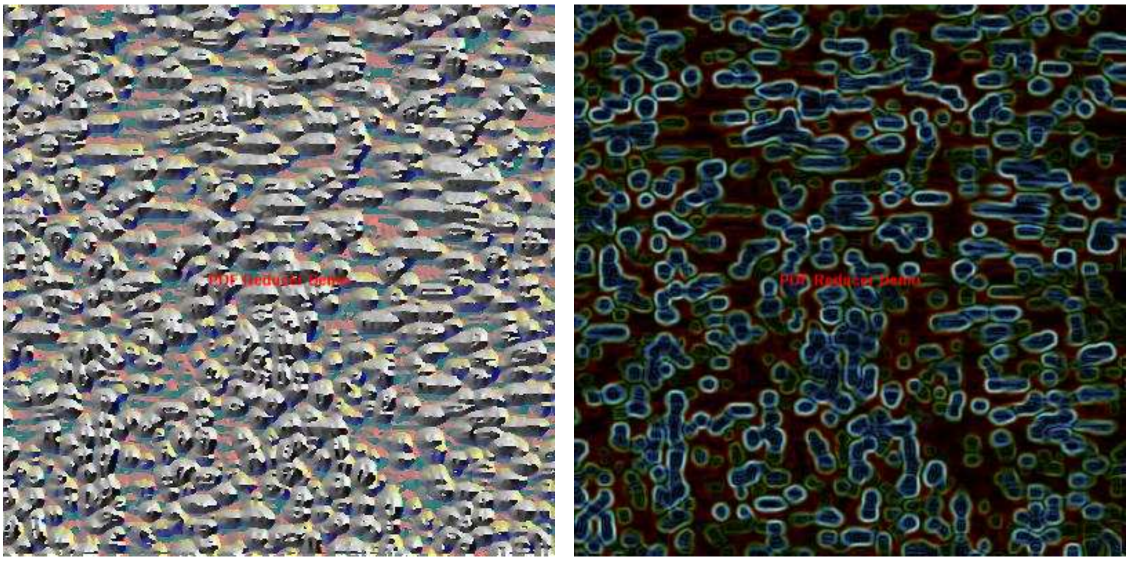

Zno: Sn (9%) after annealing

Figure (4-57) 'Sobel' edge detection for pure and doping thin films.

Figure (4-58) shows applied the (Prewitt) operator to the images in Figure (4-47). This operator gives a clear edge of the high and dips boundareas.

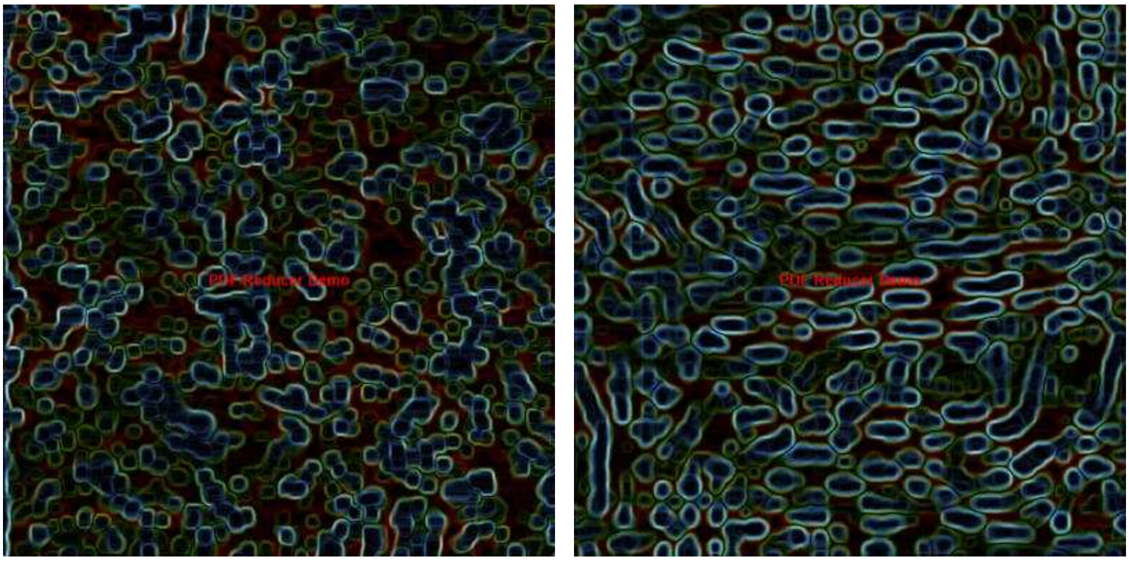

ZnO: Sn (0%) after annealing Zno: Sn (3%) after annealing

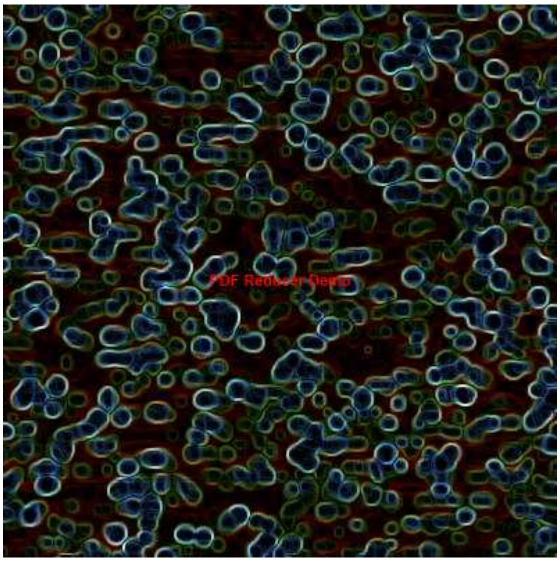
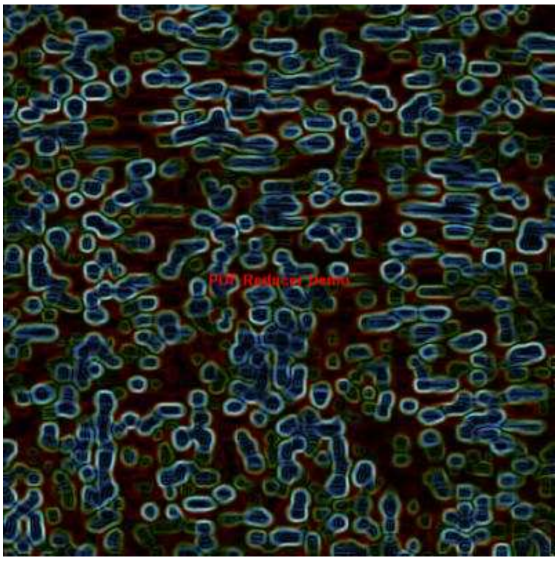

ZnO: Sn (7%) after annealing Zno: Sn (9%) after annealing

Figure (4-58) 'Prewitt' edge detection for pure and doping thin films.

Figure (4-59) shows the (Laplacian) operator when applied to the images in figure (4-47).

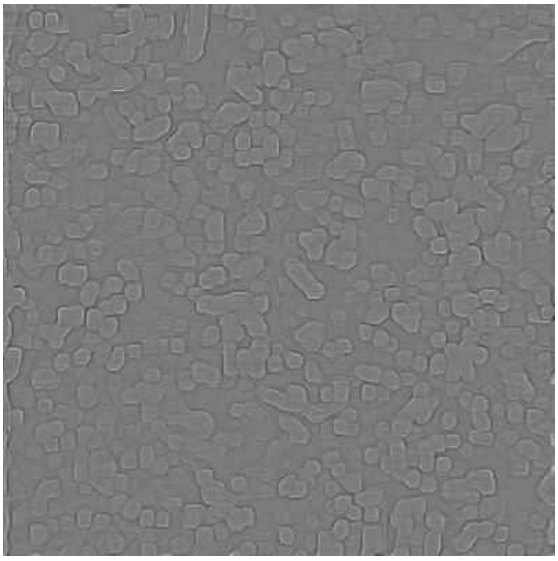
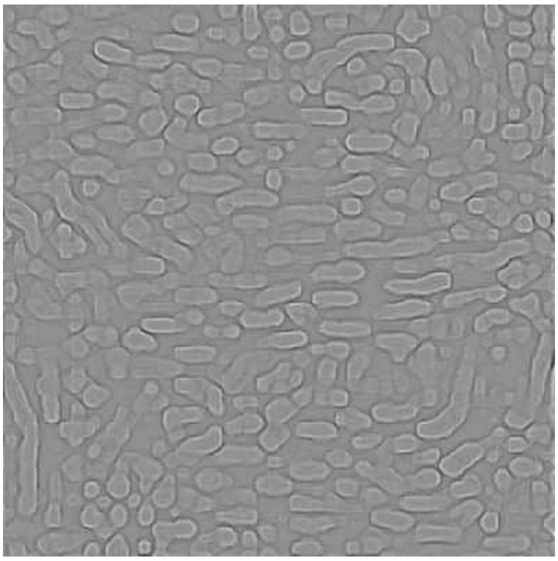

ZnO: Sn (0%) after annealing Zno: Sn (3%) after annealing

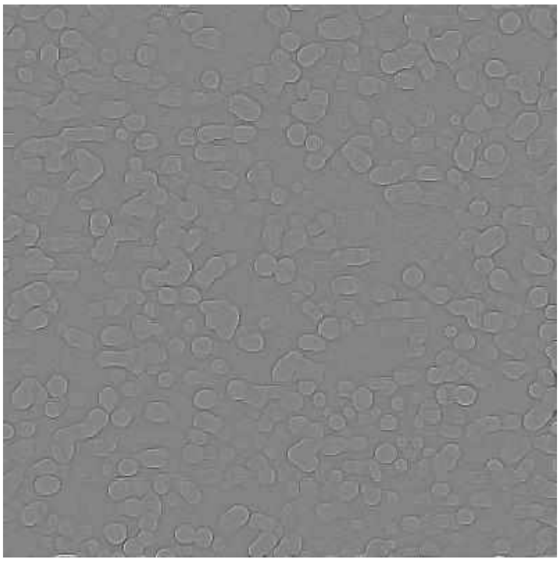
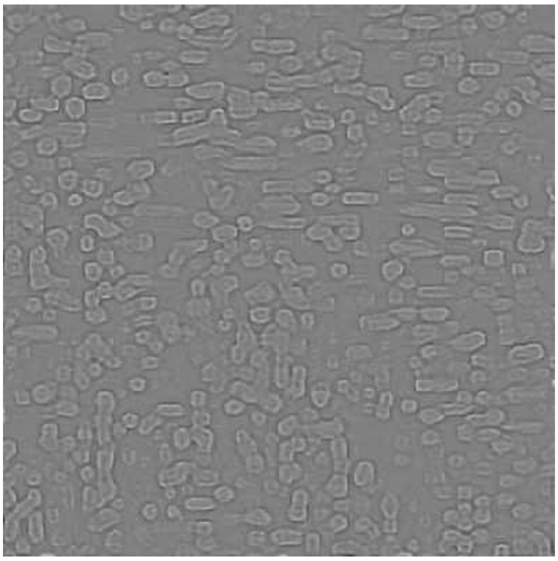

ZnO: Sn (7%) after annealing   Zno: Sn (9%) after annealing

Figure (4-59) 'Laplacian' edge detection for pure and doping thin films.

Figure (4-60) shows the (histogram stretch) operator when applied to the images in Figure (4-47). We can notice the quality of the output images specialy after anealing where the variation of the bounaries is clear and distinguishable for the listed images.

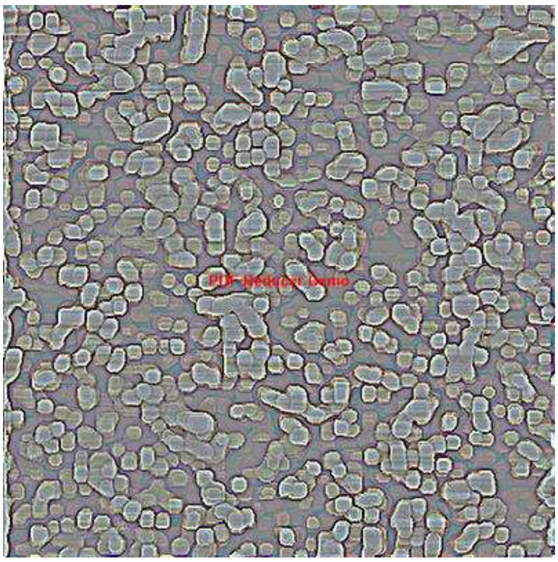
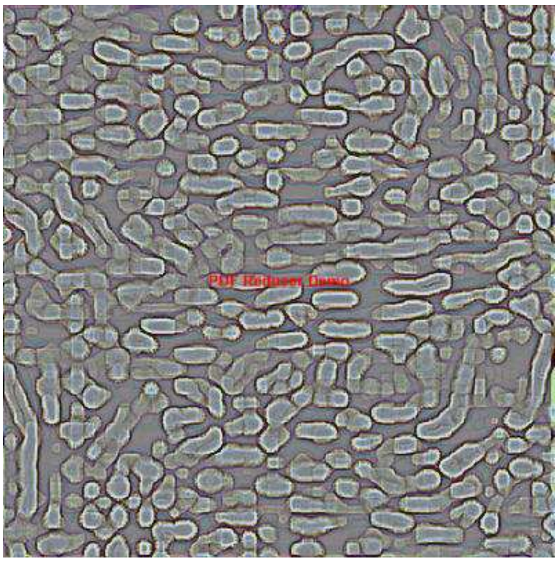

ZnO: Sn (0%) after annealing   Zno: Sn (3%) after annealing

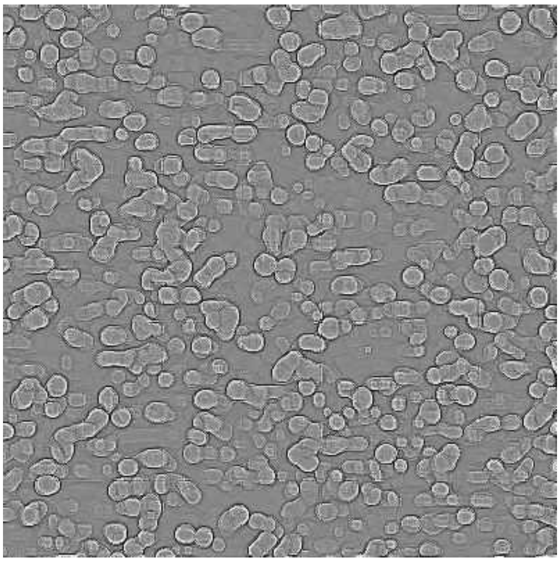

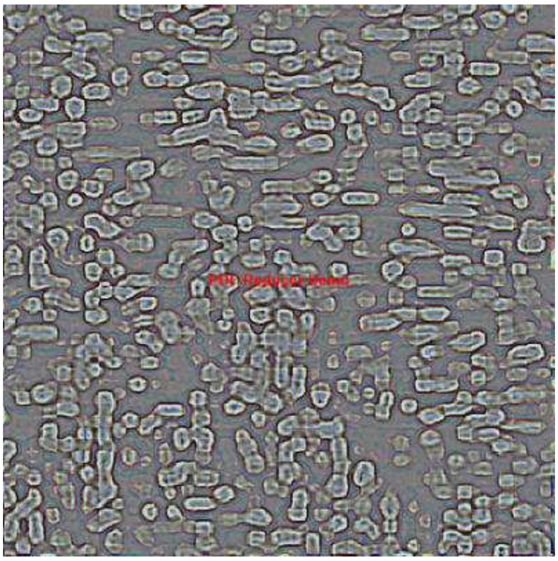

ZnO: Sn (7%) after annealing Zno: Sn (9%) after annealing

Figure (4-60) histogram stretch for pure and doping thin films.

Figure (4-61) shows the (Canny) operator when applied to the images in figure (4-47) then histogram specification.

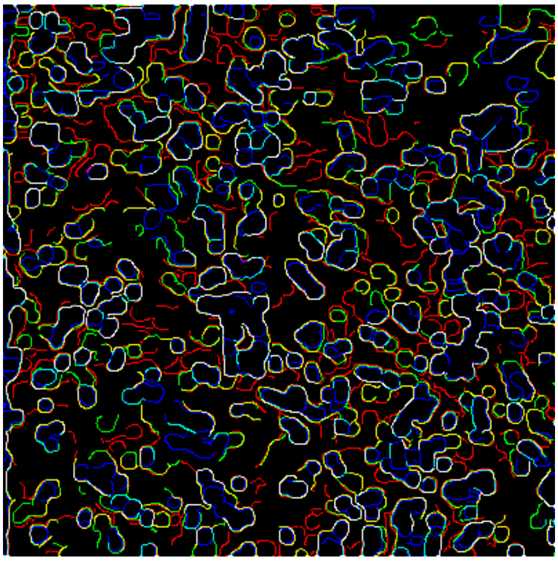

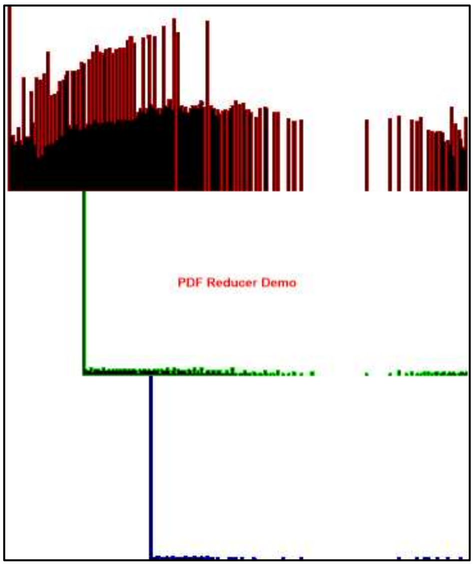

ZnO: Sn (0%) after annealing**.**

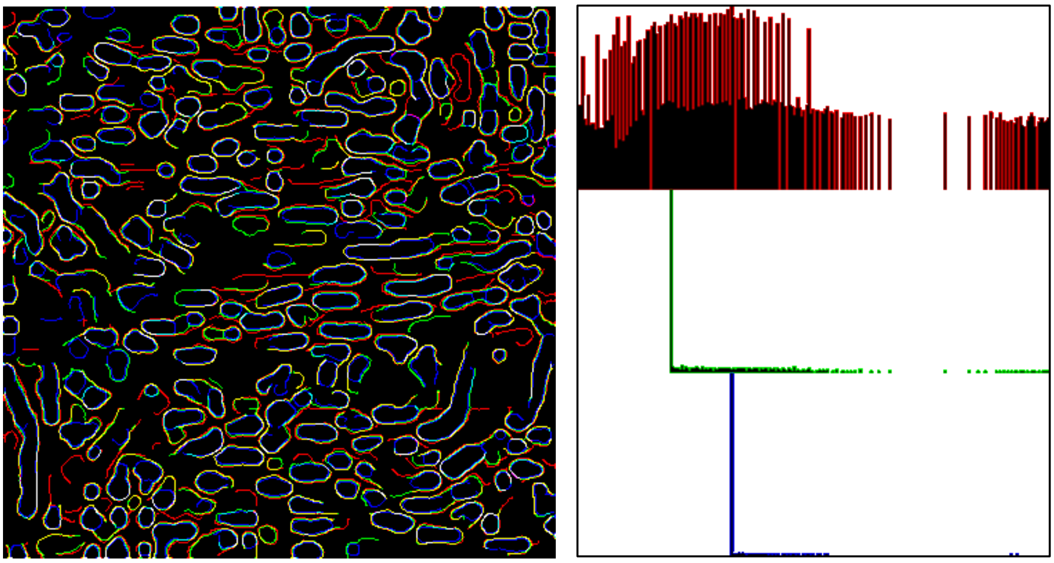

Zno: Sn (3%) after annealing

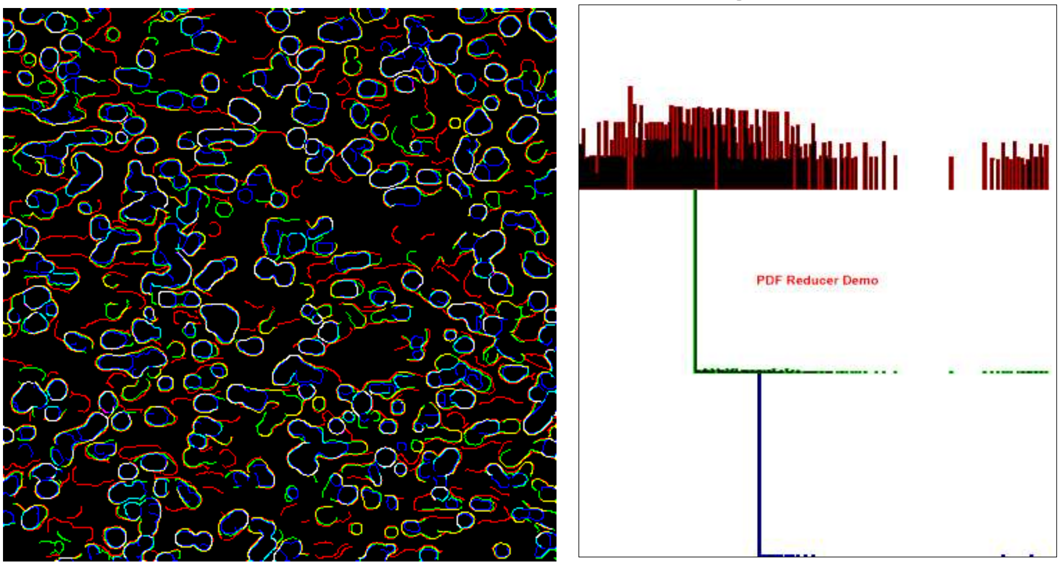

ZnO: Sn (7%) after annealing

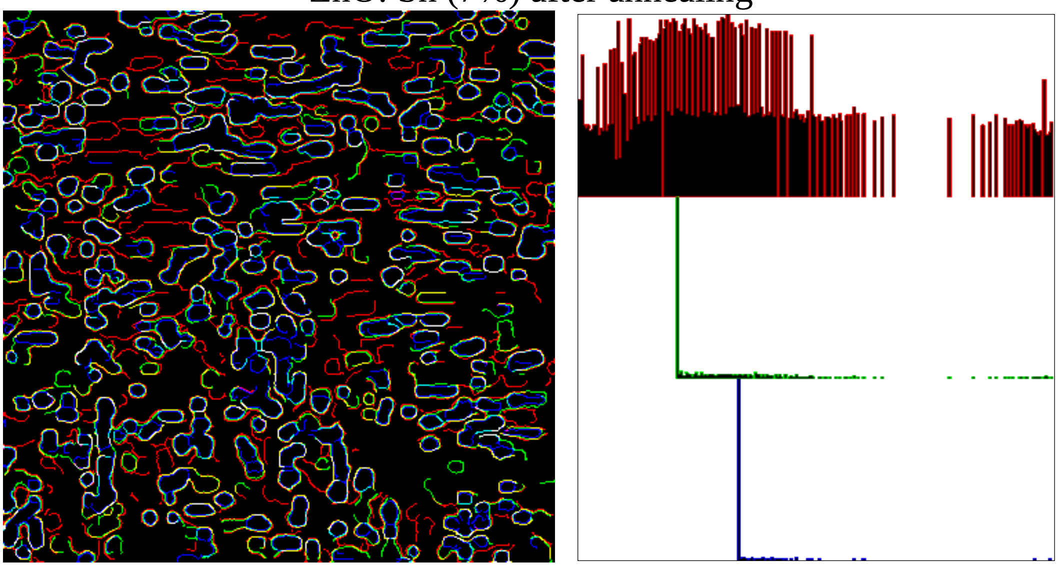

Zno: Sn (9%) after annealing

Figure (4-61) 'Canny' edge detection for pure and doping thin films.

Chapter Five

Conclusion And Future Works

Conclusions and Suggestion for Future works

5.1 conclusions

The pattern of (XRD) for pure (ZnO) thin films with thickness (200) nm are a polycrystalline hexagonal wurtzite structure, the orientation along (100), (002) and (101) planes are shifted toward the larger (2Ө). This behavior of the relation between crystalline size and the grain size are compatible for XRD and AFM techniques.

The pattern of (XRD) for doped (ZnO) thin films have a polycrystalline hexagonal wurtzite structure, and the planes are shifted toward the smaller (2θ). The (FWHM) are stable for percentage (3, 5%) while for percentage (7, 9%) increase slightly with doping. The crystalline size decrease with doping from (31.2 nm) to (19.1 nm). The UV-VIS measurement of doped thin films have higher transmission around (95%) at percentage (5%) and the lower transmission around (23%) at percentage (9%). The previous result mean that the transmission decrease with doping. The absorption coefficient for all doped thin films have direct electronic transition. The energy gap decrease with doping except for percentage (7, 9%) increase slightly with doping.

The pattern of (XRD) for doped (ZnO) thin films after annealing have a polycrystalline hexagonal wurtzite structure. The crystalline size increase with annealing for doped thin films. This results matches the results gained from (AFM) images. The transmission curves are increasing after annealing for doped thin films (ZnO:Sn), while the pure thin film decrease to reach (74%). The absorption coefficient after annealing is a direct electronic transmission. The energy gap decrease after annealing for doped thin films through (3 & 5)% percentages while it increasing for percentage (7 & 9%).

The results gained from image processing techniques are the variation of the images variables. The histogram stretch Note that the particle size and roughness are matches the previous results and clear observation for these changes. The changes in thickness, doping rate and annealing process are verified with the output images. Histogram specification Observe the clear reflectivity of the grains. The DCT sharpening give clear gain boundaries for the grains.

5.2 Suggestion for Future works

1- Apply these techniques to (SEM) images.

2- Calculating grain size and roughness utilizing image processing techniques from surfaces images.

3- Use of sputtering methods for doping thin films and comparing the obtained results between the different doping methods.

References

References

[1] M. Ohring, Materials Science of Thin Films, 2nd Edition, Academic Press, 2001.

[2] G. Hass, *Physics of Thin Films*, Academic Press, Vol. 1, Academic Press, 1963.

[3] Anthony R. West, *Solid State Chemistry and its Applications*, 2nd Edition, John willey & Sons, Singapore, 2014.

[4] Kasturi L. Chopra, *Thin Film Phenomena*, McGraw-Hill, New York, 1969.

[5] D. A. Glocker, S. I. Shah, *Handbook of Thin Film Process Technology*, Institute of Physics, Bristol, 1995.

[6] S. Franssila, *" Introduction To Micro fabrication"*, John Wiley and Sons, England, 2004.

[7] Péter B. Barna, *History of Thin Films*: *Growth, Techniques, Characterization*, Research Institute for Technical Physics and Materials Science of HAS Budapest, Hungary, 2005.

[8] G. Hass, Rudolph E. Thun, *Physics of Thin Film*, Academic Press, New York, 1964.

[9] J. Venables, *Introduction to Surface and Thin Film Processes*, Cambridge University Press, 2000.

[10] M. F. Costa, "Automated Analysis of Electrophoretic Gels by Image Digitalization and Processing ", *The Imaging Science Journal*, 48(4): 177-183, 2000.

[11] M. Mattox Donald, *Handbook of Physical Vapor Deposition PVD) Processing*, 2nd Edition, Elsevier, 2010.

[12] L. B. Freund, S. Suresh, *Thin Film Materials: Stress, Defect Formation, and Surface Evolution*, Cambridge University Press, U.K., 2004.

[13] K. Wasa, M. Kitabatake, H. Adachi, *Thin Film Materlals Technology*, William Andrew, 2004.

[14] R. K. Gupta, N. Shridhar, M. Katiyar, Structure of ZnO films prepared by oxidation of metallic Zinc, *Materials Science in Semiconductor Processing*, 5, 11–15, 2002.

[15] M. Krunks, *Thin Films for Photovoltaic by Chemical Methods*, Tallinn University of Technology, Estonia, 2004.

[16] G. Nilens, Deep Impurity in Semiconductors, Wiley-Inter Science Publication, 1973.

[17] J. C. C. Tsai, *Diffusion*, Mc Graw – Hill, New York, 1983.

[18] S. M. Sze, *Semiconductors Devices Physics and Technology*, 2nd Edition, Wiley, 2008.

[19] C. Kittel, *Introduction to Solid State Physics*, 6th Edition, Wiley, 1986.

[20] H. Mehrer, *Diffusion in Solid Metals and Alloys*, Springer Verlag, Berlin, 1990.

[21] J. Crank, *Mathematics of Diffusion*, 2nd Edition, Oxford Univ. 1975.

[22] Ali, B. Okba, S. Gareh, S. Benramache, The calculation of band gap energy in Zinc Oxide Films, *Journal of Semiconductors*, 36(1), 1-6, 2015.

[23] Roth, D. Williams, Properties of ZnO Films Prepared by Oxidation of diethyl zinc, *J. Appl. Phys.*, 52(11), 6685-6686, 1981.

[24] Z. Lin Wang, Zinc oxide nanostructures: growth, properties, and Applications, J. Phys.: Condens. Matter, 16, 2004, R829–R858.

[25] S. I. Saleh, Optical and structure properties of Mg-doped ZnO thin films, Diyala Journal for Pure Sciences, 10(2), 34-44, 2014.

[26] Jagadish, S. J. Peurton, Zinc Oxide Bulk, Thin Films, and Nano-structures: processing, properties and Application, Elsevier, 2006.

[27] S. J. Pearton, D.P.Norton, K.Ip, Y.W.Heo, T.Steiner, Recent progress in processing and properties of ZnO. Superlattices and Microstructures,

34, 3-32, 2004.

[28] F. James, Jr. Carlin, *Mineral Commodity Summary Tin*, United States Geological Survey, 2008.

[29] M. Schwartz, *Tin and Alloys Properties*, Encyclopedia of Materials, 2nd Edition, CRC Press, 2002.

[30] N. N. Greenwood, A. Earnshaw, Chemistry *of the Elements*, 2nd Edition, Oxford, Butter Worth, 1997.

[31] S. William, F. Geoffrey and H. Ralph, *General Chemistry Principles and Modern Applications*, Pearson Education, New Jersey, 2007.

[32] R. Palmieri, *Pipe Metal, Encyclopedia of Keyboard Instruments,* pp:411, New York, 2006.

[33] R. Sami Ali, " Study the structural properties for CdO Thin Films doped with Sb utilizing image processing techniques. MSc. Thesis, University of Mustansyria, 2008.

[34] S. Aksoy, Y. Caglar, S. Ilican, M. Caglar, "effect of Sn dopants on the optical and electrical properties of ZnO films", *Optical Applicata*, XL(1), 7-14, 2010.

[35] N. chahmat, A. Haddad, A. Ain-Souya, R. Ganfoudi, N. Attaf, M. Salah Aida, M. Ghers, "effect of Sn doping on the properties of ZnO thin films prepared by spray pyrolysis", *journal of modern physics*, 3, 1781-1785, 2012.

[36] S. Palimar, K. V. Bangera, G. K. Shivakumar, "Study of the doping of thermally evaporated zinc oxide thin films with indium and indium oxide", *applied nanoscience*, 3(6), pp:549–553, 2013.

[37] S. J. Mohammed, K. I. Khaleel, Q. A. Abd-Aljabbar, "Study the Doping Effect of Nickel on the Optical Properties of ZnO) Thin Films", *Tikrit Journal of Pure Science*, 18(4), pp:175-182, 2013.

[38] N. sadananda Kumar, Kasturi V. Bangera, G. K. Shivakumar,"Effect of annealing on the properties of zinc oxide nanofiber thin films grown by

spray pyrolysis technique", *applied nanosience*, 4(2), pp:209–216, 2014.

[39] K. Chongsri, Ch. Bangbai, W. Techitdheera and W. Pecharapa,characterization and photoresponse properties of Sn-doped ZnO thin films, *Sciverse Science Direct*, 34,pp 721-727, 2013.

[40] M. Fakhar-E-Alam, M.A. Asghar, U. Nazar, S. Javed, Z. Iqbal, M. Atif, S. M. Ali, W. A. Farooq,"characterization of Zinc oxide ZnO) thin films coated by thermal evaporation technique", *journal of optoelectronics and biomedical materials*, 6), pp:35-40, 2014.

[41] N. chahmat, T. souier, A. Mokri, M. Bououdina, M. S. Aida, M. Ghers, Structure, microstructure and optical properties of Sn-doped ZnO thin films, *journal of alloys and compounds*, 593, pp:148-153, 2014.

[42] S. I. Saleh,optical and structural properties of Mg doped ZnO thin films, *Diyala journal for pure sciences*, 10(2), pp: 34-44, 2014.

[43] F. Z. Bedia, A. Bedia, M. Aillerie, N. Maloufi, B. Benyoucef, Structural Optical and Electrical Properties of Sn-doped Zinc Oxide Transparent Films Interesting for Organic Solar Cells OSCs), *Energy Procedia*, 74, 539-546, 2015.

[44] Mugwang'a FK, Karimi PK, N joroge WK and Omayio O characterization of aluminum doped Zinc oxide AZO) thin films prepared by reactive thermal evaporation for solar cell applications, 5(4), pp1-6, 2015.

[45] N. H. Sheeba, S. C. Vattappalam, J. Naduvath, P. V. Sreenivasan, S. Mathew, R. R. Philip,"effect of Sn doping on properties of transparent ZnO thin films prepared by thermal evaporation technique", *chemical physical letters*, 635, pp: 290-294, 2014.

[46] Zair, A. Meftah, A. Y. Jaber, A. A. Abdelaziz, M. S. Aida, "annealing effects on the structural, electrical and optical properties of ZnO thin films prepared by thermal evaporation technique", Journal of King

Saud University – Science, 27,pp:356-360, 2015.

[47] M. Khudhr M., Kh. Haneen Abass, "effect of AL-doping on the optical properties of ZnO thin films prepared by thermal evaporation technique", *international journal of engineering and technologies,* 7,pp:25-31, 2016.

[48] Najei Hussein Al-Jamal, "Applications of Image Processing techniques on Structural and Optical Properties for different Molarities of ZnO and Sn Nanostructure thin film", Ph. D. Thesis، Al-Mustansiriya University 2016.

[49] N. Thornes "the Science and Engineering of Materials" Book, 3th, 1996.

[50] G. Streetman and S. Banerjee, "Solid State Electronic Devices", 5th Ed., Prentice Hall, Inc., New Jersey 2000.

[51] D .R .Lide, "*in chemical rubber company handbook of chemistry and physics"* CRC Press, Bocaraton,Florida USA,11th editions, 1996.

[52] N. F. Mot and E. A. Davis, "*Electronic Processes in Non-Crystalline Materials*", Clarendon Press, Oxford, 1979.

[53] J. Tauc, "*Amorphous and Liquid Semiconductors*", Plenum Press, London and New York, 1974.

[54] J. S. Blakmore, " *Solid State Physics*", Cambridge Press, 2nd edition, 1986.

[55] Kittle, "Introduction to Solid State Physics", John Wiley and Sons, Inc., 7th edition, 1996.

[56] J. S. Blakmore, "*Solid State Physics*", 2nd Edition, Cambridge University Press, 1986.

[57] W. D. Callister, "*Materials Science and Engineering: An Introduction*", John Wiley & Sons, Inc, New York, 2007 .

[58] R. West " Basic solid state chemistry", John wily and sons, 1999.

[59] Jagadish and S. J. Peurton "Zinc oxide Bulk, Thin films and Nano-

structures : processing, properties and Application" Book, Elsevier Science, 1 edition, 2006.

[60] M.A. Omer,"*Elementary Solid State Physics*", Addiso-We sly Publishing, 1975.

[61] J. P. Colinge and C. A. Colinge "*Physics of Semiconductor Devices*", Kluwer Academic Publishers, New York, 2007).

[62] B. E. Warren "*X-Ray Diffraction*", Addison-Wesley Publishing Company, Inc., USA, 1990.

[63] Y. Z. Wang and N. Yao, "*Handbook of Microscopy for Nanotechnology*",(2005.

[64] S. O. Kasap, "*principles of electronic materials and devices*", 2 nd edition,Mc Graw Hill, New York, 2002.

[65] J, Tauc "*Amorphous and liquid semiconductor*", Plenum press, London, 1974.

[66] J. I. Pankove, "*Optical Processes in Semiconductors*", Prentice-Hall, New Jersey, 1971.

[67] S. Ben, "*Solid State Electronic Devices*" Hall International, Inc, U.S.A, 1990.

[68] J. S. Blakmore, "*Solid State Physics*", 2nd Edition. Cambridge University Press, 1986.

[69] H. Clark, "Optical properties of polycrystalline and amorphous thin films and devices ", edited by Laurece. L. Kazemerki, Academic press, 1960.

[70] J. C.Wilson, "X-Ray Optics", London: Methnen & Coltd New York: John Wiley & Sons INC, PP. 1-5, 1962.

[71] Saporal and C. Herman, "Physics Of Semiconductors", University of New York, 1995.

[72] A. Neamen, " Semiconductor Physics and Devices ", University of New Mexico, 1992) .

[73] M. Abdul Majeed, A. N. Abd, N. F. Habubi," Fabrication and Characterization of Copper Oxide Nanoparticles/Psi Heterodiode" International Letters of Chemistry, Physics and Astronomy Vol. 57 pp 25-35, 2015.

[74] T. Young, G. j. Acob and L. J. Vanvliet, "Fundamentals of Image Processing",Printed in The Netherlands at the Delft University of Technology, ISBN 90-75691, NUGI 841, 1998.

[75] F. Canny, "Finding Edges and Lines in Images",Mssachusetts Institute of Technology, June 1983.

[76] http://cse3521.artifice.cc/image-convolutions transformations.html.

[77] Maini, R., & Aggarwal, H. "A Comprehensive Review of Image Enhancement Techniques" . *Jounal of Computing*, 2(3), 8-13, 2010.

[78] https://www.tutorialspoint.com/dip/gray_level_resolution.htm

[79] Gomes and L. Velho, "Image Processing for computer Graphics", Springer, New York, 1997.

[80] https://blogs.mathworks.com/steve/2012/02/20/writing-image-files/

[81] Katherine, "Genetic Influences on Brain Structure", Thompson. Loni. Vcla. edv. htmL. October, 2001.

[82] https://www.mathworks.com/help/images/examples/finding-vegetation-in-a-multispectral-image.html.

[83] R. C. Gonzalez, R. E. Woods "*Digital Image Processing*", 3rd Edition. Pearson Prentice Hall. ISBN 978-0-13-168728-8, 2008.

[84] Tsui JM, Pack CC, “Contrast sensitivity of MT receptive field centers and surrounds” *J Neurophysiol*, 106(4):1888-900, 2011.

[85] Hashemi H, Khabazkhoob M, Jafarzadehpur E, Emamian MH, Shariati M, Fotouhi A. “Contrast sensitivity evaluation in a population-based study in Shahroud, Iran.” *Ophthalmology*, 119(3):541-6, 2012.

[86] Jensen, J.R. *"Introduction to Digital Image Processing: A Remote Sensing Perspective"* .Practice Hall, New Jersey,1996.

[87] Lillesand, T. M. and Kiefer, R. *"Remote Sensing Image Interpretation"*. John Wiley, NewYork, 1993.

[88] R. Gonzales and P. Wintz, "*Digital Image Processing*",Addison Wesley Publishing Company, 1977.

[89] H. S. Kam, M. Hanmandlu And W. H. Tan, "*An Improved Image Enhancement Combining Smoothing and Sharpening*",Conference on Convergent The Technologies for the Asia-pacific Region, IEE, 2003.

[90] Oppenheim, Alan V., Ronald W. Schafer, and John R. Buck. *"Discrete-Time Signal Processing*". 2nd Ed. Upper Saddle River, NJ: Prentice Hall, 1999.

[91] https://users.cs.cf.ac.uk/Dave.Marshall/Multimedia/node231.html

[92] Suganya, Menaka, "various segmentation techniques in image processing: A survey" *proceedings of international conference on globel innovations in computing techniology*, 2, 1048-1052), 2014.

[93] https://www.imageprocessingbook.com.

[94] Barghout, Lauren, and Lawrence W. Lee, "*Perceptual information processing system,"* Paravue Inc. U.S. Patent Application 10/618,543, filed July 11, 2003.

[95] Marr, D & E. Hildreth, "Theory of edge detection", *Proc. Royal Society of London, B*, 207, 187–217, 1980.

[96] Senthilkumaran. N & R. Rajesh "Edge Detection Techniques for Image Segmentation–A Survey of Soft Computing Approaches", *International Journal of Recent Trends in Engineering*, Vol. 1, No. 2, 250-254, 2009.

[97] R. Gonzalez and R. Woods *"Digital Image Processing"*, Addison Wesley, pp 414 – 428, 1992.

[98] Gonzales, Rafael C. and Richard E. Woods. *"Digital Image Processing". 2nd ed*. Englewood Cliffs, NJ: Prentice-Hall, 2002.

[99] J. M. S. Prewitt "*Object Enhancement and Extraction*" in "Picture processing and Psychopictorics", Academic Press,1970.

[100] Young, Richard, "The Gaussian derivative model for spatial vision: I. Retinal mechanisms" *Spatial Vision*, 2 4): 273–293(21), 1987.

[101] G. R. Kandhasamy, S. Muruganand, phD, M. Pavithra," Surface study of ZnO thin film using image processing Techniques", *international Journal of Computer Application*, V70, no23: pp 26-28, 2013.

[102] K. L. Chopra and I. Kaur, " *Thin Film Device Applications* ", Plenum Press, New York, 1983.

[103] P. Prashanth," *Presentation of Thermal Evaporator* ", Indian Institute of Science Publication, 2010) .

[104] Venaables," Introduction to Surface and Thin Film Processes " Cambridge University Press,(2003.

[105] R. Phillip Scott, "*Measuring the Thickness of Thin Metal Films*",the faculty Brigham Young University – Idaho,MSc, 2012.

[106] Samir A. Maki, Alli A. Shehaband, Enase Y. Abed, "A study of structure and optical properties of ZnO thin films deposited by thermal evaporation technique under different flow rate of oxygen O_2" *Ibn Al-Haitham Jour. For pure & Appl*. Sci, 26 1), 137:143, 2013.

[107] E.Y. Abed, 2012) "Thickness influence on structure and optical properties of ZnO thin films prepared by thermal evaporation" *Ibn Al-Haitham Journal for pure and applied science*, 3,25, 179:185, 2012.

[108] A. Van der Drift *" Evolution are selection a principle governing growth orientation in vapor – deposited layers "* Philips Res, Rep., 267 -288, 1968.

[109] Y. J. Kim and H. J. Kim, "Trapped Oxygen in the Grain Boundaries of ZnO polycrystalline Thin films prepared by plasma-enhanced Chemical Vapor Deposition", *Materials Letters*, 41, 159-163, 1999.

[110] H. I. Adbulgafour N, Z. Hassan, N. Al-Hardan, F. K. Yam, "Growth of Zinc Oxide Nanoflowers by thermal evaporation Method", *physica B* 405, 2570-2572, 2010.

الخلاصة

في هذا البحث تمت دراسة الخواص التركيبية والبصرية لأغشية أوكسيد الزنك المحضرة بطريقة التبخر الحراري في الفراغ. بترسيب معدن الزنك النقي على قواعد زجاجيه بدرجة حرارة الغرفة (300K). حضرت الاغشية الرقيقة وبسمك nm (200). تمت عملية الاكسدة على اغشية الزنك عند درجة حرارة (673K) لمدة ساعة كاملة بوجود تدفق الهواء lit/s (2.5). أيضا تمت دراسة تأثير التشويب بمعدن القصدير على الخصائص التركيبية والبصرية بنسب تشويب wt%(3, 5, 7, 9). من ناحيه أخرى تمت دراسة تأثير عملية التلدين عند درجة حرارة (472K) على الخصائص التركيبية والبصرية. نمط حيود الاشعة السينية للأغشية المحضرة النقية والمشوبة أظهرت انها ذات تركيب سداسي متعدد التبلور، اما بالنسبة للاغشية المشوبة فان الحجم البلوري يزداد من (29.9 nm) للغشاء النقي الى (30.4 nm) للغشاء المشوب عند النسبة (5%) ثم يقل عند النسبة %(9 & 7). اما تأثير التلدين عند درجة حرارة (473K) على الحجم الحبيبي تكون بتناقص مستمر مع زيادة نسبة التشويب. ومن تقنية UV-visible عند المدى nm (1100 -300) تم حساب النفاذية والامتصاصية ومعامل الامتصاص وفجوة الطاقة البصرية.

تم استخدام تقنيات معالجة الصور الرقمية لصور مجهر القوة الذرية AFM . لقد تم تحسين الصور الرقمية واستخدام تقنيات التحويل وتقنيات اظهار الحواف لمشاهدة طبيعة سطوح الاغشية الرقيقة. تم استخدام الصفات التركيبية والبصرية للحصول على صفة مرجعية لتحديد نوعية الغشاء المحضر. الطرق الأخرى المستخدمة في هذا البحث هي تأثير التشويب والتلدين على طبيعة سطوح الاغشية. لقد أظهرت تقنية الرسم البياني نتائج واعدة لتحديد نوعية الغشاء.

جمهورية العراق
وزارة التعليم العالي والبحث العلمي
جامعة بغداد
كلية التربية للعلوم الصرفة / أبن الهيثم
قسم الفيزياء

دراسة تأثير التشويب والتلدين على الخصائص التركيبية والبصرية لأغشية ZnO الرقيقة باستخدام معالجة الصور

رسالة مقدمة إلى

كلية التربية للعلوم الصرفة / ابن الهيثم – جامعة بغداد

وهي جزء من متطلبات نيل درجة الماجستير علوم في الفيزياء

من قبل

شهد علي حسين

بإشراف

الاستاذ المساعد الدكتور

عدي حاتم شعبان

١٤٣٩هـ **٢٠١٨**